# POLITECNICO DI TORINO

## MASTER's Degree in BIOMEDICAL ENGINEERING


## MASTER's Degree Thesis

# Design and characterization of a supramolecular hydrogel containing nanoparticles with antioxidant and antibacterial properties to treat chronic wounds

**Supervisors**
**Prof. CLARA MATTU**
**Prof. TZANKO TZANOV**
**Prof. GIANLUCA CIARDELLI**
**Prof. MONICA BOFFITO**

**Candidate**
**GIULIANA ORLANDINI**
**s279863**

**DECEMBER 2022**

# Summary

Chronic wound (CW) treatment represents one of the main challenges of modern medicine. As CWs result from a variety of causes, their treatment is particularly difficult and can adversely affect patient's life. A serious obstacle to CW treatment is the bacterial resistance to antibiotics. This thesis aimed at the design of a hydrogel intended to be placed in contact with the CWs to stimulate wound remission, without the use of antibiotics. To achieve this, an injectable supramolecular (SM) polyurethane (PU) hydrogel was loaded with antioxidant and antibacterial nanoparticles (NPs).

The NPs were obtained by combining two plant-derived polyphenolic compounds with antioxidant properties, such as lignin, and tannic acid. The project focused on the optimization of a green synthesis exploiting the enzymatic activity of laccase to promote lignin phenolation, in order to increase the NP antioxidant and antimicrobial properties. As a result, phenolated lignin NPs (PheLig NPs) were obtained. The NPs were further modified by enzymatic grafting of a metalloproteinase (MMP) inhibitor to control the activity of the overexpressed in CWs MMPs responsible for wound chronicity. L-tyrosine hydroxamate (LTH) was conjugated to the PheLig NPs via laccase-catalysed reaction obtaining LTH-PheLig NPs. Finally, Co was loaded into the NPs via a redox reaction, to confer bactericidal properties, obtaining Co-LTH-PheLig NPs.

All NPs were characterized in terms of size, PDI and ζ-potential. LTH-PheLig NPs had similar size and ζ-potential compared to PheLig NPs, while Co-LTH-PheLig NPs resulted in a smaller average dimension. LTH conjugation increased NP antioxidant properties, as demonstrated by the myeloperoxidase (MPO) residual activity measured after incubation with NPs. Co inclusion was proved via inductively coupled plasma spectroscopy (ICP). In addition, NP inhibitory effects over bacterial growth as well as their antibacterial properties were measured. Finally, viability tests were conducted on fibroblasts and keratinocytes. PheLig NPs and LTH-PheLig NPs showed good cytocompatibility and inhibitory effects over bacterial growth, but lower antibacterial effects compared to Co-PheLig NPs. Co inclusion increased NP cytotoxicity. However, Co-PheLig NPs showed good bactericidal and antioxidant effects at lower concentration.

NPs were then loaded within an injectable SM network based on two PUs (CHP407 and SHF68) and α-cyclodextrins. The latter are toroidal-shape molecules with a hydrophobic cavity and a hydrophilic surface and allow the formation of supramolecular crystalline structures called poly(pseudo)rotaxanes (PPRs) thanks to host-guest complexes between their inner cavity and the hydrophobic domains of PUs The NP loading increased the system stability, as demonstrated by rheological tests. This is probably related to the establishment of new crosslinking points between NP phenolic groups and SHF68 primary amines. Finally release studies showed a quite linear and controlled kinetics, with no burst release. The overall system showed no swelling behaviour but a weight loss over time as a function of the amount of fluids the system was put in contact with the material. This is due to an exchange of fluids between the environment inside and outside the

hydrogel: the greater the volume of fluid with which the system was in contact, the greater the flow rate.

Overall, the developed formulations represent promising platforms for wound healing applications although further investigations are necessary. Future research perspectives would be the optimisation of the NPs content within the system to achieve a good compromise between biocompatibility and release kinetics, as well as the characterisation of the system in contact with wound exudates.

# Thesis goal

The treatment of chronic wounds (CWs) represents one of the main challenges of modern medicine. The development of CWs, in fact, is associated with a huge number of different pathologies and is the result of a wide variety of causes. Its treatment is therefore particularly difficult and can adversely affect the life of a subject. A serious obstacle to the treatment of chronic infections such as those developed at the level of a wound is represented by bacterial resistance to antibiotics.

The final aim of the thesis is the design of a hydrogel intended to be placed in contact with the bed of a CW to stimulate its remission, without the use of antibiotics. In order to obtain this result, a polyurethane network with a pseudo-crystalline structure will be developed, inside which NPs with antioxidant and antibacterial properties will be encapsulated. The NPs will be obtained using green synthesis by combining two plant-derived polyphenolic compounds with antioxidant properties, lignin, and tannic acid. Moreover, a hydroxamic group (L-tyrosine hydroxamate) and a metal ion (cobalt) will be added inside the nanoparticles to specifically inhibit the activity of metalloproteases, which overexpression commonly occurs in CWs, and confer bactericidal properties to the NPs. The overall system will be designed to promote fluid exchange between the internal environment of the hydrogel, rich in nanoparticles, and the external one, rich in exudates, maintaining a moist environment and preventing the formation of bacterial colonies at the wound site.

# Acknowledgements

*To zia Mimmy*
*wherever you are, you will always be one step away from me*

Before proceeding with the discussion, I would like to dedicate a few lines to all those who have been close to me on this path of personal and professional growth.
Firstly, I would like to express my deepest gratitude to my internal supervisors, Professor Clara Mattu, Professor Gianluca Ciardelli and Professor Monica Boffito for their patience and support. Words cannot express my gratitude to my external supervisor Professor Tzanko Tzanov for guidance and for the constant feedback that helped me in my project decisions.
I would like to extend my sincere thanks to doctoral students Giulia Crivello and Angela Gala Morena for their advice and suggestion and for the theoretical and practical expertise shared with me during the experiments and the thesis editing. I am also thankful to all the members of Professor Tzanov's research group for constant support and helpfulness.
I would like to acknowledge my parents, my grandmother and all my big family for moral and financial support they have offered me during this long course of study and for always believing in me.
I would like to extend my sincere thanks to all the special people the university has allowed me to meet and who have made the whole university experience more enjoyable and fun.
Lastly, I would like to mention Luca, Sara, Federica, and Marta. Thank you for all shared moments, smiles and tears, your constant emotional support and for always understanding me, especially in times of difficulty and despair.
Finally, my thanks go to myself, to my dedication and to all the times I chose to try, even if I did not believe it all the way.

# Contents

# List of Figures

# Acronyms

**AgPLN NPs** Silver/Phenolated Lignin nanoparticles
**BDI** 1,4-budandiisocyanate
**BP** Baird Park
**CDs** Cyclodextrins
**CDM** 1,4–cyclohexanedimethanol
**CE** Cetrimide
**CF** Chloroform
**CMT** Critical micelle temperature
**CW** Chronic wounds
**Co NPs** Cobalt nanoparticles
**Co-LTH-PheLig NPs** Cobalt phenolated lignin nanoparticles containing L-tyrosine hydroxamate
**CUPRAC** Cupric reducing antioxidant capacity
**CUR** Curcumin
**DCE** Dichloroethane
**DE** Diethyl ether
**DMF** Dimethylformamide
**DMSO** Dimethyl sulfoxide
**DSC** Differential scanning calorimetry
**ECM** Extracellular Matrix
**EDX** Energy Dispersive X-ray
**EO** Ethylene Oxide
**FFF** Filament fabrication application
**FTIR** Fourier Transform Infrared
**HClO** Hypochlorous acid
**HDI** Hexamethylene diisocyanate
**LB** Lithium Bromide
**Lig** Lignin
**LCST** Lower critical solution temperature
**LTH** L-tyrosine hydroxamate
**LTH-PheLig** Phenolated lignin conjugate with L-tyrosine hydroxamate
**LTH-PheLig NPs** Phenolated lignin nanoparticles containing L-tyrosine hydroxamate
**LVE** Linear viscoelastic range
**MBC** Minimal Bacterial Concentration

**MIC** Minimal Inhibitory Concentration
**MMPs** Metalloproteinases
**MPO** Myeloperoxidase
**MT-MMPs** Membrane-type metalloproteinases
**NB** Nutrient Broth
**NPs** Nanoparticles
**OD** Optical density
**PBS** Phosphate buffered saline
**PCL** Poly(ε-caprolactone)
**PDI** Polydispersity Index
**PEG** Poly(ethylen) glycol
**PEO** Poly(ethylene oxide)
**PEU** Poly(ether) urethane
**PheLig** Phenolated lignin
**PheLig$_{bs}$** Phenolated lignin obtained via a double step protocol
**PheLig$_{ss}$** Phenolated lignin obtained via a single step protocol
**PheLig NPs** Phenolated lignin nanoparticles
**PLA** Poly(lactic acid)
**PO** Propylene oxide
**PPO** Poly (propylene oxide)
**PPRs** Poly(pseudo)rotaxanes
**PU** Polyurethane
**RID** Refractory Index Detector
**ROS** Reactive Oxygen Species
**SEC** Size-exclusion chromatography
**SEM** Scanning Electron Microscopy
**SM** Supramolecular
**TA** Tannic acid
**TEM** Transmission Electron Microscope
**TGF-$\beta$** Transforming Growth Factors-$\beta$
**TIMPs** Metalloproteinases inhibitors
**UCST** Upper critical solution temperature
**US** Ultrasounds
**XRD** X-Ray Diffraction

# Chapter 1

# Introduction

## Pathogenesis of a chronic wound

### Structure and function of the skin

Skin is a complex organ of the human body with several functions such as thermoregulation and physical protection. Its structure is composed by three layers: epidermis, dermis, and hypodermis with different mechanical properties (Figure 1).[1]

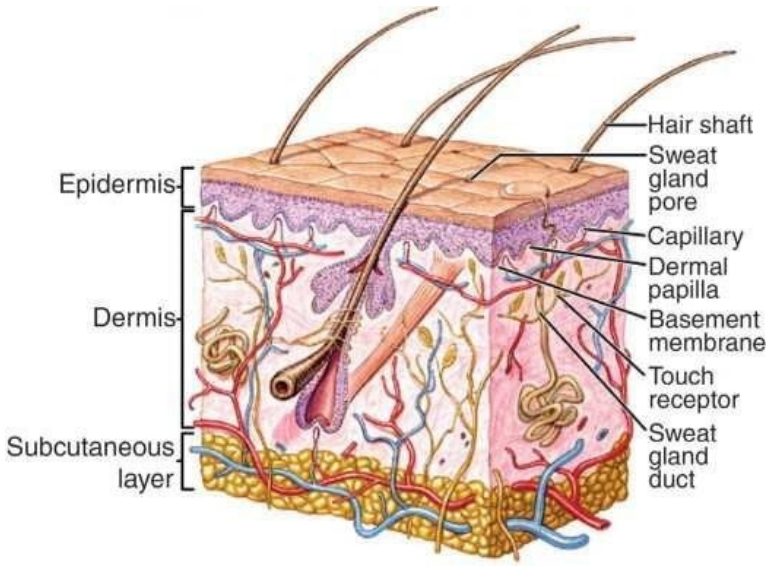


**Figure 1** General scheme of the human skin (*MacNeil et al.*).[1]

The epidermis is the outer layer and acts as a protective barrier, preventing the entrance of pathogens within the body and defending it from infections.[2] In addition, it is involved in the regulation of body temperature thanks to the presence of the ducts of the sweat glands that release sweat on the skin surface.[3] Its structure is composed of two layers of proliferative basal and differentiated suprabasal keratinocytes. The outermost part of the epidermis is the corneum.[4] This layer is rough and flexible, and composed by non-viable cells which offer specific barrier properties. [5]

The middle layer, called dermis, is a fibre network positioned under the epidermis. Its matrix contains few cells, predominantly fibroblasts capable of producing the different components of the ECM (Extracellular Matrix), mainly polysaccharides and proteins such as

collagen and elastin embedded in proteoglycans.[6] These macromolecules provide elasticity, high tensile strength, and compressibility to the ECM.[7]

Finally, the deepest layer, the hypodermis, is composed predominantly of adipocytes forming a loose fatty subcutaneous layer. It provides structural support and shock absorption and insulate the body from cold.[8] The layers are crossed by blood and lymph vessels, nerves endings, hair follicles and sweat glands.[5] Nociceptor, proprioceptor, thermoreceptors, and mechanoreceptors present as nerve free endings, and avoid the perception of external stimuli like pain, itch, temperature, and touch. The vascular system cooperates with the lymphatic system to promote homeostasis.[9] Sweat glands are a key component of the skin not only because they contribute to the maintenance of a thermic balance, but also because they are able to remove metabolic waste and excess micronutrients.[10] Hair follicles produce keratinocytes and undergo a repetitive cycle of anagen (growth), telogen (quiescence) and catagen (apoptosis). They receive mechanical external stimuli from the hair and send the information to the central nervous system.[11]

## Physiologic and pathological wound healing

### Physiological wound healing

Chronic wounds (CWs) affect more than 40 million people worldwide. For this reason, they represent one of the main challenges of medical research. An analysis conducted in 2004 highlighted that CWs annually cost around $9.7 billion in the United States and represent the largest direct medical cost of all human skin diseases.[12] In physiological conditions, after a superficial wound, the activation of different biological processes allows the elimination of foreign materials and the restoration of the skin essential function. Wound healing is a multiphase process which main stages are haemostasis, inflammation, proliferation, and remodelling.[13] The first stage of the wound healing process is the haemostasis: during this phase, the activation of circulating platelets triggers the formation of a fibrin network that consequently promotes the migration and proliferation of all the different cells involved in the wound healing[13]. During the inflammation phase, pathogens are removed from the wound site and the damage is restricted in a localized area. This process is regulated by cytokines and begins when the concentration of neutrophils and monocytes at the wound site increases thanks to a vasodilation process which locally enhances the vascular permeability.[14] Activated neutrophils release reactive oxygen species (ROS) and reactive nitrogen species (RNS) to kill the invading agents.[15] The phase culminates with the conversion of pro-inflammatory prostaglandins to anti-inflammatory lipoxins; the latter inhibit the recruitment of neutrophils and trigger the recruitment of monocytes that evolve into macrophages. Finally, macrophages can phagocyte and digest tissue debris and wastes and lead to the beginning of the remodelling phase (maturation).[14]

During the proliferative phase, that lasts for 2-4 weeks from the injury, fibroblasts migrate at the wound site and produce collagen and other components of the ECM. The network of fibrin is replaced by new granulation tissue and endothelial cells promote angiogenesis, resulting in the formation of a new vascular network from the initial granulation tissue. The granulation tissue is invaded by new angiogenic capillaries that rapidly compose a new microvascular structure.[16] The remodelling phase starts with the development of the granulation tissue. During this phase, the components of the ECM are degraded and resynthesized to reach the final ECM structure around 21 days after the injury. Figure 2 shows the general scheme of wound healing.[17]

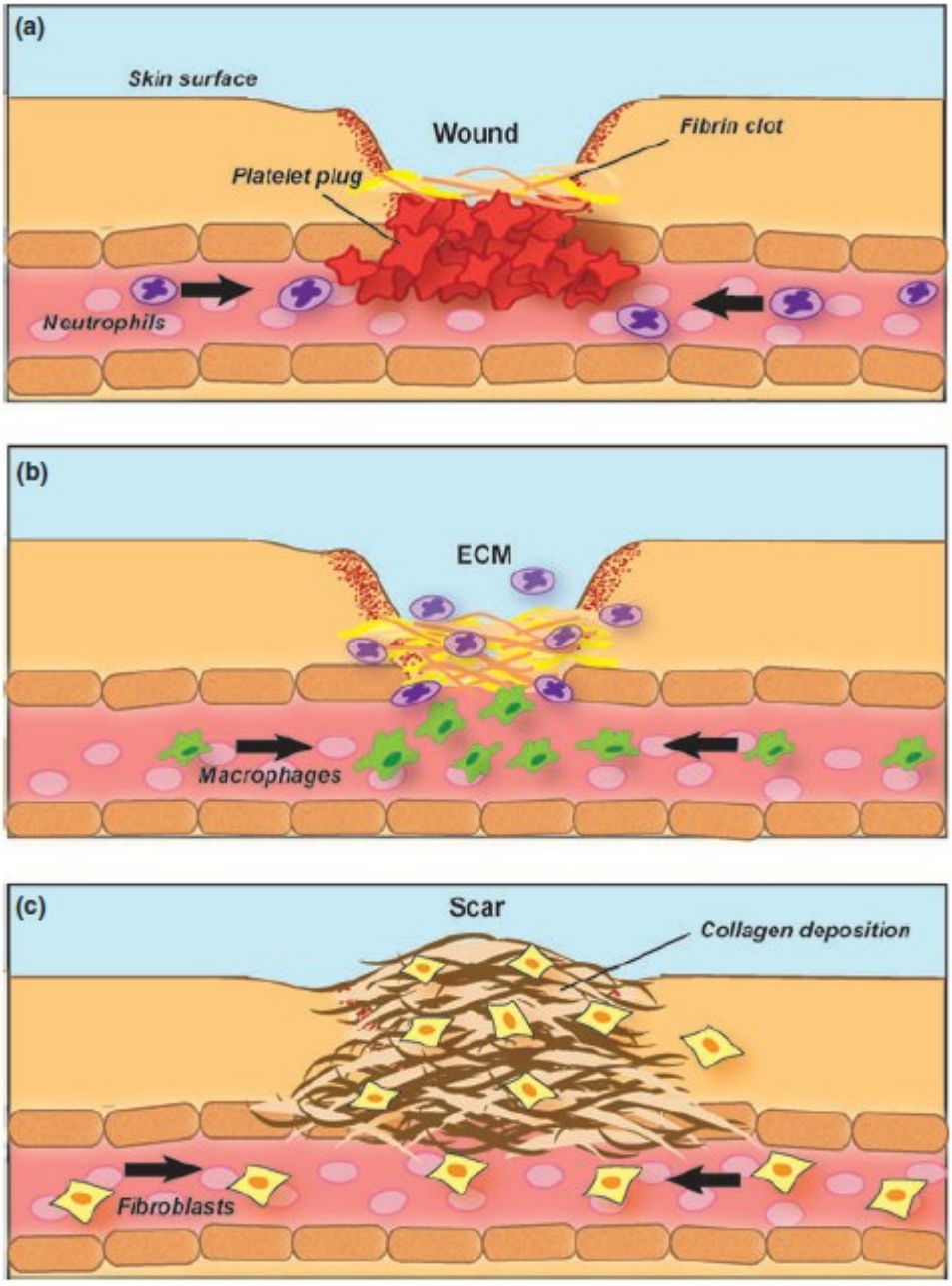


**Figure 2** General scheme of the wound healing: a) coagulation and early stage of inflammation; b) late stage of inflammation; c) proliferative and remodelling phase (*Nauta et al.*).[17]

The final healing is possible thanks to new interactions occurring between fibroblasts and the ECM. In addition, the overall process is influenced by local and systemic factors like oxygenation, stress, age, and sex hormones in aged individuals.[18] It requires a continuous oxygen supply to interact with cytokines, neutrophils and proliferating cells.[16] Another crucial factor to obtain a proper physiological healing is the maintenance of a proper balance of nutrients, such as proteins, vitamins, and zinc, at the wound site. The healing process can also be influenced by external factors, such as alcohol consumption, smoking, temperature, and moisture as well as by patient pathological conditions such as diabetes, keloids, fibrosis, hereditary healing disorders, jaundice, uraemia, cancer, and AIDS.[19,18]

**Pathological wound healing**

The development of a CW is the consequence of the degeneration of a physiological wound healing process. The potential causes of a CW can be different. Figure 3 illustrates the main factors that contribute to the formation of CWs.[20] The most common are chronic diseases, vascular insufficiency, nutritional deficiency, diabetes, neurological diseases, and age.[12] At the molecular levels, the main actors involved are cytokines, proteases, ROS, and senescent cells. Moreover, as many other chronic diseases, the evolution of CWs is characterized by a persistent infection combined with an increase in the number of dysfunctional stem cells. In tissues developing CW, the concentration of some growth factors such as TGF-$\beta$ (Transforming Growth Factors-$\beta$) increases, as well as the number of residual fragments deriving from ECM.[20] The resulting environment causes a local increase of the immune response with the activation of the proinflammatory cytokine cascade. The latter persists for a prolonged period and triggers the increase in levels of proteases and the consequence proteolytic degradation of ECM.[21]

This prevents the passage to the proliferative phase of healing while attracting neutrophils that produce new ROS, further degrading the matrix components.[12] The oxidative stress causes further damages to the DNA and promotes cell senescence, altering proliferative and secretory properties of cells.[22] As a result, the healing process is blocked in an inflammatory loop from which it is difficult to escape.

## Role of metalloproteinases and their inhibitors

Metalloproteinases (MMPs) are a class of 23 endopeptidases which are able to degrade the proteins that form the ECM and are involved in several physiological processes regulated by hormones, growth factors and cytokines.[23] MMPs are calcium dependent, contain zinc ($Zn^{2+}$) and share a common structure: they possess a propeptide of about 80 amino acids, a catalytic domain of about 170 amino acids, a linker peptide and a hemopexin domain of about 200 amino acids. MMPs contain a cysteine sulfhydryl group that chelates their active site $Zn^{2+}$ and keeps them in their inactive zymogen form.[24] In the development of a CW, one of

the most studied factors is the imbalance between MMPs and tissue inhibitors of metalloproteinases (TIMPs), which coincides with a local increase in MMPs levels. TIMPs are a class of proteins capable of forming reversible 1:1 complex with MMPs, participating in the activation and uptake/removal of MMPs from the extracellular environment.

The activity of MMPs is a regulated process, divided into 4 steps: (1) transcription, (2) activation of zymogen precursors, (3) interaction with ECM, (4) inhibition by TIMPs.

Based on their affinity with specific components of the ECM, MMPs can be classified into membrane-type metalloproteinases (MT-MMPs), collagenases, gelatinases, stromelysins and matrilysins. Through all the different types of MMPs, collagenases (MMP-1, MMP-8, MMP-13, and MMP-18) and gelatinases (MMP-2 and MMP-9) are involved in different molecular processes which balance is fundamental to obtain a physiological wound healing.[23] Increased levels of MMP-1, -8 and -9 are associated with slow wound healing processes. In particular, MMP-8 is the collagenase involved in the initial phase of dermal wound healing and its deficiency has been associated with dysregulations of the inflammatory process during cutaneous wound healing in murine models.[25] In physiological conditions, MMP-1 is present in very low concentrations. Its main role is the degradation of collagen and gelatin, but it is also fundamental in the modification of pro-MMP-9 into its active form. MMP-2 and MMP-9, respectively gelatinase A and gelatinase B, have a distinct collagen-binding domain and act as proteolytic agents in several physiological and pathological processes, including inflammation. MMP-10 is expressed by macrophages and epithelium in response to injury and influences the scar formation during the wound repair. Conversely, MMP-11 contains a laminin receptor and is expressed during the tissue remodelling phase.[24]

Abnormal regulation of MMPs and TIMPs is one of the main causes of most pathological conditions, including chronic inflammation. For this reason, a control of the interactions


**Figure 3**. Multicellular factors involved in the formation of a CW (red circles) and the agents required to overcome them (green circles)
(*Frykberg et al.*).[20]

between MMPs and TIMPs is a valid strategy in the management of a CW and in the restoration of physiological conditions.[23]

Another important factor during an inflammatory state is the activity of myeloperoxidase (MPO). MPO is an inflammatory enzyme with a critical role in the mediation of oxidative stress since it triggers the production of ROS and RNS. It also catalyses the reaction between chloride and $H_2O_2$ to produce hypochlorous acid (HOCl) that degrades several biological molecules, among which TIMPs. The decrease of TIMPs activity results in a MMP over-activation that causes excessive degradation of the ECM and impairs the wound healing process.[26]

# Bacteria in a chronic infected wound and antibiotics resistance

In the development of chronicity, a fundamental factor to consider is the development of bacterial infections. Wounds can be easily contaminated, and infections result in a delay of the healing process. In a study of the Microbiology laboratory of Pescara Hospital conducted over 6 months on 312 wound samples, 69.5 % of the analysed wounds were infected by one or more microbial species. More in details, 28 different microbial species were isolated: 44.2 % were Gram-positive and 55.8 % were Gram-negative. The bacteria species detected in greater quantity, generally associated within the same wound, were the Gram-positive *Staphylococcus aureus* (37 %) and the Gram-negative *Pseudomonas aeruginosa* (17 %).[27] Given the variety of pathogens involved, in health care practice, wounds are analysed to identify the pathogenic agents located at the infected site and to select the correct antibiotic therapy. However, microorganisms can form biofilms, self-produced extracellular matrixes that protect the pathogens, making infection elimination difficult with traditional antibiotic treatment. In addition to that, the spreading of antibiotic resistance is becoming a growing concern in the health care system. The World Health Organization has indicated this issue as one of the three most important medical challenges of the 21st century.[28] The use of antibiotics for long periods of time, as it is done for treating chronic diseases, is one of the causes of the spreading of antibiotic resistance. Therefore, the development of more effective treatments is highly required to improve patient wellbeing and reduce the risk of antibiotic resistance spread.

# Management of a chronic wound

Since the ancient Egypt, men have studied methods to treat open wounds. The first papyruses about the wound healing date back to 1400 BC. However, it was in 280 BC, during the ancient Greek, when it was noted that syringes could be good for injecting liquids and removing them from the wounds.[29] With the advance of the modern medicine, the wound bed preparation has become crucial.[12] A solution to treat a CW is to act on the environment

that is promoting the pathology in order to restore an environment similar to that of healing wounds. Debridement is often used to promote wound healing as it can be exploited to remove necrotic tissue and bacteria from the wound bed, leaving a clean surface.[30] The removal of the non-viable tissue has the aim to expose the underlying healthy vascularized tissue. This promotes the migration and proliferation of the epithelial cells at the wound site, and thus the recovery of the normal structure of the tissue. For this reason, the treatment of a CW should comprise the removal of necrotic tissue and the application of a wound dressing able to:

- absorb the excess of exudate;
- maintain a moisture environment;
- have an antimicrobial activity;
- avoid trauma on removal;
- avoid allergic reactions and pain.[12]

In addition, CW management should include control strategies over the MMPs and MPO levels and alternative treatments to antibiotics to manage and/or prevent bacterial infections.[23] Starting from the analysis of the most important factors involved in the treatment of a CW, the current study aimed to develop a new wound dress able to treat CWs without the use of antibiotics but exploiting the properties of novel materials with antioxidant and/or antimicrobial properties. Concretely, the antimicrobial effects of the system were tested considering their efficacy against *P. aeruginosa* and *S. aureus*, as they are the most common bacteria present in an infected wound. The study also focused on strategies to control MMP and MPO levels, in particular by means of MMP inhibition. The selection of an amphiphilic hydrogel as wound dressing has permitted to obtain an injectable cream that could be applied on the wound site to cover and protect it after wound debridement and cleaning. The gel is capable to exchange external exudates with internal nanosized moieties with antioxidant and antimicrobial properties according to a concentration gradient.

# Chapter 2

# Poly(ether urethane)-based hydrogels

## Introduction

### Injectable hydrogels

Hydrogels are 3D polymeric networks which structure is based on the formation of crosslinking points through the interaction of the different macromolecules they are composed of. These systems can be used for different purposes in the fields of tissue engineering and regenerative medicine thanks to their tuneable physical, biological, and chemical properties. Examples of these are the high absorbing capacity and biocompatibility.[31]

Hydrogels can be variously classified as

- synthetic, natural or hybrid;
- physically or chemically crosslinked;
- cationic, anionic or neutral;
- non-degradable, degradable;
- low swelling, high swelling or superabsorbent.

Their properties are influenced both by the synthesis conditions and their composition. One of their major applications consists in the exploitation of hydrogels as platform for drug release. This is possible thanks to their porous structure that permits to encapsulate therapeutic agents and release them in a controlled way.[32] By modifying the porosity of the gel, it is possible to change the release kinetics of the therapeutic agents.

The formation of a hydrogel happens through a "sol-gel transition" during which interactions at the molecular level occur, allowing a transition from the liquid to the gel form. This interaction can be a chemical or physical crosslinking, and this influence the mechanical properties of the final structure. Usually, chemical crosslinking allows the formation of more stable structures due to the stronger nature of the chemical bond. On the other hand, physically crosslinked hydrogels provide a more biomimetic environment that can be put in contact with biological elements such as cells or bioactive molecules. In fact, the presence of physical crosslinking is associated with the development of less mechanical force within the system, resulting in a system which morphology is able to adapt more in response to external stimuli.[32] Another factor that strongly influences the mechanical properties, and the biocompatibility of the final structure is the hydrophilicity of the polymer composing the hydrogel.[32] One class of materials used in hydrogels synthesis is composed by amphiphilic

polymers, which possess both hydrophobic and hydrophilic moieties. Thanks to this, they can simultaneously retain a large amount of water, due to the presence of hydrophilic domains, and possess better mechanical properties compared to homopolymer hydrophilic hydrogels, due to the presence of hydrophobic domains.[31]

An interesting category of hydrogels are smart systems in which the sol-to-gel transition is triggered by physical, chemical or biological stimuli. Depending on the type of stimulus activating the phase transition, these systems can be categorised into pH-responsive, temperature responsive, glucose-responsive, enzyme responsive, photo-responsive, electrically responsive, and shear stress responsive hydrogels.[37] Among all the possible stimuli-responsive materials, thermosensitive polymers are particularly interesting for developing drug releasing formulations. Indeed, they can respond to temperature changes undergoing a consequent sol-to-gel transition. This can be exploited to trigger the drug release but also to obtain injectability properties.[33] Thermosensitive hydrogels can be divided into negative temperature-sensitive systems and positive temperature-sensitive systems. The first class has a lower critical solution temperature (LCST) upon which the sol-to-gel transition occurs. On the contrary, positive-temperature sensitive hydrogels undergo a sol-to-gel transition below an upper critical solution temperature (UCST).[34] The most common type of thermosensitive hydrogels used for biomedical applications are liquid at room temperature and undergo a sol-to-gel transition at 37 °C.[35] One of the most common amphiphilic materials used to obtain thermosensitive materials are copolymers of poly(ethylene oxide) (PEO) and poly(propylene oxide) (PPO), known as Pluronics® or Poloxamers®.[36]

Another factor that should be analysed when designing a hydrogel is related to its application methods. Injectable hydrogels are a category of promising systems for biomedical applications. A broadly studied application target is the controlled delivery of drugs, cells, or bioactive molecules to treat inflammatory diseases, cancer or stimulate tissue regeneration.[37] One of the main advantages of injectable hydrogels is their minimal invasiveness, as they can be implanted at the site of interest via injection.[37] The injectability of hydrogels may be related to *in situ* or to *ex vivo* gelation mechanisms: in the first case a flowable solution or a liquid can be converted into a gel *after* injection, thanks to the formation of covalent or non-covalent crosslinking points; in the second type of systems, the sol-to-gel transition happens *before* injection thanks to its shear-shinning and self-healing properties.[38] Figure 4 shows the formation of injectable hydrogels that passes through a sol-to-gel transition caused by a crosslinking reaction.[32]

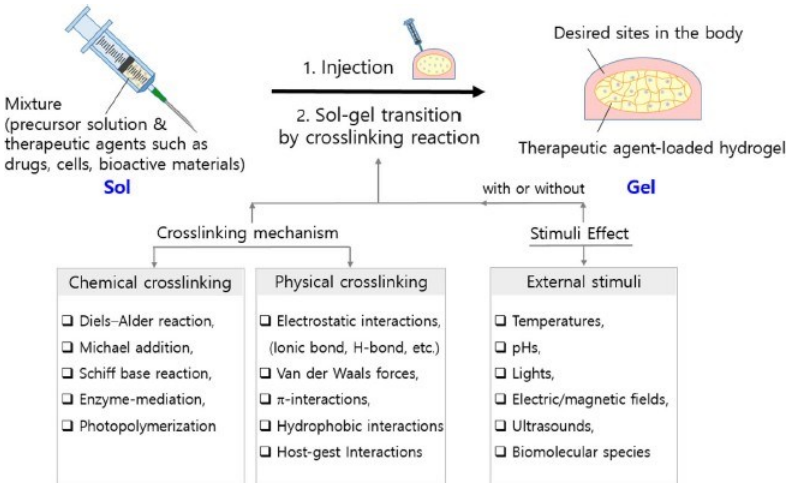


**Figure 4** Preparation of injectable hydrogels induced by physical or chemical crosslinking reactions with or without external stimuli (*Lee et al.*).[32]

The system studied in this master's thesis project is an amphiphilic and injectable hydrogel. The amphiphilic nature of the polymer was exploited to combine the possibility to have hydrophobic interactions at the most hydrophobic portions of the polymer chains, with the ability to retain aqueous solution at the most hydrophilic parts. An additional advantage of the injectability of the hydrogel is that it can be easily applied on the site of interest. Finally, the possibility to form the gel and then inject it without losing its integrity permitted to better control the NP internalization and homogeneity inside the gel. Indeed, *in-situ* gelation could result in uncontrolled NP dispersion after the injection since the time required for the gelation to take place may result in NP precipitation.

## Supramolecular hydrogels based on poly(ether urethane)s and cyclodextrins

One strategy to develop drug delivery systems lies in the design of supramolecular (SM) hydrogels. SM hydrogels are a specific class of hydrogels which formation is due to a self-assembly process of small molecules that results in a three-dimensional solid phase. This class of hydrogels, able to retain more than 97 % of water, shares common features in terms of amphiphilicity and non-covalent interactions with some biological structures allowing high biocompatibility and biodegradation.[39] By exploiting specific interactions that can arise among the different polymeric components of the hydrogel, it is possible to obtain a physical crosslinked structure that allows a high control over the release kinetics of an encapsulated cargo and the degradation/dissolution profiles. This master's thesis project aimed to exploit a SM hydrogel based on custom-made poly(urethane)s and cyclodextrins to obtain a platform to treat CWs.

**Poly(urethane)s**

Poly(urethane)s (PUs) are a class of polymeric materials composed of repeating urethane groups produced through the reaction between macromolecules presenting hydroxyl groups (R'-$(OH)_{n \geq 2}$) and compounds presenting isocyanate moieties (R-$(N=C=O)_{n \geq 2}$). The reaction is initiated by the presence of catalysts or ultraviolet light.[40] Depending on the nature of the macromolecules used, the final PUs present additional groups such as ethers, esters, urea, or aromatic compounds, which give different mechanical, physical and chemical properties. Generally, the final structure is composed by stiff and rigid segments due to the presence of the isocyanate, soft segments, composed by polyols with high molecular weight that can move more freely, and short-chain diols which act as chain-extenders. The properties of PUs depend on those of the polyols, the number of functional reactive groups, their molecular structure, and their molecular mass. Moreover, depending on the chain-extenders structure and their amount, it is possible to obtain different features in terms of morphological design, surface, thermal and mechanical properties of the selected PUs.[40,41]

The PUs used in this work were synthesized starting from two different macrodiols, the Poloxamers® 407 (P407) and F68 (F68), the diisocyanate 1,6-hexamethylene diisocyanate (HDI) and two different chain extenders, N-Boc-serinol and 1,4–cyclohexanedimethanol (CDM). Poloxamers®, available commercially also as Pluronic®, exhibit a triblock structure of ethylene oxide -propylene oxide - ethylene oxide ($EO_x$-$PO_y$-$EO_x$) which final structure is obtained thanks to the sequential polymerisation of blocks of EO and PO in the presence of sodium hydroxide or potassium hydroxide. The resulting system shows reversible thermosensitive properties in aqueous solutions: by increasing the temperature, a phase transition can be observed due to the formation and packing of micelles induced by the interaction of the most hydrophobic components of the polymeric chains. Thanks to their properties, Pluronics® can be used to form *in situ* gels and to enhance the solubilisation of hydrophobic compounds. This makes them excellent candidates for controlled-release systems[40,42]. *Al Khateb et al.* studied and compared the thermal properties of F68 and P407 via differential scanning calorimetry (DSC): in 20 wt % P407 solution micelle formation started at 13.7 °C and ended at 27.0 °C, while in 20 wt % F68 solution the temperature of gelation beginning and end was higher, respectively 39.5 °C and 60.8 °C.[42] In addition, *Al Khateb et al.* studied the properties of different P407/F68 mixtures demonstrating that the critical micelle temperature (CMT) remains similar if the polymeric concentration of the final solution of P407/F68 remains constant, while the P407/F68 ratio varies.[42] With the aim to obtain a reproducible system, this property is a considerable advantage. In fact, by varying the reciprocal concentration of the two polymers, it is possible to modify the mechanical properties and responsivity of the system, while maintaining the thermal behaviour of the hydrogel. This makes the system largely adaptable.

Poly(ether urethane)s (PEUs) are a sub-group of PUs characterized by a copolymeric structural chain composed by hard urethane segments which allow high modulus and strength and soft ether

segments which offer elasticity and elongation. The hard segments are composed by the reaction between a diisocyanate and a chain extender that normally is a low-molecular weight diol or a diamine. The diisocyanate can be aromatic, aliphatic, cycloaliphatic, or polycyclic. HDI is an aliphatic diisocyanate often used in PU synthesis thanks to its relatively non-toxic degradation products. Furthermore, it offers good mechanical properties to the final polymers.[43]

Another fundamental element that influences the crystallinity and the mechanical properties of PUs is the chain extender. *Sartori et al.* studied the influence of the chain extenders n PUs properties.[44] They synthesized different biodegradable PUs by using poly(ε-caprolactone) diol (PCL), 1,4-butandiisocyanate (BDI) and four different chain extenders, including CDM and N-Boc-serinol. The PU containing N-Boc-serinol as chain extender showed high crystallinity and optimal elastomeric behaviours. On the other hand, the PU with CDM as chain extender presented a lower crystallinity associated to a less ordered structure, but better biological response in terms of viability, adhesion, spreading and proliferation of murine myoblasts.

**Cyclodextrins**

Cyclodextrins (CDs) are natural oligosaccharides composed by units of glucopyranose disposed to form a toroidal geometry. Depending on the number of glucopyranose units, namely 6, 7 or 8 units, they are coded as α−, β− or γ−CDs, respectively. CDs, shown in Figure 5, have a hydrophobic cavity that allows them to host hydrophobic molecules in their cavity, while the external hydrophilic surface can interact with aqueous solvents, allowing the formation of host-guest complexes, that are highly stable in aqueous solutions.[45] Moreover, by exploiting their hydrophobic inner cavity, cyclodextrins can thread along polymer chains and establish Van der

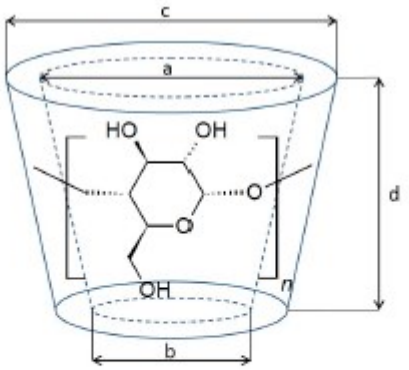


| | Glucose units | Dimensions [nm] | | | |
|---|---|---|---|---|---|
| | | a | b | c | d |
| α-CD | 6 | 0.57 | 0.44 | 1.37 | 0.78 |
| β-CD | 7 | 0.78 | 0.65 | 1.53 | 0.78 |
| γ-CD | 8 | 0.95 | 0.74 | 1.69 | 0.78 |

**Figure 5** Molecular dimensions and glucose units of cyclodextrins (*Adrian et al.*).[45]

Waals or hydrophobic interactions. The resulting structures are known as poly(pseudo)rotaxanes (PPRs) and can aggregate in water forming crystalline clusters with a channel like geometry.
The formation of PPRs in the hydrogel occurs in two stages:

1. In the first stage polymeric chains penetrate in the CDs cavity thanks to host-guest interactions occurring between CDs and the hydrophobic sections of the polymer, creating the PPRs (Fig. 6.b).
2. In the second phase neighbouring CDs molecules form hydrogen bonding and create a crystalline structure (Figure 6.c).

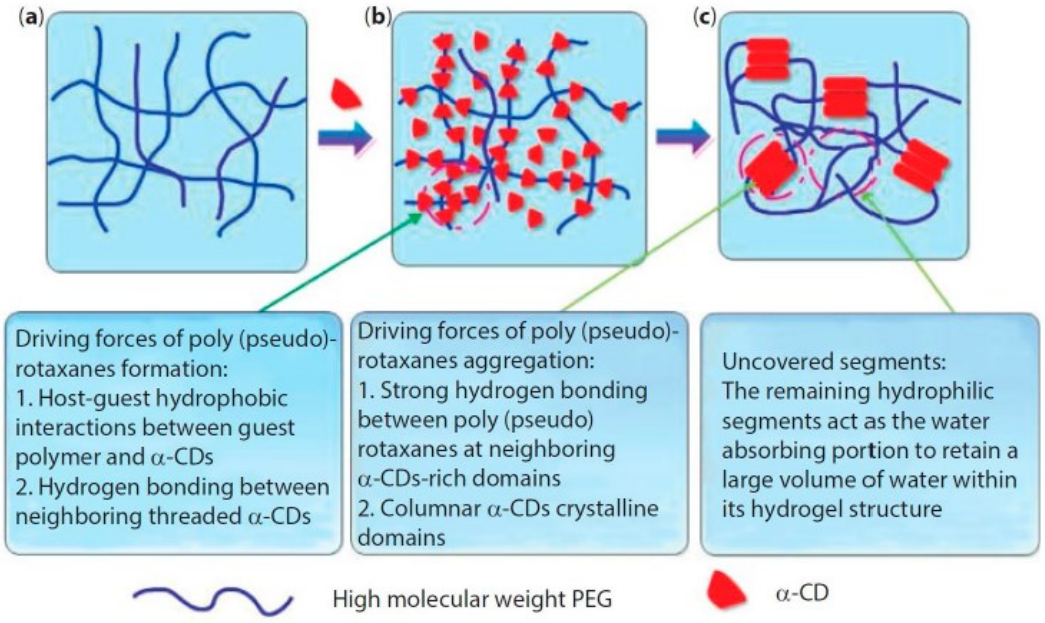


**Figure 6** Gelation of a hydrogel through the formation of a PPR-based structure (*Adrian et al.*).[45]

Many developed PPR-based SM hydrogel are composed of α-CDs and poly(ethylene glycol) (PEG). Figure 6 shows the sol-gel transition in a PPR-based hydrogel: the formation of the final structure occurs thanks to host-guest interaction between α-CDs and polymer chains of PEG.[45] The PPR-based hydrogel formation depends on the size of the CDs inner cavity, the negative binding enthalpy related to the hydrophobic interactions between the inner cavity and the polymer chains, and the length of the polymer chains. The last property influences the self-assembly behaviour of PPRs: for polymers with small molecular weight the crystalline domains can growth without limitations as the CDs can completely cover the polymer chains. At the contrary, in systems presenting high molecular weight polymers, both cluster of CDs and uncovered chains are present. The presence of non-crystalline domains is a fundamental requirement to obtain a SM hydrogel; in fact, the presence of uncovered chains gives the hydrogel the ability to retain water and to remain stable in aqueous solutions.[45]

**CHP407-SHF68 SM hydrogel**

In this scenario, high molar mass amphiphilic Poloxamer-based PEUs and α-CDs were used in this work to form PPRs, and their aggregation led to the formation of PPR-based SM stable hydrogels. More in details, a mixture of two PEUs, respectively CHP407 and SHF68, and α-CDs was used to obtain the final three-dimensional structure. CHP407 was obtained using Poloxamer 407 as macrodiol, HDI as diisocyanate and CDM as chain extender; while SHF68 was synthesized starting from Poloxamer F68 as macrodiol, with the same diisocyanate HDI and using N-Boc serinol as chain extender. The latter required an additional deprotection reaction to remove the N-BOC group from the chain extender and expose free primary amines along the polymeric chains. The exposure of free amino groups aimed to increase the responsivity of the hydrogel, by enhancing the hydrophilicity of the network, as well as to allow further functionalisation of the hydrogel. To obtain the final structure two previous works performed in the lab were taken into account: *Torchio et al. and Boffito et al.* [46,47]

In the study of *Torchio et al.* custom made poly(ether)urethanes (PEUs) (CHP407 and NHP407, based on P407, HDI and CDM or N-Boc serinol, respectively) and α-CDs were used to obtain SM structures. In the study the authors demonstrated that the presence of α-CDs and the formation of PPRs structures play a fundamental role in stabilizing the hydrogel. To infer these conclusions, *Torchio et al.* characterized the resulting PPRs through X-Ray Powder Diffraction (XRD), Attenuated Total Reflectance-Fourier Transformed Infrared (ATR-FTIR) Spectroscopy and Proton Nuclear Magnetic Resonance (H-NMR) Spectroscopy, evidencing the formation of crystalline domains given by PPRs assembly, as shown in Figure 7, 8, 9.[47] XRD spectra (Figure 7) evidenced the typical peaks provide the SM self-assembly into hexagonal channel-like crystals.

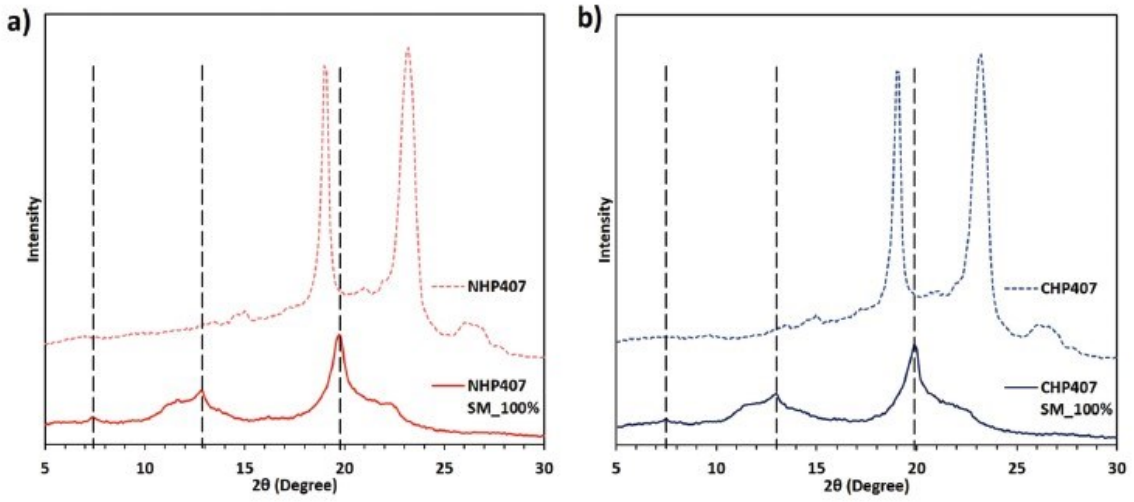


**Figure 7** XRD spectra of PEUs and their SM crystals: vertical dashed lines positioned at 2Θ = 7.6 °, 13 °, 19,8 ° indicate the SM self-assembly into hexagonal channel-like crystals, while no peaks related to pure PEU conformation are visible (*Torchio et al.*).[47]

ATR-FTIR spectra (Figure 8) evidenced the co-presence of PEU and CD bonds in the SM samples with -OH bands shifted from 3308 $cm^{-1}$ to 3340 $cm^{-1}$ and C = O bands shifted from 1720 $cm^{-1}$ to 1740 $cm^{-1}$.

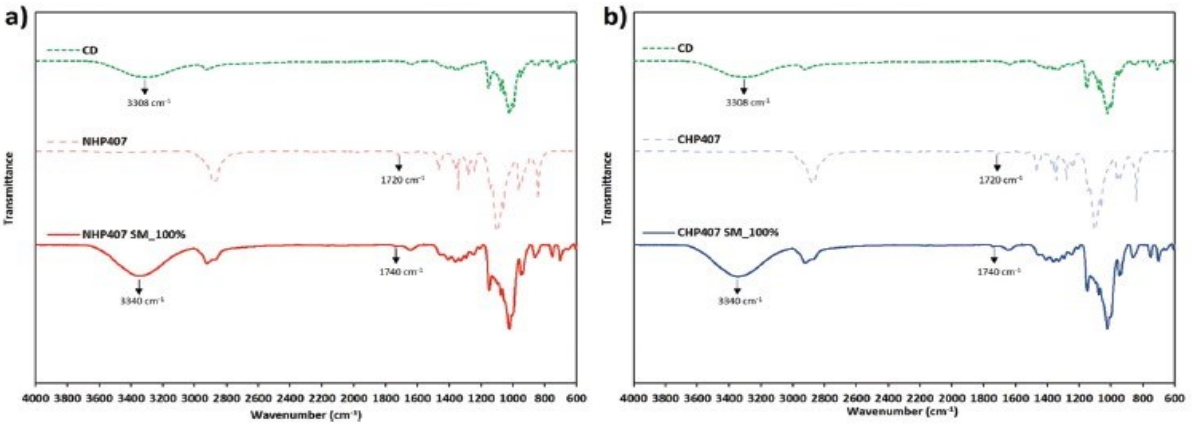


**Figure 8** ATR-FTIR spectra of CDs, PEUs and SM complexes (*Torchio et al.*).[47]

Also, $^{1s}$H-NMR spectra (Figure 9) demonstrated the co-presence of CD and PEUs in the SM crystals proved by the appearance of the typical peaks of both the components in CHP407SM 100% and NHP407SM 100 % spectra.

Moreover, *Torchio et al*. demonstrated that a better SM-assembly based on PPR formation can be reached at lower PEU concentration and higher CD concentration.[47] On the contrary, an increase in the concentration of PEUs compared to the concentration of α-CDs promoted the formation of a micelle-based structure, reducing the amount of PPRs-based crystalline phase. They also studied the influence the concentration of α-CDs had on the gelation kinetics: an increase in the α-CDs concentration from 7-8 % w/v to 9-10 % w/v allowed a significant increase in gelation speed of the hydrogel. Finally, they compared the differences in the gelation kinetics of CHP407 and NHP407. Their conclusion was that due to the absence of steric hindrance of lateral groups, the PEUs with CDM as chain extender (CHP407) was able to better interact with α-CDs, resulting in the faster gelation.

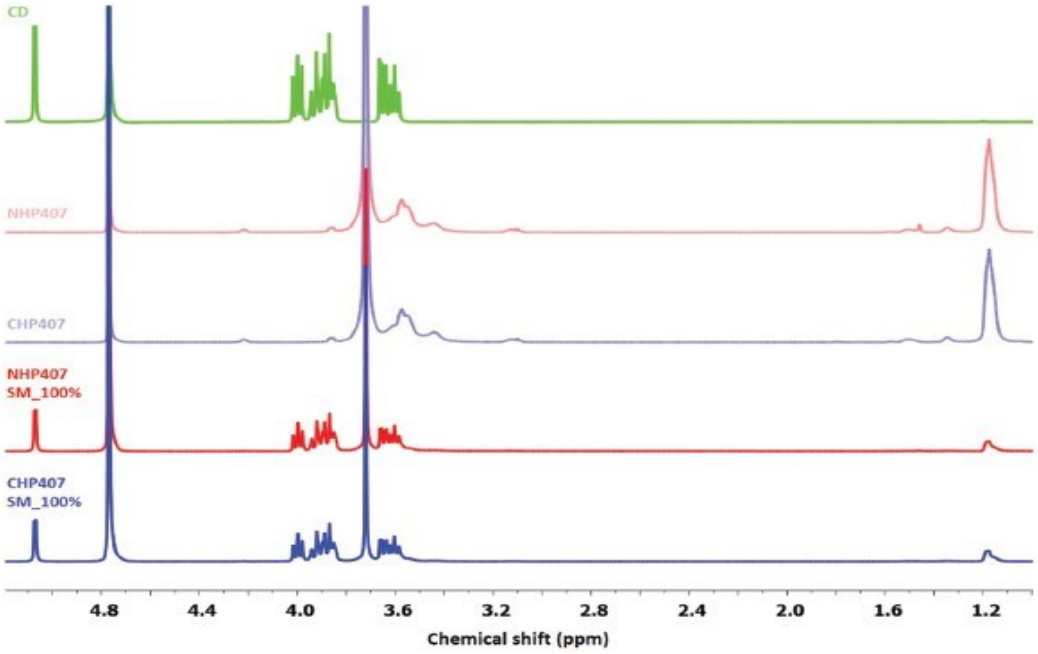


**Figure 9** [1]H-NMR spectra of CDs, CHP407, NHP407 and the SM hydrogel based NHP407 or CHP407 (*Torchio et al.*).[47]

In the second work, *Boffito et al.* designed a thermosensitive hydrogel starting from the same PEU (NHP407) developed by *Torchio et al.* [46,47] This PEU possesses primary amines, protected by N-Boc-serinol group. The PU building blocks were subjected to a deprotection reaction allowing the exposure of free primary amine group (SHP407) and enhancing the responsiveness of the hydrogel to different external acid pH environment. From the analysis of the stability properties emerged that NHP407 based hydrogels, compared to the SHP407-based ones, showed a lower dissolution and destabilization in aqueous environment.[46]

Starting from these works, the SM hydrogel system studied in this project used PEUs at low concentration (*i.e.*, 3 % w/v) and a CDs at high concentration (*i.e.*, 10 % w/v). The final SM-hydrogel was obtained by mixing the two PEUs at a CHP407:SHF68 weight ratio of 80:20.

# Materials and methods

## Synthesis of CHP407 and SHF68

### Synthesis of CHP407 and NHF68

The synthesis of CHP407 and NHF68 was done starting from the protocol proposed by *Boffito et al.* and *Torchio et al.*[46,47] The synthesis of poly(ether urethane)s required three days of preparation. Water molecules have undesired hydroxyl groups that can interfere with the reaction. Therefore, they should be eliminated as much as possible from the reagents and the solvents. To obtain this,

the Poloxamer® macrodiols P407 and F68 were weighted and incubated under alternate dynamic and static vacuum at 100 °C for 8 h, and then cooled down to 30 °C to allow easy handling. The chain extenders 1,4 –cyclohexanedimethanol (CDM) and N-Boc-serinol were weighted and stored overnight in the dark under vacuum at room temperature. To absorb the water molecules, the solvent 1,2-dichloroethane (DCE) was previously anhydrified over activated molecular sieves, under the fume hood in an inert atmosphere overnight. The synthesis was conducted during the second day in a three-necked flask connected to a condenser to avoid the evaporation of the highly volatile solvent (DCE). The process was carried out under nitrogen flow to maintain an inert atmosphere, while the flask was maintained at a specific temperature though the use of a silicon oil bath. The reaction consisted in two steps:

1. P407 and F68 were solubilised in anhydrified DCE with a concentration of 20 % w/v and the diisocyanate 1,6-hexamethylene diisocyanate (HDI) was added in a molar ratio 2:1 respect to the macrodiol to obtain prepolymeric chains with two isocyanate ending groups. The catalyst Dibutyltin dilaurate (DBTL) was also added in a concentration of 0.1 % (w/w) with respect to the macrodiol to promote the beginning of the reaction. The reaction continued for 2.30 h at 78-80 °C, then the temperature was lowered down to 60 °C.
2. The chain extenders used were CDM for P407 and N-Boc-serinol for F68. They were solubilized in anhydrified DCE (3 % w/v) and added to the solution of the prepolymers in a molar ratio of 1:1 with respect to the macrodiol. The reaction continued for 1.30 h; then, the system was led to room temperature and methanol was added in excess to stop the reaction. The system was maintained in agitation for 20/30 min. Finally, the synthesized polymers were precipitated with excess of petroleum ether (volume ratio 4:1 of the total DCE volume used) and dried overnight.

The third day of the synthesis consisted in the purification process. DCE was added maintaining the system under stirring at 50 rpm and 50 °C to reach a polymer concentration of 20% w/v. Then, a non-solvent solution of diethyl ether (DE) and methanol (2 % v/v) was used to precipitate the polymer at 5:1 volume ratio with respect to the DCE volume. The polymer was then collected by centrifugation at 6000 rpm, for 20 min at 4 °C. The supernatant was removed, and the polymer was maintained under chemical fume hood overnight to permit the complete solvent evaporation. The dried polymers were stored under vacuum at 4 °C.

The names of the polyurethanes obtained depended on the components they were composed of. For CHP407, C refers to the chain extender CDM, H to the diisocyanate HDI and P407 to the Poloxamer used. Similarly, for NHF68, N refers to N-Boc-serinol, H to the diisocyanate HDI and F68 to the Poloxamer used.

**Deprotection of Boc-protected primary amines in NHF68 to obtain SHF68**

The deprotection reaction was performed in accordance with the protocol proposed by *Boffito et al.*[46] The deprotection of the Boc groups allowed the exposure of the amino groups present in the chain extender. NHF68 was weighted and solubilized in chloroform (CF) through stirring (250

rpm) for 120 min under chemical hood. To obtain the deprotection of the Boc groups, trifluoroacetic acid (TFA) was added to the CF solution to obtain a final polymer concentration of 4 % w/v with a CF/TFA volume ratio of 90:10. After 1 hour, the deprotected PU solution was subjected to evaporation at reduced pressure to allow the complete evaporation of the solvents. Subsequently, the concentrated solution was washed twice with CF and resuspended in bi-distilled water by vigorous stirring at 4 °C overnight. To remove residual traces of TFA and CF and well as the N-Boc groups, the solution was subjected to dialysis (cut of 10000 – 12000 Da) in distilled water for 3 days. Finally, the sample was lyophilized and stored at 4 °C, under vacuum. The name of the obtained polymer was changed from NHF68 to SHF68 to indicate the deprotection of the serinol moieties.

## PU characterizations

**Size-exclusion chromatography (SEC) analysis**

Size-exclusion chromatography (SEC) analysis was used to discriminate polymeric chains with different molecular weight. The analysis was carried out using an Agilent Technologies 1200 Series (California, USA) equipped with two Waters Styragel columns (HR1 and HR4) and a refractory index detector (RID). For the analysis the mobile phase used was N,N-dimethylformamide (DMF) with lithium bromide (LiBr,0.1 % w/v). Samples of SHF68, CHP407, NHF68, F68 and P407 were solubilized in the mobile phase at 2 mg/ml concentration, vortexed and filtered with a PTFE filter (0,45 µm) before being analysed (flow rate 0.4 ml/min at 55 °C). As output, an elugram showing the refractory index intensity in function of the elution time was registered. To obtain the numeral and ponderal average molecular weights and the polydispersity index (PDI), a calibration curve built starting from standards of PEO was used.

**Attenuated Total Reflectance Fourier Transform infrared (ATR-FTIR) spectroscopy**

ATR-FTIR analysis was used to assess the presence of the urethane groups within CHP407 and SHF68, comparing their spectra with the one of the starting Poloxamers (*i.e.*, P407 and F68). Moreover, the analysis was used to verify the absence of urea groups that could form when residual water molecules are present during the polyurethane synthesis. The analysis was conducted in the range of 600 $cm^{-1}$ – 4000 $cm^{-1}$ in 32 scans using a Perkin Elmer Spectrum 100 equipped with an ATR accessory with diamond crystal (UATR KRSS). Finally, the spectra of the materials were analysed using the Perkin Elmer software.

**Kaiser Test**

The Kaiser Test is a colorimetric assay used to evaluate the presence of primary ammino groups by exploiting their reactivity towards ninhydrin molecules. Firstly, a calibration curve was obtained starting from a serial dilution of glycine (0.5 mg/ml) in ethanol at 60 % ($EtOH_{60\%}$). 600 µl of each dilution of glycine were mixed with sequentially 75 µl of phenol, 100 µl of potassium

cyanide and 75 µl of ninhydrin. The solution was incubated at 120 °C for 10 min and the absorbance at 570 nm was measured to obtain a calibration curve. The same process was used for the samples SHF68 and NHF68, the latter used as negative control. The absorbance value used to determine the primary amino groups concentration in SHF68 was measured as follows:

$$\boldsymbol{Absorbance = Absorbance_{(570\,nm)_{SHF68}} - Absorbance_{(570\,nm)_{NHF68}}}$$

Thus, the absorbance was used to calculate the amino groups concentration starting from the calibration curve.

In this test it is important to avoid the saturation of the signal that could be due to:

- High signal intensity that cannot be detected by the spectrophotometer. This can be solved by diluting the sample.
- Saturation of the available ninhydrin molecules. This could happen when the moles of ninhydrin used are not exciding the amines present. In this case, it is necessary to estimate the moles of amines present so that there is no saturation of the signal.

# Results

## PU characterization

### SEC analysis

The SEC analysis was performed to study the molecular weight and the size distribution of the polyurethanes obtained after the synthesis of CHP407 and NHF68 and after the deprotection of

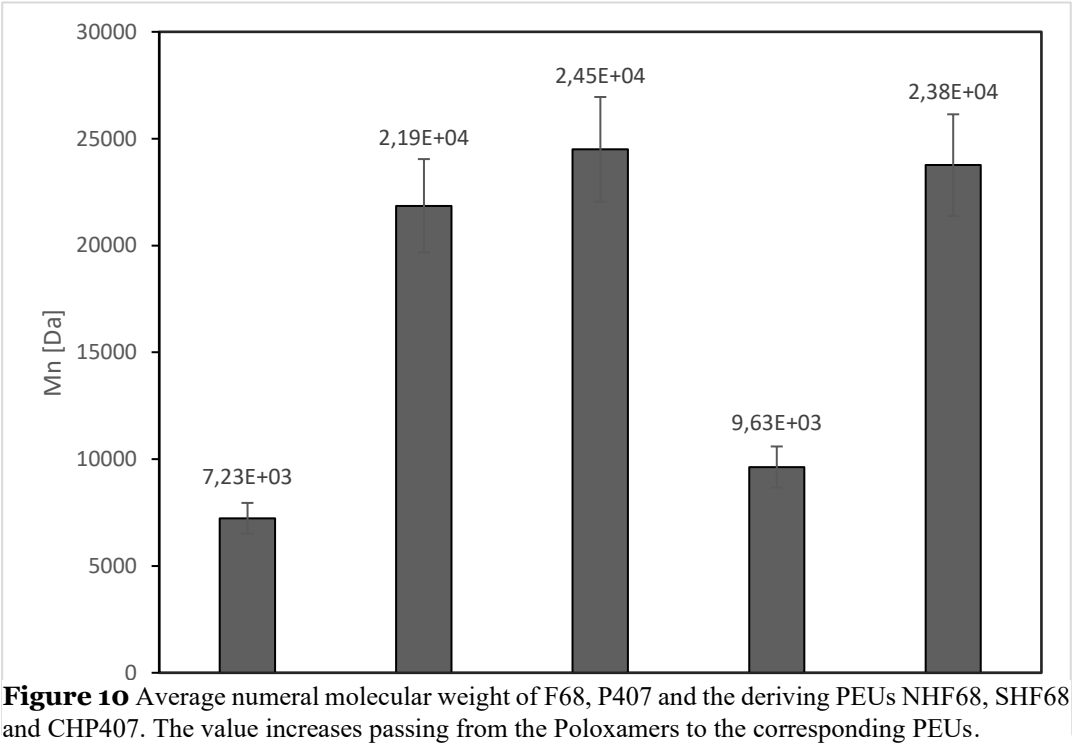


**Figure 10** Average numeral molecular weight of F68, P407 and the deriving PEUs NHF68, SHF68 and CHP407. The value increases passing from the Poloxamers to the corresponding PEUs.

NHF68 to SHF68. Figure 10 shows the number of the average molecular weights ($\overline{M}_n$) obtained from SEC analysis for the different PUs compared to the corresponding Poloxamers.

The measured $\overline{M}_n$ for F68, P407, NHF68, SHF68 and CHP407 were respectively 7.2 kDa, 9.6 kDa, 22 kDa, 25 kDa and 24 kDa with a corresponding PDI of 1.04, 1.13, 1.77, 1.68, and 1.70, respectively. The $\overline{M}_n$ of NHF68 , SHF68 and CHP407 was significantly higher than the $\overline{M}_n$ of the Poloxamers, confirming the successful synthesis of the PEU. A further increase in the molecular weight of SHF68 can be observed. This could be a consequence of the post-deprotection purification involving the removal of low molecular weight chains through dialysis, as well as to the instrument measurement errors which is 10 %.[46] Figure 11 represents the molecular mass distribution of the different PUs. Figure 11.1 shows a comparison between the molecular mass distribution of NHF68 and SHF68, while Figure 11.2 compares the results associated to SHF68 and CHP407.

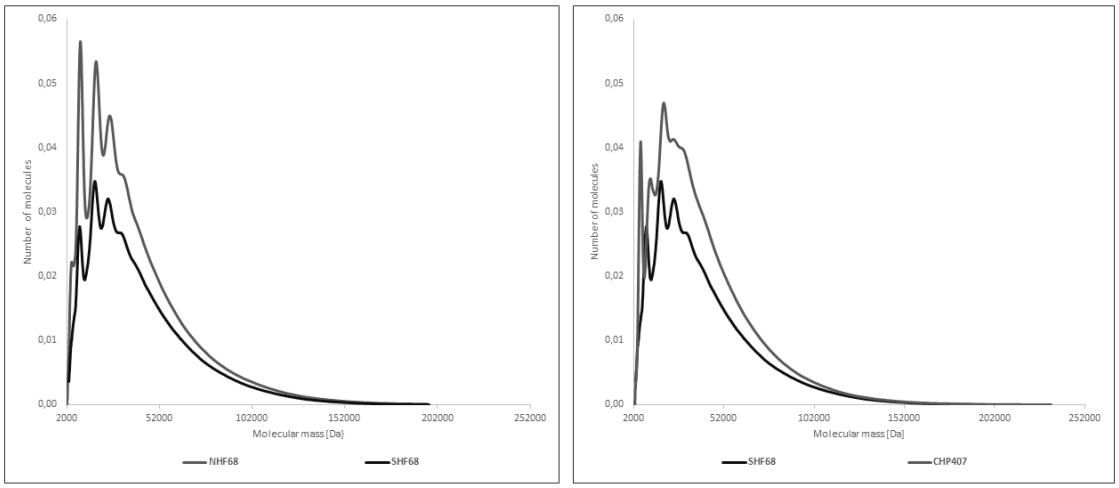


**Figure 11** Molecular mass distribution profiles of the PEUs. 1) Comparison between NHF68 and SHF68. 2) Comparison between the final PEUs used for the hydrogel preparation, SHF68 and CHP407.

**ATR-FTIR analysis**

To further verify the success of PU synthesis, ATR-FTIR analysis was performed. Figure 12 shows the ATR-FTIR spectra of the Poloxamer 407 and the derivative PU CHP407. According to *Torchio et al.* in each compound it was possible to find the following common peaks:

- around 2880 $cm^{-1}$, corresponding to -$CH_2$ stretching vibrations;
- around 1242 $cm^{-1}$, corresponding to -$CH_2$ rocking vibrations;
- around 1098 $cm^{-1}$, corresponding to -$CH_2$-O-$CH_2$- asymmetric vibrations.[47]

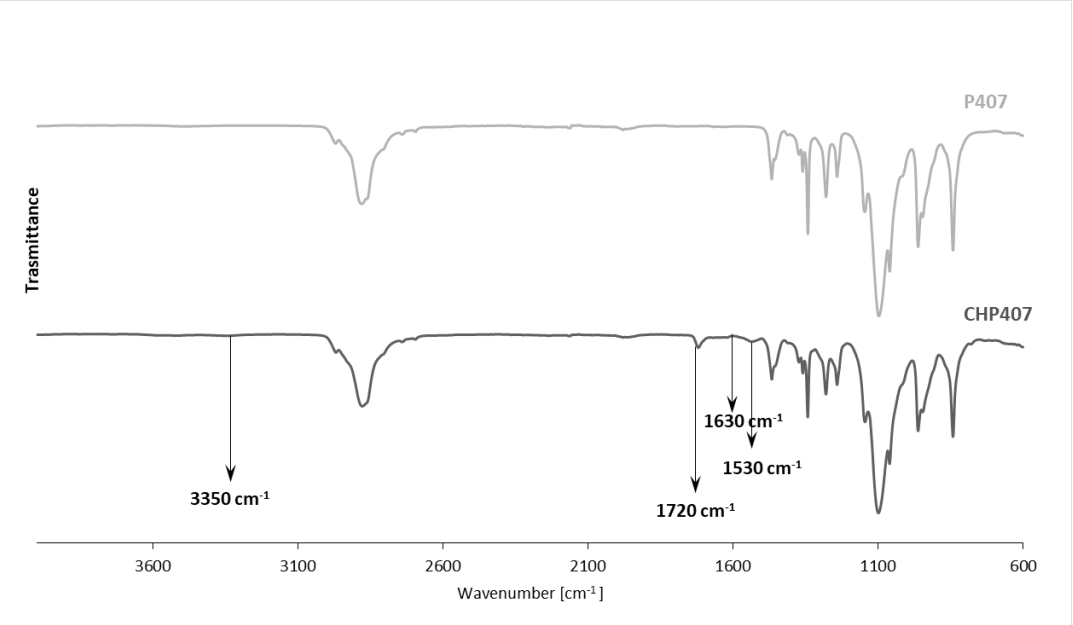


**Figure 12** ATR-FTIR spectra of the Poloxamer P407 and the deriving CHP407: the presence of the peaks identified with arrows demonstrates the PEU formation.

Conversely, the presence of the new urethane groups was testified by the appearance of new absorption peaks for SHF68, NHF68 and CHP407. More in detail:

- the peak around 3347 $cm^{-1}$ is related to -NH stretching vibrations;
- the peak around 1720 $cm^{-1}$ is related to -C=O stretching vibrations;
- the peak around 1630 $cm^{-1}$ is related to -NHCO stretching vibrations;
- the peak around 1534 $cm^{-1}$ is related to -NH bending and -OH stretching.[47]

A comparison between SHF68, NHF68 and F68 is presented in Figure 13. NHF68 and SHF68 spectra were similar and overlapped also with CHP407 spectrum.

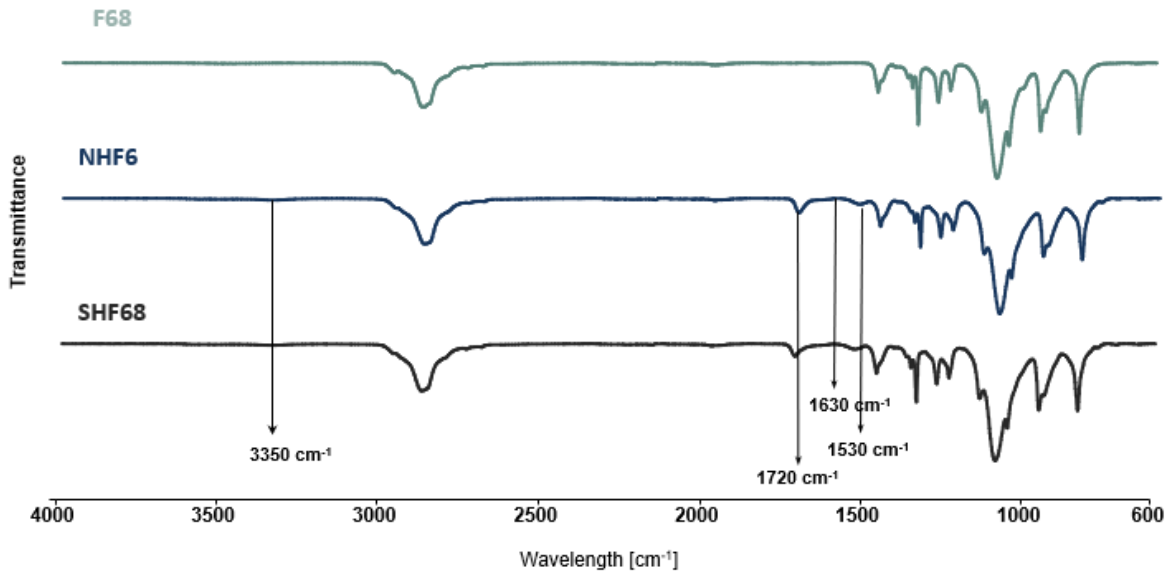


**Figure 13** ATR-FTIR spectra of F68, NHF68 and SHF68. The results confirmed the presence of the urethane group in the PEUs.

### Kaiser Test

The colorimetric Kaiser Test was performed to prove the success of the deprotection process and quantify the number of amines exposed on the polymer backbone. The quantity of amines exposed after the deprotection of the N-Boc-serinol was measured to be $2.17\ 10^{15} \pm 2.46\ 10^{14}$ $NH_2$/mg PU, demonstrating the success of the reaction.

## Conclusions

The synthesis of the PEUs composing the SM hydrogel was confirmed by the results of SEC analyses, ATR-FTIR spectroscopy as well as the colorimetric Kaiser Test. The preparation of the hydrogel in this project has followed just one root according to an already optimized formulation: the preparation and characterization of the hydrogel was performed considering a single composition (80 % of CHP407 and 20 % of SHF68 in weight) as well as a single combination of PEUs/CDs concentrations (PEUs at 3 % w/v, CDs at 10 % w/v).

The selection of these specific PEUs and CDs concentrations was the result of a previous optimization that allowed to obtain a system which sol-to-gel transition was predominantly driven by the formation of a PPRs crystalline phase, rather than the aggregation of the hydrophobic components of PEUs into micelles. This aspect is fundamental to allow the formation of a SM hydrogel with an optimal biocompatibility. The aggregation of CDs to form PPRs permits to obtain a stable SM structure, while maintaining a low polymer concentration, which strongly increases the biocompatibility of the hydrogel. In fact, a system with a low concentration of

synthetic polymers will release a lower amount of potentially cytotoxic degradation/bioerosion products, thus increasing the safety of the hydrogel.
The selected ratio of the two polyurethanes (80 % of CHP407 and 20 % of SHF68 in weight) was also a parameter previously optimized. This combination allowed to obtain the best compromise between mechanical properties, responsivity, gelation kinetics and stability. However, a future perspective could be the characterization of systems obtained starting from different combinations of CHP407 and SHF68. In the perspective of including NPs within the hydrogel, an increase in the SFH68 content could promote more interactions between the NPs and the amine lateral groups exposed by SHF68.

# Chapter 3

# Nanoparticles

## Introduction

The term nanoparticles (NPs) refer to a class of materials with at least one dimension in the nanoscale. The small size offers to nanodimensioned systems new properties different from their bulk counterpart. These new unique properties have encouraged the development and application of NPs in different fields such as electronics, environmental and energy economics, cosmetics, medicine, pharmaceutical and biomedical applications.[48] In the field of nanomedicine, one of the possible applications consists in the use of NPs to develop new treatments. The nanosize of these systems dramatically increases the surface area to volume ratio and, consequently, leads to advanced physicochemical properties and increases the treatment efficacy. Among the possible applications, the use of nano systems for treating non-healing wounds is gain growing interest in the research. NPs can be exploited as delivery systems of gaseous molecules, natural products, bioactive plant derived compounds, and growth factors at the wound site. For example, they can be used to deliver soluble curcumin with proved anti-inflammatory, antimicrobial and antioxidant effects.[49,50]

One of the most effective strategies in the treatment of CWs is the development of metal-based NPs. Among several existing metallic materials used in the development of antibacterial NPs, silver (Ag), gold (Au) and zinc oxide (ZnO) offered the best results in terms of antimicrobial effects and biocompatibility.[50,51] *Wu et al.* synthesized silver nanoparticles (Ag NPs) and used them as coating materials of bacterial cellulose nanofibers (Ag NPs-BP). The resulting systems exhibited antibacterial properties against *E. coli, P. aeruginosa* and *S. aureus* and no cytotoxic effects in epidermal cells.[52]

Gold can be conjugated to antimicrobial moieties to increase their antibacterial properties. *Shih-Chun et al.* conjugated gold nanoparticles (Au NPs) with the proangiogenic vascular endothelial growth factor-$A_{165}$ (VEGF-$A_{165}$) and the antibacterial (11-mercaptoundecyl)-N,N,N-trimethylammonium (11-MTA) cation to form 11-MTA/VEGF-Au NPs. The final system applied on infected wounds of diabetic mice exhibited strong antimicrobial activity as well as low cytotoxicity and stimulated the reepithelization.[53]

Zinc ($Zn^{2+}$) is a metallic ion involved in several physiological and pathophysiological processes, including wound healing, oxidative stress, inflammation, and tissue reepithelization.[54] $Zn^{2+}$ is a cofactor for many metalloenzymes whose deficiency has a significant effect on T lymphocytes involved in the regulation and suppression of the inflammation.[55] *Rashmirekha et al.* synthesized

zinc oxide-based NPs (ZnO-NPs) with strong antibacterial and antibiofilm effects on *S. aureus*. Moreover, *in vivo* analysis showed the NPs reduced the skin infection and inflammation in murine models.[56]

While gold, silver and zinc represent the most studied materials used in the production of NPs used in the wounds care, cobalt is still a poorly known but promising material in the management of a chronic infection. *Koyyati et al.* developed and characterized cobalt nanoparticles by an eco-friendly and cost-effective method using *Raphanus sativus var. longipinnatus* leaf extract. The NPs showed good antibacterial activity in Gram-negative bacteria and a dose dependent cytotoxicity.[57]

Another strategy widely employed in the management of a CW is based on the curative properties of polyphenolic compound extracted from plants as secondary metabolites. The most common use of this class of compounds is as incorporated moieties in wound dressings. In particular, in the management of CWs this compound could play a fundamental role thanks to their antioxidant capacities, their scavenging activity over free radicals and non-radical reactive species, as well as their anti-inflammatory, antimicrobial and wound healing promoting properties.[58]

One of the cornerstones of this thesis project was the provision of antioxidant and antibacterial properties to the designed hydrogel through the inclusion of polyphenolic NPs. The next paragraphs will be focused on a detailed analysis of the chemistry of phenolic compounds with a particular attention to the use of lignin (Lig) and tannic acid (TA) for the development of innovative NPs. The study will also focus on the inclusion of cobalt (Co) in the NPs as this material has demonstrated abilities to chemically interact with polyphenolic groups. The final aim is the development and characterisation of cobalt-based polyphenolic NPs to be included in an innovative antibacterial and antioxidant system to treat CWs.

## Phenolic compounds

Polyphenols are natural compounds that belong to the class of phytochemicals. They are extracted as secondary metabolites from fruits, seeds, flowers, vegetables, nuts, and stems and can be classified in phenolic acids, flavonoids, and non-flavonoids. Each phenolic compound contains one or more carbon-based aromatic phenyl ring. It is possible to classify phenolic compounds in phenols, composed by only one phenolic OH group, polyphenols with two or more phenolic OH groups grafted to the aromatic ring. It is possible to classify phenolic compounds in phenols, composed by only one phenolic OH group, polyphenols with two or more phenolic OH groups grafted to the aromatic ring. The latter have attracted interest as anti-cancer agents thanks to their strong antioxidant properties.[59] The antioxidant action of polyphenols is connected to four possible mechanisms:

- free radical scavenging
- oxidase inhibition and consequent suppression of free radicals
- transition metal ions chelation

- activation of antioxidant enzymes.[59]

In more details, the antioxidant properties of the phenols are connected to the formation of phenoxy radicals. In fact, the phenolic groups can oxidase to quinones, conferring to these compounds strong antioxidant and anti-inflammatory properties.[60,61] Figure 14 shows the oxidation process of a phenolic groups.[62] The reaction is triggered by the presence of an oxidizing agent and brings to the formation of free phenoxy radicals, shown in Figure 14 (3). This is due to the cleavage of the -OH caused by the loss of a hydrogen atom (Figure 14 (1)) and the formation of a phenoxide anion. The latter loses one electron, as shown in Figure 14 (2) and leads to the formation of a phenoxy radical that is resonance-stabilized by the delocalization of the unpaired electron over the aromatic ring as shown in Figure 14 (3a-3d).[62]

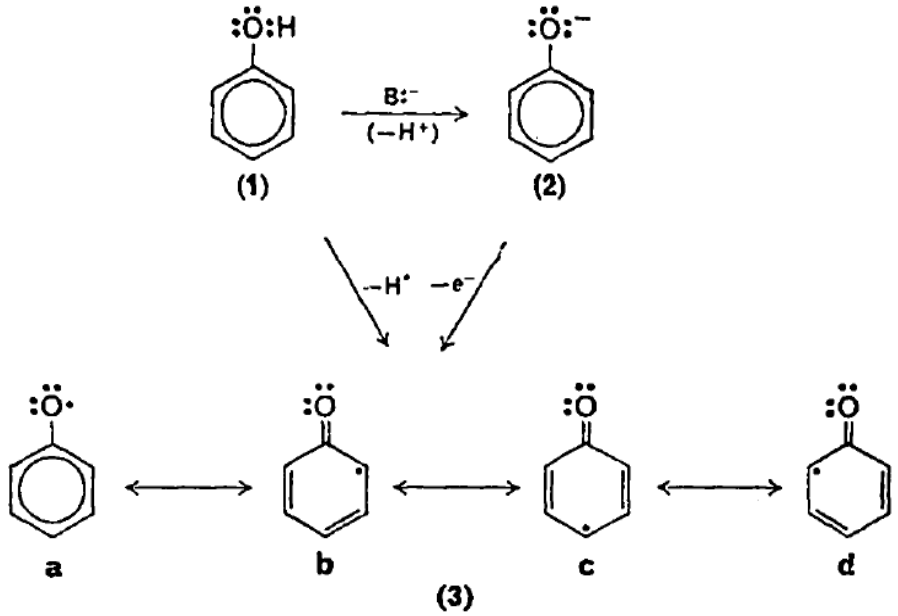


**Figure 14** Mechanism of phenolic oxidation. 1. The reaction begins with the loss of -H in presence of an oxidizing agent; 2. The deriving phenoxide anion loses an electron: the deriving phenoxy radical is resonance-stabilized by the delocalization of the unpaired electron (*Mihailovi et al.*).[62]

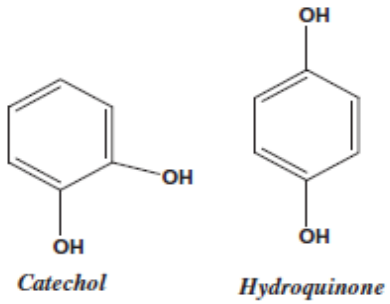


**Figure 15** Chemical structure of catechol and hydroquinone (*Teodor et al.*).[63]

The oxidation of phenols is followed by hydrolyse in *ortho*- and *-para* positions to obtain catechol and hydroquinone whose chemical structure is shown in Figure 15.[63] As shown in Figure 16, in presence of an oxidizing agent, catechol and hydroquinone are consequently transformed to *o*- (1) and *p*-quinones (2) respectively which can react with nucleophilic reactants or can undergo an autopolymerisation.[59,62] In the current study, an enzymatic oxidation of Lig allowed its phenolation promoting the reaction of the deriving reactive phenoxy radical with TA. The presence of a polyphenolic nanosystem was considered a fundamental factor not only to obtain a system with antioxidant properties but also to obtain further crosslinking useful in the formation of the hydrogel. It was supposed that the o-quinone intermediates deriving from the oxidation of polyphenolic Lig could be able to react with the nucleophile amine groups exposed as lateral group by the deprotected chain extender N-Boc serinol of SHF68.

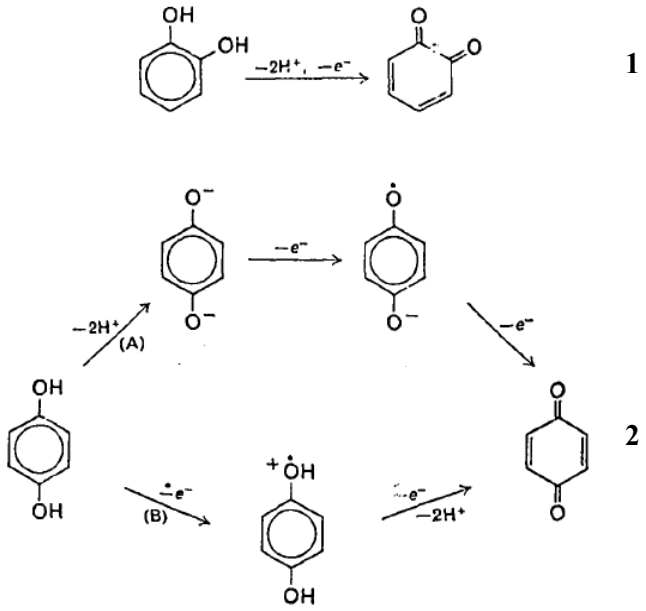


**Figure 16** Oxidation of catechol group into o-quinone.
2) Oxidation of hydroquinone into p-quinone. (*Mihailovi et al.*).[62]

**Lignin and tannic acid**

Among all the natural phenolic compounds, Lig is the second most abundant plant-derived biopolymer.[64] It is extracted from lignocellulosic biomasses where is strongly bound to

cellulose and hemicellulose via covalent and non-covalent interactions. Depending on the separation method as well as on the biomass source, the properties of the resultant extracted lignin can be different. In addition, the resulting features are depending on several external key factors such as temperature, pH, pressure, solvent/solute volume that takes part in the reaction and its dissolving power.[65] There are 4 processes methods for lignin extraction: Kraft process, sulphite process, soda process and organosolv process. The main properties of the corresponding Lig products are summarized in Table 2.[65] The main separation method is Kraft pulping during which about 90-95 % of Lig is degraded to fragments with low water solubility and high phenolic content. Another separation method is based on the sulphite pumping that produces lignosulfonates with a higher water solubility and a lower phenolic content.[66] The lignin (Protobind6000) used in this project is obtained through the soda process.[67] This type of Lig derives from non-wood materials and has a mean molecular weight (MW) of 2400 Da but this value can range between 1000 and 3000 Da, depending on the carbon content. In addition, it contains no sulphur and consequently precipitates in aqueous solutions.[65] According to this, Protobind6000 has 0.71 % of S. In addition, it is characterized by a high percentage of C (59.1 %) and a small amount of N (2.32 %); the latter may be derived from the plant resources and is not connected to the presence of amines. Finally, it contains water and a hemicellulose derivative (xylose) and can be differentiated from other Protobind lignins according to the hydroxyl content but also because of the total absence of any added chemicals.[68] Thermogravimetric analysis allowed to study Lig degradation temperature range demonstrating that the major degradation takes place between 200 and 700 °C.[68]

Lig is largely exploited in several applications fields: its increasing request is connected to its reactivity, low costs, and eco-friendly nature. Depending on its properties, lignin can be exploited in applications such as dyes, binders, emulsifiers, synthetic flooring, dispersal agents, paints as well as for the production of polymer building blocks and chemicals.[66] In the biomedical field, Lig has been employed in tissue engineering applications and as drugs delivery systems for several medical fields thanks to its cytocompatibility and its anti-tumoral, anti-viral, antidiabetic, antioxidant, and antimicrobial effects.[66]

**Table 1** Extraction process of Lig and deriving properties; [a]Conventional process; [b]Value referred to softwood.[65]

| EXTRACTION PROCESS | TREATMENT CONDITIONS | SOLUBILITY[69] | LIGNIN MW [DA] | COOH % | OH PHENOLIC % | METHOXY % |
|---|---|---|---|---|---|---|
| **KRAFT** | **1st** Sodium hydroxide and /or sodium sulphide (pH=13-14 and T≈170 °C) **2nd** : Sulfuric acid (pH=5-7.5) | Alkali; Organic solvent | 1000-15000 | 4.1[b] | 2.6[b] | 14[b] |
| **SULPHITE** | Metal sulphite + Sulphur dioxide ($Ca^{2+}$, $Mg^{2+}$, or $Na^{2+}$) (pH=2-12 and T=120-180 °C, for 1 to 5 h) | Water | 1000-50000 | ND | ND | ND |
| **SODA** | 13-16 % wt of Sodium hydroxide (T=140-170 °C) + Anthraquinone (catalyser) | Alkali | 1000-3000 | 7.2-13.6 | 2.6-5.1 | 10-16 |
| **ORGANOLV** | Organic solvents (ethanol, methanol, acetic and formic acid), usually mixed with water (T=170–190 °C) | Wide range of organic solvents | 500-5000 | 3.6-7.7 | 3.4-3.7 | 15.1-19 |

According to *Spiridon et al*. the development of Lig-based formulations could become an important topic in the market of wound healing products.[64] As example, *Dominguez et at*. designed poly(lactic acid) (PLA) filaments and combined them with Lig. The resulting fibres were employed to obtain a 3D printed dressing for wound healing applications. Then, to obtain advanced properties without the inclusion of any antibiotics, the network was coated with curcumin (CUR), an antioxidant and antibacterial natural product widely employed to treat infections.[70] In this master thesis project Lig was employed to obtain Lig-based NPs which were included in the designed hydrogel to provide the system with antioxidant properties by using a highly biocompatible and low-cost natural compound. The reactivity of Lig depends on the total phenolic hydroxyl content of Lig. *Aracri et al.* measured the total -OH amount of Protobind6000 was of 0.84 mmol per g of lignin.[71] Starting from this assumption, an increasing in the reactivity of Lig was considered essential to obtain a highly effective product; for this reason, the designed Lig-based NPs were conjugated with the polyphenolic compound TA.

TA is a natural molecule that belongs to the class of tannins. It can be found in several beverages and foods such as red wine, beer, coffee, black tea, and green tea as well as grapes, pears, bananas, sorghum, black-eyed peace, lentils, and chocolate.

The chemical structure of TA is shown in Figure 17: it has a "core-shell" form containing a central hydrophobic glucose molecule esterified at external hydrophilic hydroxyl groups with gallic acid molecules.[72,73] According to *Khan et al.,* TA is a potent antioxidant and exhibits anticarcinogenic and antimutagenic activities, decreasing the tumorigenicity risk in skin and other organs. The antioxidant activity of this compound is related to its ability to quench hydroxyl radical and cleavage plasmid DNA.[74] In this study, TA was bound with Lig by exploiting a biografting process whose efficacy is related to the propensity of phenolic compounds to undergo coupling reactions with phenoxy radicals.[71] For this reason, the biografting required an initial Lig activation step during which the polymer was enzymatically oxidated to phenoxy radicals. More in detail, Lig activation was mediated by the catalytic action of laccase that possess several natural functions including Lig polymerization (lignification) and depolymerization (delignification).

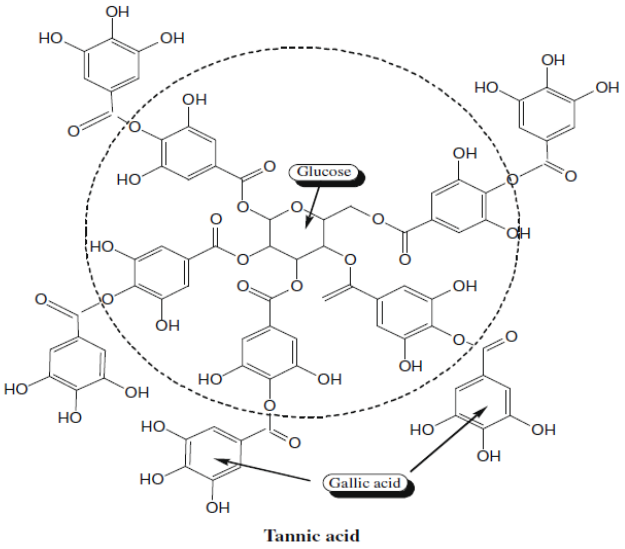


**Figure 17** Chemical structure of TA.

**Laccase-mediated phenolation of lignin**

Laccase belongs to multicopper proteins family able to transfer four electrons from a reducing substrate. Among all the substrates, lignin-derived phenols and aromatic amines are of considerable interest. The laccase reaction mechanism shown in Figure 18[75].

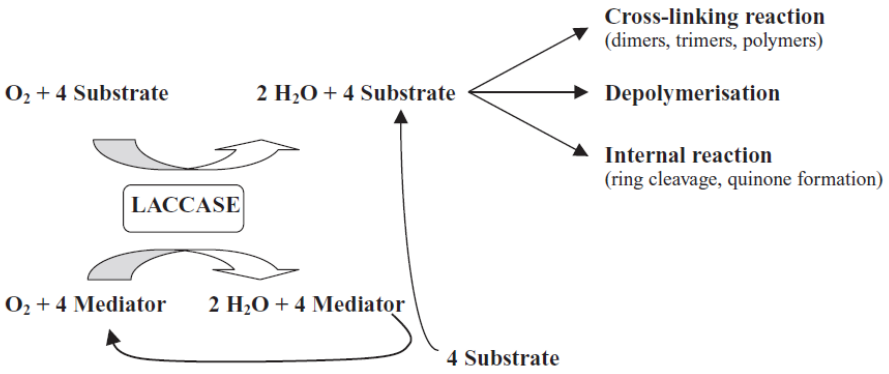


**Figure 18** Laccase mediated oxidation mechanism (*Strong et al.*).[75]

The oxidation of a phenolic compound leads to the production of radicals which can react with each other and form new crosslinking points, as shown in Figure 19.[76]

The enzymatic catalysis used to graft functional molecules onto Lig represents an eco-friendly solution and avoids the use of hazardous chemicals reducing the amount of toxic residuals produced during the synthesis process. For this reason, this type of reaction was considered the best option for the final application the overall system was projected for. Thus, phenolated lignin nanoparticles (PheLig NPs) were obtained according to the protocol proposed by *Morena et al.*[76].

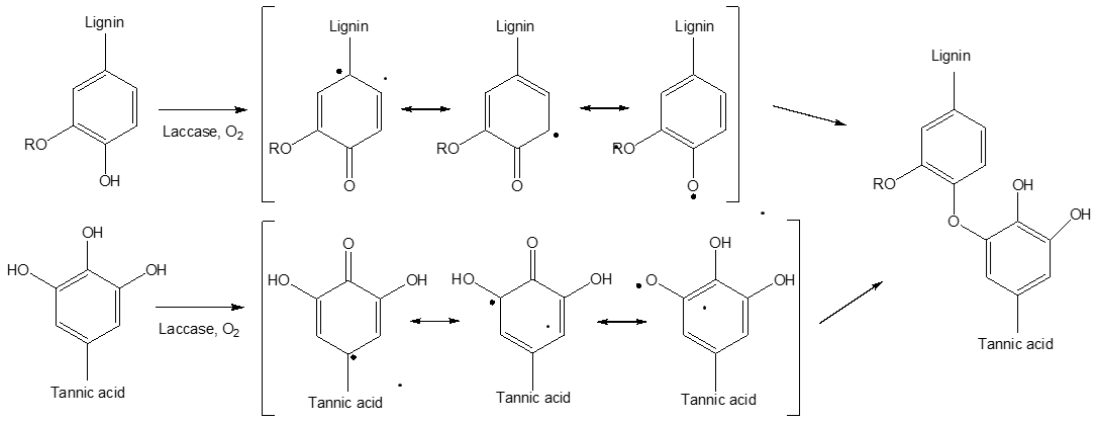


**Figure 19** Laccase mediated oxidation of Lig with TA (*Morena et al.*).[76]

*Diaz-González et al.* demonstrated that syringyl-type phenols methyl syringate and acetosyringone were the most efficient natural enhancer in laccase-mediated oxidation.[77] For this reason, the process required an enzymatic preactivation of Lig using acetosyringone. The second synthesis step was the addiction of TA and the application of ultrasounds (US) to promote simultaneously crosslinking reactions between TA and Lig and the formation of NPs. On the contrary, without the use of US, it is possible to obtain in bulk phenolated Lig, as shown in Figure 20.[76] PheLig NPs showed antibacterial effect against both Gram-positive and Gram-negative bacteria as well as cytotocompatibility.[76] The aim of the thesis work was not only to include such PheLig NPs within the hydrogel to characterise the final system, but also to modify these NPs to achieve an increase in the control of MPO and MMPs levels as well as to increase their bactericidal effects.

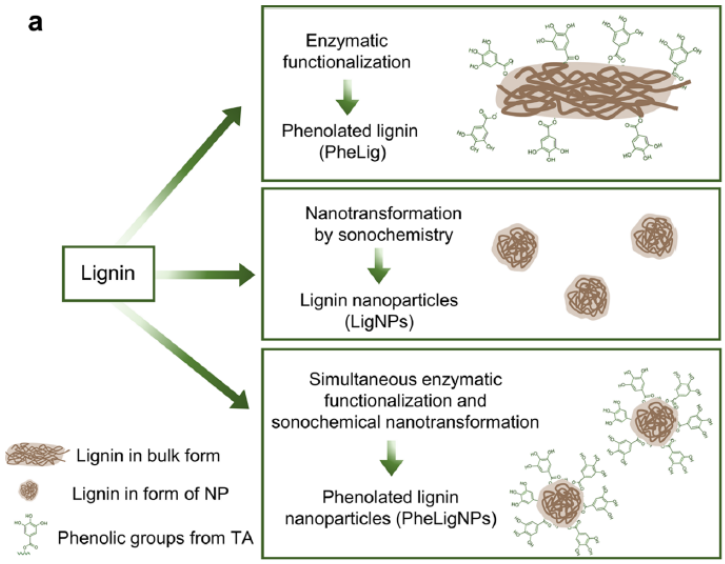


**Figure 20** Schematic representation of all the possible Lig can undergo. The activation of Lig by the mediation of acetosyringone can be used to obtain LigNPs via sonochemistry, PheLig NPs via US in presence of TA or phenolated Lig (PheLig) in bulk without the use of US (*Morena et al.*)[76]

## Hydroxamates as inhibitors of MMPs

Hydroxamic acids are organic compounds composed by the functional group RCONOHR'. In zinc-proteases, the catalytic action of the zinc ion depend on its binding with three protein ligands and a water molecule at the active site of the MMP.[78] hydroxamic acids are good inhibitors of zinc-proteases and of several other MMPs due to their higher affinity with the metal ion in the active site compared to regular substrate.[79] However, their action is not limited to the active site. In the case of MMP-2, beside the catalytic active zinc ion site, hydroxamic groups also interact with two hydrophobic domains called S1' and S2' pocket and with the enzyme backbone through hydrogen bonds.[80] Different peptides can be modified with an hydroxamic acid residue becoming inhibitors for MMPs. The state of art reports different applications of hydroxamic functional groups used to obtain systems designed to manage MMPs activities. *Liang et al*., synthesized hydroxamic acid-methacrylated collagen conjugate to obtain an innovative MMP-modulating hydrogel. The resulting network proved

to induce a percentual of relative fluorescence units (RFU %) of around 13 % and 32 % connected to the activity reduction of respectively MMP-9 and MMP-3.[81] *Giustiniano et al.* synthesized small amino acid derivatives inhibitors containing hydroxamic groups as chelating groups able to interact with the zinc ion in MMPs catalytic site.[82] *Xian-Chao et al*. designed and synthesized a series of L-tyrosine derivatives which exhibited inhibitory effects against MMP-2.[80] For this reason, among all the different hydroxamic acid functional groups, L-tyrosine hydroxamate (LTH) attracted interest. As shown in Figure 21, its chemical structure is composed by an hydroxamic functional group and a phenolic terminal group. LTH was used to decorate PheLig NPs (LTH-PheLig NPs) to enhance the control over MMPs expression thanks to the presence of the hydroxamic residue, allowing a bond between the active site of the MMPs and the NPs. The presence of a phenolic ring was exploited to obtain a laccase-mediated biografting of LTH with Lig and TA. The resulting LTH-PheLig NPs should promote specific interactions between NPs and the active site of MMPs supporting an active targeting.

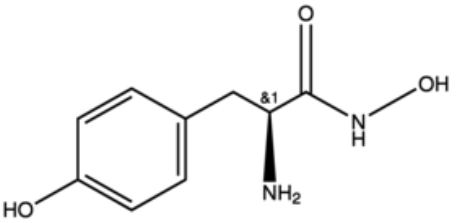


**Figure 21** LTH chemical structure.

## Cobalt nanoparticles

The successive step of the work consisted in the study of strategies to enhance the bactericidal effects of the system. In fact, although the developed PheLig and LTH-PheLig NPs demonstrated to have good inhibitory effects over the % of bacterial growth, they did not show evident and sufficient bactericidal properties. In the optimum to obtain a platform able to treat CWs, one cornerstone was the inclusion into the hydrogel of NPs able to kill bacteria and, thus, to provide a strong defence against the formation of an infected wound. The state of art reports many examples of polyphenols employed as metals reducing agents for different purposes. For example, *Lee et al.* used the cupric reducing antioxidant capacity (CUPRAC) method to reduce Cu(II) in the presence of neocuproine (2,9-dimethyl-1,10-phenanthroline), by tannic acid to obtain a spectrophotometric measure of total polyphenols content in wine.[83]

In this thesis research, Co (II) was investigated as an antimicrobial component in LTH conjugated PheLig (LTH-PheLig) to synthesize innovative cobalt NPs (Co-LTH-PheLig NPs) with antimicrobial properties. The selection of Co (II) was connected to both its reduction standard potential of -0.28 $E^0$/V and its unique properties fitting several requirements of the current study.[84]

Co belongs to the class of transitional metal ions available for biological processes and it is able to bind strongly polarizable donors.[85] It can be found in three metastable phases with different crystallographic structures, hexagonal closed packed, face-centered cubic, and

epsilon phases. Moreover, it is one of the most important ferromagnetic metals.[86] Co NPs have been widely employed in several medical fields, thanks to their biocompatibility as well as their ability to respond to external magnetic fields which, for example, makes them optimal candidates for theragnostic applications.[87] Cobalt is part of vitamin $B_{12}$ and is used in the anaemia treatment as it promotes red blood cells formation. The most interest properties of Co NPs are their antibacterial, anticancer, antioxidant antifungal and enzyme inhibition properties.[86] Co demonstrated to have antimicrobial effects not only when it is coordinated with antibiotics but also when it is complexed with other natural or synthetic materials. *Zahih H. Chohan et al*. synthesized complexes of the antibiotic Kefzol coordinated with Co (II) and studied their antibacterial activity against *S. aureus*, *Escherichia coli*, *P. aeruginosa*, *Klebsiella pneumoniae* and *Proteus mirabilis*, demonstrating an enhancement Kefzol activity against all the tested bacterial strains when it was conjugated with Co(II).[88]

For what concerns the synthesis methods, there are several possible Co NPs preparations which can be classified in physical synthesis, thermal decomposition, hydrothermal and solvothermal synthesis, reduction of Co salts and polyol processes.[87] Co salts reduction and polyol process were considered the most interesting for the final purpose of the developed project. The reduction of cobalt salts is one of the most common preparation methods of metal NPs and it consists on the use of a reducing agent such as hydrogen, alcohol, hydrazine or borohydride mixed with a metal salt in the presence of ligands, polymers, dendrimers, surfactants which act as stabilizing agents to prevent the formation of agglomerations.[87] *Ella L. Dzidziguri et al.* developed Co NPs by cobalt nitrate reduction in alkali solution, followed by hydrogen reduction at high temperature. In that case, ($Co(NO_3)_2 \cdot 6H_2O$) and NaOH were used as precursors for $Co(OH)_2$ NPs synthesis to obtain a chemical precipitation according to the following reaction:

$$Co(NO_3)_2 + 2NaOH \rightarrow Co(OH)_2 + 2NaNO_3$$

Then, the resulting Co hydroxide was washed and dried via lyophilization. The following steps were a calcination process at 400 °C to obtain Co(OH) and a final metallization carried out in a quartz reactor at 220 °C in $H_2$ atmosphere to obtain the final NPs. The synthesized Co NPs are shown in Figure 22.[89]

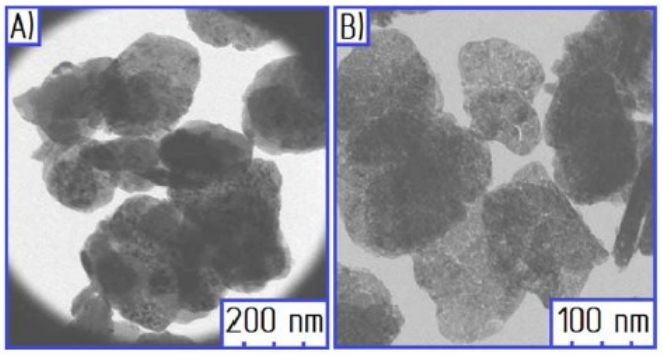


**Figure 22** $Co(OH)_2$ NPs (A) and Co(OH) NPs (B) (*Ella L. Dzidziguri et al*.).[89]

Although the described method efficiently produced Co NPs, the extreme temperature conditions used were considered not compatible to be used with natural polyphenols.

The term “polyol process” was used for the first time in the late eighties by *Fiévet, Lagier* and *Figlarz* and is an eco-friendly method in which the polyol acts as reducing agent in mild conditions (low temperature and normal pressure).[87,90] This process consists in reducing a metal salt by a polyol and was used to reduce both ions of noble metals and more electropositive metals, such as Co, to the zero-valent state.[91] To obtain this, the following steps are required:

1. dissolution of the metal precursor at room temperature or at high temperatures
2. possible formation of intermediates which act as cation reservoirs
3. nucleation from monomer species
4. growth and formation of metal particles.[91]

Depending on the preparation, it is possible to distinguish micrometer-sized and sub-micrometer-sized Co particles. Micrometer-sized particles are the results of a homogeneous nucleation process obtained by adding already formed foreign metallic nuclei during the reaction. On the contrary, sub-micrometer-sized Co particles can be obtained by initiating the formation of foreign nuclei via the addition of a metal precursor, such as a nitrate, at the beginning of the reaction.[91] In addition, according to *Fiévet et al*., the reaction conditions in terms of basicity of medium and temperature strongly influence the Co NPs features and it is possible to shift from metallic cobalt to cobalt carbide.[91] *Feldmann et al*. demonstrated that via polyol processes it is possible to obtain monodispersed oxide nanoparticles, such as CoO and ZnO, with a mean size in the range of 30-300 nm.[92]

The main idea of this work was to exploit the green synthesis of PheLig to obtain a new capping agent reducing Co (II). The final aim was to produce a nanosystem via redox reaction, through a hybrid protocol in which aromatic PheLig was used as reducing agents of cobalt in mild conditions starting from the precursor salt cobalt nitrate. The antioxidant optimal properties connected with the presence of polyphenolic compounds could be associated with the transitional metal Co, allowing the synthesis of a final structure that contemporary:

- possesses antioxidant properties
- allows a control over MMPs and MPO activities
- has strong bactericidal effects on both Gram-positive and Gram-negative bacteria

An example of Co NPs green synthesis starting from plant extracts have been already reported by *Urabe et al.* In that case, Co oxide ($Co_3O_4$) NPs were synthesized starting from plant extract of *Camellia sinensis* and *Apium graveolens.* Fresh extracts were added to a solution of $CoNH_3$ (0.02 M) and stirred at 85 °C for 30 min. Then, sodium hydroxide was added for 60 min at 60 °C to maintain the pH at 14: the synthesis of $Co_3O_4$ NPs could be qualitative seen by observing the colour variation from pink to grey. The mixture was

maintained at room temperature overnight and then centrifuged and dried. A graphical abstract of the process is shown in Figure 23.[93]

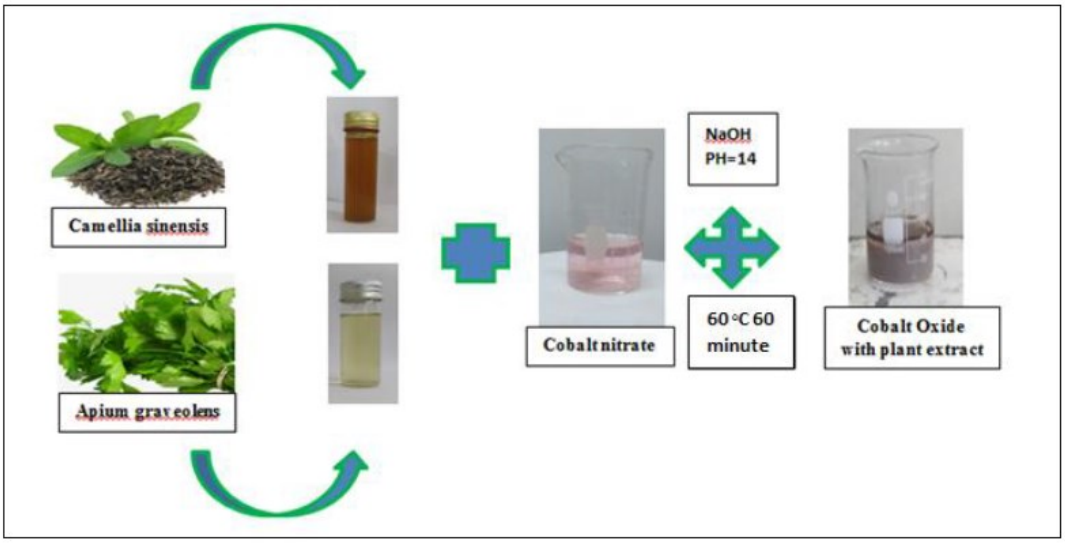


**Figure 23** $Co_3O_4$ NPs synthesis according to *Urabe et al*.[93]

In this work, the protocol developed by *Morena et al.* to synthesize Silver/ Phenolated Lig NPs (AgPL NPs) was adapted. In *Morena et al.* study, phenolated lignin obtained with a laccase-mediated biografting of TA was used as Ag reducing agent to obtain the final AgPL NPs in an US assisted process.[26] The developed NPs were included into polyurethane foams were PheLig acted also as additive reactive agents with isocyanate. The final nanoparticles-embedded polyurethane foams imputed to manage CWs showed *in vitro* bactericidal effects both against *S. aureus* and *P. aeruginosa* depending on the NPs concentration, as shown in Figure 24.[26]

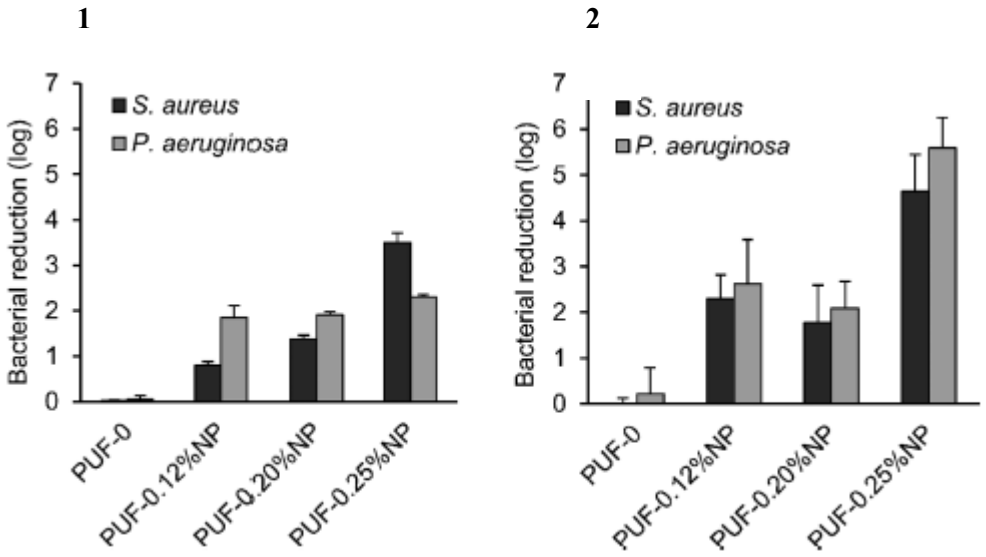


**Figure 24** Bacterial reduction. 1) Release killing test. 2) Contact killing test (*Morena et al.*).[26]

# Materials and methods

## Determination of the enzymatic activity of laccase

Before the phenolation of Lig it was necessary to determine the enzymatic activity of fungal laccase Novozym 51003 from *Myceliophthora thermophila*, starting from a serial dilution of the enzyme (dilution factor from $10^{-4}$ to $10^{-7}$). 10 µl of each dilution were mixed with 215 µl of sodium acetate buffer (pH 5, 0.05 M) and 25 µl of ABTS 10 mM. Finally, the absorbance was measured at 436 nm, at different time points (0, 60, 120, 180, 240, 300, 360, 420, 480 and 540 s), at 25 °C. Starting from the analysis of the absorbance over time, the dilution with the highest absorbance spectra was selected and the values of two successive time points were used to measure the enzymatic activity (U/ml) using the following formula:

$$Activity\ (\frac{U}{ml}) = \frac{\left[\frac{\Delta A_{436}}{\min(test)} - \frac{\Delta A_{436}}{\min(blank)}\right]\ x\ final\ volume\ (ml)\ x\ dilution\ factor\ of\ the\ enzyme}{Millimolar\ extinction\ coefficient\ ABTS\ (mM^{-1}\ cm^{-1}) x\ pathlenght\ (cm) x\ volume\ of\ enzyme\ (ml)}$$

## Synthesis of PheLig NPs and LTH-PheLig NPs

The phenolation of lignin (Protobind 6000) was performed starting from the protocol of *Morena et al.*[76] The lignin was soaked in 50 ml of a sodium acetate buffer (pH 5, 50 mM) with the enzyme laccase.

To promote the beginning of the enzymatic oxidation of Lig, it was necessary to previously dissolve the mediator acetosyringone in the buffer (1.5 mg/ml) at 50 °C under stirring (500 rpm) for 30 min. Laccase (348 U/ml) and Lig (10 mg/ml) were added, and the solution was incubated at 50°C under stirring (250 rpm) for 1 h. Subsequently, TA (10 mg/ml) was added, and the mixture was maintained under stirring (250 rpm) for 5 min at 50 °C. For the synthesis of LTH-PheLig NPs preparation LTH (0.5 mg/ml) was added in the Lig solution contemporary with TA (10 mg/ml) to promote the binding of the phenolic groups of LTH and TA to the phenoxy radicals of enzymatically activated Lig.

To promote the suspension of PheLig NPs and LTH-PheLig NPs, the solution was sonicated (20 kHz, 50 % amplitude) for 2 h at 50 °C (VCX 750 ultrasonic processor, Sonics, USA) and centrifuged at 25000 xg for 15 min at 4°C to remove the residues of TA in the supernatant. Then, PheLig NPs and LTH-PheLig NPs were suspended in 5 ml of milli-Q water and sonicated (Sonics and Materials instrument, Ti-horn, 20 kHz and 50% amplitude) for 1 min at low intensity to disaggregate the NPs.

Finally, the suspension was centrifuged at 500 xg for 5 min to remove the heaviest NPs and the undissolved residuals of Lig. The synthesized PheLig NPs and LTH-PheLig NPs were analysed at Dynamic Light Scattering (DLS) stored at 4 °C. Figure 25 shows a graphical abstract of the synthesis protocol.

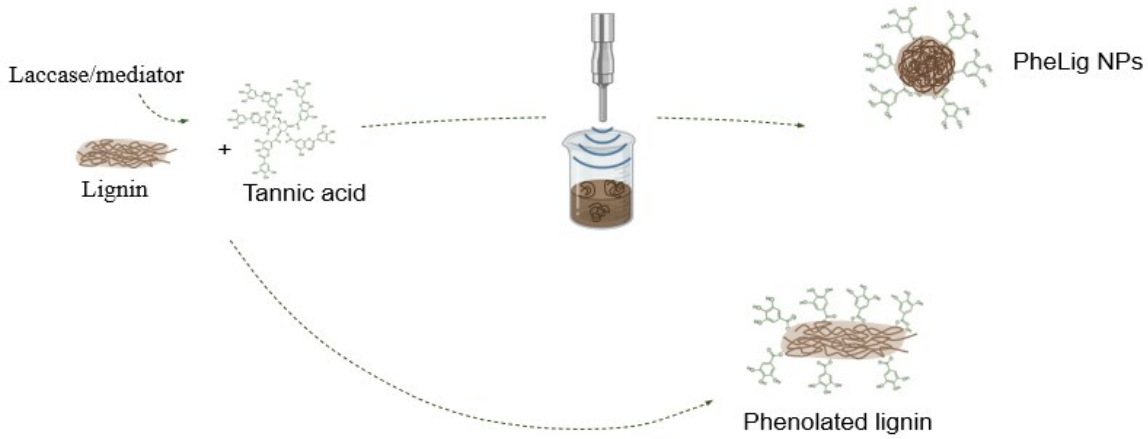


**Figure 25** PheLig NPs synthesis via high-intensity US.

**Synthesis of Co PheLig NPs via stirring**

The pH of the phenolated lignin with L-tyrosine hydroxamate (5 mg/ml) was adjusted to 8 to promote the oxidation of the phenolic groups. Then $Co(NH_3)$ was added, and the solution was maintained under stirring for 2 h at 60 °C to promote the reduction of Co (II) and the formation of the NPs. Table 2 reports all the different combinations of concentration and volumes assessed. The solution was centrifuged at 6000 rpm for 15 min at 4 °C to remove the residuals and

resuspended in 5 ml of Milli-Q water. Finally, the solution was sonicated for 1 min at 50 % of amplitude to promote the suspensions of the NPs.

**Table 2** Different concentrations and volumes of PheLig and $CoNH_3$ used to synthesize via stirring Co-LTH-PheLig NPs.

| PheLig (mg/ml) | $CoNH_3$ (mg/ml) | Volumes % |
|---|---|---|
| 5 | 4 | 50 : 50 |
| 5 | 4 | 60 : 40 |
| 5 | 4 | 40 : 60 |
| 2.5 | 2.5 | 25 : 75 |
| 2.5 | 4 | 40 : 60 |

## Characterization of PheLig NPs and LTH-PheLig NPs

### Final concentration, Dynamic Light Scattering (DLS) and Nanoparticle tracking analysis (NTA)

To measure the concentration of the synthesised NPs, 1 ml of the final solution was freeze dried using a Telstar LyoAlfa 15 freeze-dryer and weighted. The hydrodynamic size, the PDI, and the ξ-potential of PheLig NPs, LTH-PheLig NPs and Co-LTH-PheLig NPs were measured using a Zetasizer Nano Z (Malvern Instrument Inc, U.K.). In the case of Co-LTH-PheLig NPs, the DLS analysis allowed not only a measurement of their average size, PDI and ξ-Potential, but also an optimization of the synthesis protocol offering a comparison between different results deriving from different concentrations and volume ratios of $CoNH_3$ and Lig (Table 2) as well as different tested synthesis methods (US and stirring). NTA is an alternative method to visualize and analyse particles in liquids and to determine the size distribution profile and the concentration of the NPs. The instrument was used to compare the results with the previous ones obtained via DLS.

### Inductively Coupled Plasma Mass Spectrometry (ICP-MS)

ICP-MS is a sensitive analytic technique based on mass spectroscopy combined with plasma used to detect several inorganic substances. In this case, ICP-MS analysis was used to

1. measure the amount of cobalt in the synthesized NPs, by the analysis of the final NPs aqueous solution obtained starting from different synthesis conditions
2. measure the Co uptake respect with the initial amount during the synthesis evaluating the yield % of the process . In this case the analysed solutions were:
   a. Lig (5 mg/ml)/$CoNH_3$ (4 mg/ml) solution before centrifugation at 6000 rpm

b. the supernatant collected after the centrifugation at 6000 rpm the volume of which was measured using a micropipette.
c. the final NPs solution post centrifugation at low intensity and pellet resuspension in 5 ml of Milli-Q water.

The analysis required the NPs destruction to free the Co from the NPs. To do this, it was necessary the NPs were dissolved in nitric acid (20 % wt). The solution was maintained in incubation at 95 °C for around 3 h to allow the destruction of NPs and the consequent cobalt release. Then, the solution was diluted 1:10, filtered with a 0.22 µm filter and analysed using ICP-MS 7800, Agilent Technologies.

**Amino content**

Amino content assay was used to quantify the presence of primary amines in the NPs to confirm the correct conjunction of LTH composed by an amino group in LTH-PheLig NPs. Firstly, a calibration curve was obtained starting from a solution of L-methionine (1 mg/ml) in Milli Q water and preparing multiple dilutions. Then, aqueous solutions (1 mg/ml) of LTH-PheLig NPs and PheLig NPs, as negative control, were prepared. 75 µl of the samples (1 mg/ml) were mixed with 25 µl of 3 mg/ml Fluorescamine reagent dissolved in DMSO, and incubated at room temperature for 3 min. Finally, the fluorescence at $\lambda_{excitation}$= 390 nm and $\lambda_{emission}$ = 470 nm was measured using the spectrophotometer Infinite M200 (Tecan, Austria) to measure the amino groups concentration in each analysed sample.

**FT-IR Analysis**

ATR-FTIR spectroscopy was performed at room temperature on PheLig NPs and LTH-PheLig NPs powder. Spectra resulted from 16 scans with a spectral region ranging between 4400 and 550 $cm^{-1}$ using a PerkingElmer Spectrum 100.

**Phenolic content**

The concentration of phenolic groups was measured spectrophotometrically using the Folin-Ciocalteau phenol reagent**.** Firstly, a calibration curve was obtained starting from a solution of gallic acid (1 mg/ml) in Milli Q water and preparing multiple dilutions. Then, aqueous solutions (1 mg/ml) of Lig, TA, LTH-PheLig in bulk obtained both via a single and via a double step protocol, LTH-PheLig NPs, Co-LTH-PheLig NPs and a negative control were prepared. 20 µl of each solution was mixed with 100 µl of sodium carbonate (20 % wt) and 80 µl of Folin-Ciocalteau (0.2 N) and then analysed at spectrophotometer Infinite M200 (Tecan, Austria) at 765 nm.

**Scanning Electron Microscopy (SEM)**

SEM analysis was used to study the morphology and distribution of PheLig NPs, LTH-PheLig NPs and Co-LTH-PheLig NPs. 10 µl of each sample (1 mg/ml) were placed on holey carbon films on copper grids and observed using JEOL JSM 7100 F microscope. Nanoparticles sizes were measure using the software Image J.

## Cytotoxicity

The cytotoxicity of PheLig NPs, LTH-PheLig NPs and Co-LTH-PheLig NPs was tested toward human fibroblasts (cell line BJ-5tα) and human keratinocytes (cell line HaCaT). The cells were grown in 100 µl of in Dulbecco's Modified Eagle's Medium (DMEM, Sigma-Aldrich) in a 96-well plate (60 000 cells per well) in a controlled humidified atmosphere with a $CO_2$ concentration constant at 5 % and a temperature of 37 °C. After 24 h of cell growth, PheLig NPs (3.59 mg/ml), LTH-PheLig NPs (3.39 mg/ml) and Co-LTH-PheLig NPs (2.35 mg/ml) were incubated with the cells for 24 h in a controlled atmosphere (T= 37 °C and $CO_2$ at 5 %). Then, the NPs were removed from the wells, and the cells were recovered for 24 h in 100 µl of fresh DMEM. The cell viability assessment was performed using the AlamarBlue assay, evaluating the metabolic activity of cells incubated with the NPs. After removing the culture medium, 100 µl of AlamarBlue (10 % v/v) was added and incubated at 37 °C for 3 h. Then, the fluorescence was measured ($\lambda_{excitation}$ = 550 nm, $\lambda_{emission}$ = 590 nm). The maximum percentage of cell viability was calculated using the fluorescence values of a growth control containing only cells and AlamarBlue reagent. In addition, wells containing only AlamarBlue reagent were used as the blank group. The percentage of cell viability was calculated as follows:

$$Cell\ viability\ \% = \frac{(Fluorescence_{sample} - Fluorescence_{\ blank})}{(Fluorescence_{control} - Fluorescence_{\ blank})}\ 100$$

# Antibacterial Tests

### Bacterial Inhibition and Bacterial Reduction

The antibacterial properties of PheLig NPs (3.59 mg/ml), LTH-PheLig NPs (3.39 mg/ml) and Co-LTH-PheLig NPs (2.35 mg/ml) against both *S. aureus* and *P. aeruginosa* was measured. The bacteria were seeded on selective agar plates, *S. aureus* on Braid-Parker (BP) and *P. aeruginosa* on Cetrimides (CE) and incubated at 37 °C overnight. Then, the bacteria were soaked in 5 ml of medium Nutrient Broth (NB) and incubated at 37 °C overnight under shaking. Next, their concentrations were measured in absorbance at 600 nm using the spectrophotometer Infinite M200 (Tecan, Austria) in order to measure the required number of bacteria to obtain an optical density (OD) of 0.01 in 20 ml. 100 µl of each sample were added in triplicate in a multi plate and 50 µl of NB were added in the successive 7 rows of the multi-plate to have multiple dilutions. Finally, 50 µl of culture medium with bacteria were added to all the plates obtaining a total volume of 100 µl in each plate and the multi-well was incubated at 37 °C. A positive and a negative control were also prepared. At 0 h and 24 h of incubation, the solutions were analysed in absorbance at 600 nm to measure the bacterial inhibition over time, using the following formula:

$$\%\ Bacterial\ inhibition = 100 - \frac{(Absorbance_{sample_{600\ nm}} - Absorbance_{blank_{600\ nm}})_{24h} - (Absorbance_{sample_{600\ nm}} - Absorbance_{blank_{600\ nm}})_{0h}}{(Absorbance_{control_{600\ nm}} - Absorbance_{blank_{600\ nm}})_{24h} - (Absorbance_{control_{600\ nm}} - Absorbance_{blank_{600\ nm}})_{0h}} 100$$

The Colony Forming Unit (CFU) counting was used to study the bactericidal effects of PheLig NPs, LTH-PheLig NPs and Co-LTH-PheLig NPs by studying the % of bacteria reduction. The concentrations selected were 1 mg/ml for PheLig NPs and LTH-PheLig NPs and 0.75 mg/ml for Co-LTH-PheLig NP. To perform the test, the bacteria incubated for 24 h with NPs were serially diluted in PBS with a 10 fold dilution factor. Then, 10 µl of each dilution were put in a selective agar. The plates were incubated overnight at 37 °C and the number of colonies formed were counted. Two controls of bacteria without NPs were also prepared. In one case, the bacteria were immediately diluted in PBS and plated in selective agar plates, while in the second case the bacteria were prior incubated for 24 h. The test was performed in triplicate for each combination of sample and bacteria. The bacterial reduction was calculated as follows:

$$\log\ reduction\ \% = \frac{log_{10}(\frac{A}{B})}{log_{10}(A)} 100$$

where A and B are the average number of bacterial colonies before the treatment and after 24 h.

## MPO inhibition assay

The ability of Lig, TA, LTH, LTH-PheLig, PheLig NPs, LTH-PheLig NPs, Co-LTH-PheLig NPs to reduce the activity of MPO was measured as follows. Firstly, the enzymatic activity of MPO was measured starting from a serial dilution (dilution factor from $10^{-4}$ to $10^{-7}$). 32 µl of each dilution were put in contact with 150 µl of water and 96 µl of guaiacol (167 mM). 190 µl of each solution was mixed with 10 µl of $H_2O_2$ (10 mM) and analyzed in absorbance at 476 nm for 10 min every 30 s. Starting from the analysis of the absorbance over time, the dilution with the highest absorbance spectra was selected and the values of two successive time points were used to measure the enzymatic activity (U/ml) using the following formula:

$$Activity\ (\frac{U}{ml}) = \frac{\left[\frac{\Delta A_{476}}{\min(test)} - \frac{\Delta A_{476}}{\min(blank)}\right]\ x\ final\ volume\ (ml)\ x\ dilution\ factor\ of\ the\ enzyme}{Millimolar\ extinction\ coefficient\ H_2O_2\ \ (mM^{-1}\ cm^{-1}) x\ pathlenght\ (cm) x\ volume\ of\ enzyme\ (ml)}$$

After the measurement of the enzymatic activity of MPO, 150 µl of each sample (1 mg/ml) were mixed with 96 µl of guaiacol (167 mM) and 32 µl of MPO (0.25 U/ml) and incubated at 37 °C for 1.5 h. In parallel, for each sample, a negative control incubated without MPO was prepared. Finally, 190 µl of the resulting solution were mixed with 10 µl of $H_2O_2$ (10 mM) and analyzed in absorbance at 476 nm for 10 min every 30 s. $H_2O_2$ in the presence of active free MPO can react with Guaiacol and the reaction speed is correlated with the amount of MPO available. The linear regression of the absorbance over time was calculated. The slope of the obtained curve

corresponded to the reaction speed associated with the active MPO still available A positive control (MPO in water) was prepared to assess the maximum activity of MPO at the concentration of 0.25 U/ml. The % activity of MPO was measured as follows:

$$Activity\ \% = \frac{slope_{s_i}}{slope_{100\%}} 100$$

## MMPs inhibition assay

EnzCheck Gelatinate Collagenase Assay was used and the protocol adapted to study the inhibitory activity of the synthesized NPs over the MMPs. The inhibitory efficiency of the LTH-PheLig NPs and PheLig NPs against collagenase was estimated by measuring the increase in fluorescence intensity of fluorescently labelled gelatin (EnzCheck substrate) cleaved in the presence of collagenase. The assay was also performed over a sample of Lig, TA and LTH as control. Briefly, sample were solubilized at 1 mg/ml in buffer (80 ml 1 M Tris HCl buffer pH 7.1 and 20 ml 1 M $CaCl_2$). Then, 5 µl of 500 U/ml collagenase were added to 500 µl of the sample solutions to obtain a final concentration of 2 U/ml and incubated for 24 h at 37 °C. Then, the samples were centrifugated at 5000 xg for 5 min and the supernatants were collected to be analyzed. 100 µl of each incubated solutions were transferred in a 96-well microplate and mixed with 80 µl of the reagent buffer and 20 µl of DQ Gelatin (50 µg/ml). The fluorescence was measured at 493/528 nm. All measurements were performed in triplicate, repeating the measurement at-different time point and the results were expressed as collagenase residual activity compared to the collagenase control solution.

# Results

In this work, three different nanoparticles were synthetised with the aim of obtaining systems acting in the

- prevention against possible bacterial contaminations, avoiding the development of bacterial resistance
- control of MMPs and MPO expression levels
- bacterial killing to avoid eventual bacterial infections

The first nanosystem, PheLig NPs was synthesized starting from the work of *Morena et al.* to obtain a solution able to offer enhanced antioxidant and antibacterial effects without passing through the use of antibiotics and avoiding the appearance of bacteria resistance.[76] The selection was oriented towards a polyphenolic NP: the presence of the phenolic groups should promote multiple non-specific interactions between the surface of NPs and bacteria, hampering the development of bacterial resistance. The inclusion of PheLig NPs within a biocompatible hydrogel in contact with a clean wound bed should prevent the development of bacterial contaminations at the wound site, avoiding the formation of an infected CW.

The second type of NP, LTH-PheLig NP, was studied with the aim to have a better control over the MMPs and TIMPs levels, the dysregulation of which represents one of the main factors involved in the development of chronicity at molecular level. The selected strategy was the inclusion onto the NP of a moiety that could act as a substitute MMPs inhibitor, fighting their overexpression that lead to an uninterrupted process of ECM degradation and, thus, to the persistence of the inflammatory phase.

Finally, the last nanosystem, Co-LTH-PheLig NP, was developed to enhance the bactericidal effects of the final systems: the presence of a transitional metal ion was considered the best option to enhance the efficacy of the system in the case of existing bacterial infections to reduce and consequently eliminate the pathogens.

A graphical abstract of the conducted processes of synthesis is shown in Figure 26

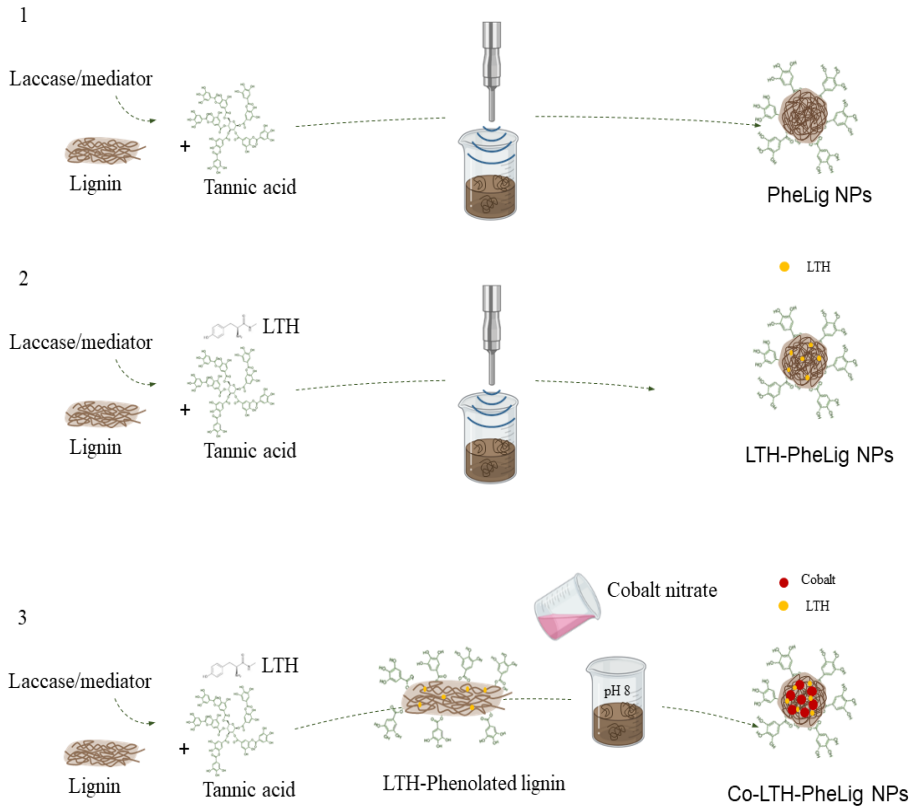


**Figure 26** Graphical abstract of the three synthesis procedures. 1) Synthesis of PheLig NPs 2) Synthesis of LTH-PheLig NPs 3) Synthesis of Co-LTH-PheLig NPs preceded by the enzymatic phenolation of Lig with TA and LTH.

The first part of this chapter focuses to the discussion of the main NPs characterizations in terms of laccase activity, average size, colloidal stability, phenolic content, amino content and metallic

content, while a second section is dedicated to a comparison between the main chemical and morphological features of the different NPs. Finally, in the last part of the chapter, the analysis and comparison of the properties of the different NPs in terms of biocompatibility, antibacterial properties and inhibition ability of MMPs and MPO, is discussed.

## Laccase activity test

Before performing the phenolation of Lig, it was necessary to determine the enzymatic activity of laccase. The measured enzymatic activity of laccase was 348.3 ± 169.4 U/ml. This measurement was carried out once, before the synthesis took place. Nevertheless, the assay should be repeated periodically as the enzyme could reduce its enzymatic activity with time and thus, the required laccase volume for the NPs synthesis could change.

## Characterization of PheLig NPs and LTH-PheLig NPs

### Dynamic Light Scattering (DLS) and Scanning Electron Microscopy (SEM)

DLS analysis was used to measure hydrodynamic size, PDI and ξ-potential of PheLig NPs and LTH-PheLig NPs. As summarized in Table 3, PheLig NPs presented an average size of 269 nm, a PDI of 0.18 and a ξ-potential of -29.0 mV, while LTH-PheLig NPs showed an average size of 294 nm with a PDI of 0.29 and a ξ-potential of -30.9 mV.

**Table 3** DLS results of PheLig NPs and LTH-PheLig NPs.

| Sample | Average hydrodynamic diameter [nm] | PDI | ξ-potential [mV] |
|---|---|---|---|
| PheLig NPs | 269 | 0.18 | -29.0 |
| LTH-PheLig NPs | 294 | 0.29 | -30.9 |

The increase in the average size of the LTH-PheLig NPs compared to the PheLig NPs could be related with the conjugation of LTH to the NPs. On the contrary, this conjugation does not seem affecting the colloidal stability of the NPs, as demonstrated by the similar value of ξ-potential. From the SEM analysis emerged that the mean size calculated for PheLig NPs and LTH-PheLig NPs was respectively 216 ± 9.5 nm and 219 ± 12.7 nm, as shown in Figure 27. These results are in accordance with what obtained at the DLS: although the size of the NPs obtained via DLS seems to be higher than the corresponding results obtained via SEM analysis, it is important to consider that the DLS measurement offers a calculation of the average hydrodynamic diameter, rather than the effective size of the NPs. In addition, the difference between the size of PheLig NPs and LTH-PheLig NPs is less evident in the SEM analysis results: this could be a further

demonstration of the exposition of amino groups by LTH-PheLig NPs that increases the hydrophilicity of the NPs and thus their hydrodynamic average size.

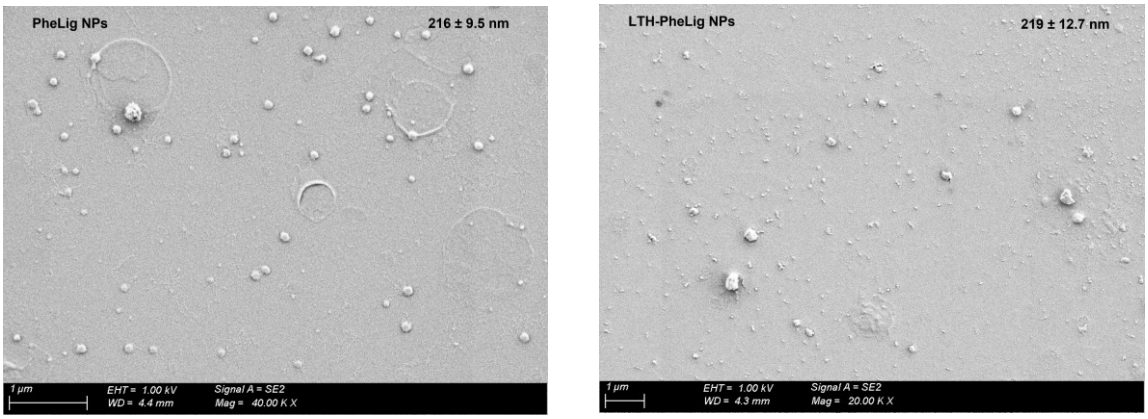


**Figure 27** SEM analysis results. 1) PheLig NPs 2) LTH-PheLig NPs. The NPs have a circular shape and similar size but the monodispersion is slightly reduced by the presence of LTH.

However, the images resolution obtained was considered not sufficiently high to obtain precise results. A better resolution could be obtained using a Transmission Electron Microscope (TEM).

**FT-IR Analysis**

The FT-IR Analysis was used to confirm the PheLig NPs synthesis as well as the presence of the hydroxamic group in LTH-PheLig NPs. *Gilca et al*. studied the ATR-FTIR spectra of Lig NPs obtained via US irradiation reporting the presence of:

- a broad O-H band at around 3400 $cm^{-1}$
- C-H stretching of methyl or methylene groups around 2900 $cm^{-1}$
- C=O stretching at around 1700 $cm^{-1}$
- aromatic skeletal vibration around 1600 $cm^{-1}$
- stretching of aromatic skeletal around 1510 $cm^{-1}$
- C-H skeletal vibration around 1460 $cm^{-1}$
- C-H vibration of methyl group around 1420 $cm^{-1}$
- syringyl units vibration around 1330 $cm^{-1}$
- OH stretching of primary alcohol 1030 $cm^{-1}$
- a peak at around 1120 $cm^{-1}$ associated to the presence of aromatic units.[94]

The presence of phenolic C-O from TA can be seen around 1200 $cm^{-1}$, according to *Chowdhury et al.*[95] Finally, according with *Jian Fui et al.* the presence of the hydroxamic acid is related with:

- a C=O stretching peak shifting from 1727 $cm^{-1}$ to lower wavelengths, indicating the conversion of ester groups into hydroxamic acids
- a peak at 1648 $cm^{-1}$ connected with the N-H bending mode
- a broad band at 3119 $cm^{-1}$ corresponding with the overlap of O-H and N-H stretching mode.[96]

As shown in Figure 28, PheLig NPs and LTH-PheLig NPs FT-IR spectra confirm the results of *Gilda et al.* and *Chowdhury et al.* [94,95]

In the specific:

- a OH broad band was found at 3360 $cm^{-1}$
- C-H stretching of methyl or methylene groups was found at 2919 $cm^{-1}$
- aromatic skeletal vibration was found at 1600 $cm^{-1}$
- stretching of aromatic skeletal was found at 1510 $cm^{-1}$
- C-H skeletal vibration was found at 1454 $cm^{-1}$
- C-H vibration of methyl group was found at 1423 $cm^{-1}$
- syringyl unit vibration was found at 1331 $cm^{-1}$
- OH stretching of primary alcohol was found at 1032 cm
- a peak associated with the presence of aromatic units was found at 1117 $cm^{-1}$
- C-O phenolic groups associated with the presence of TA was found at 1210 $cm^{-1}$

**Amino content**

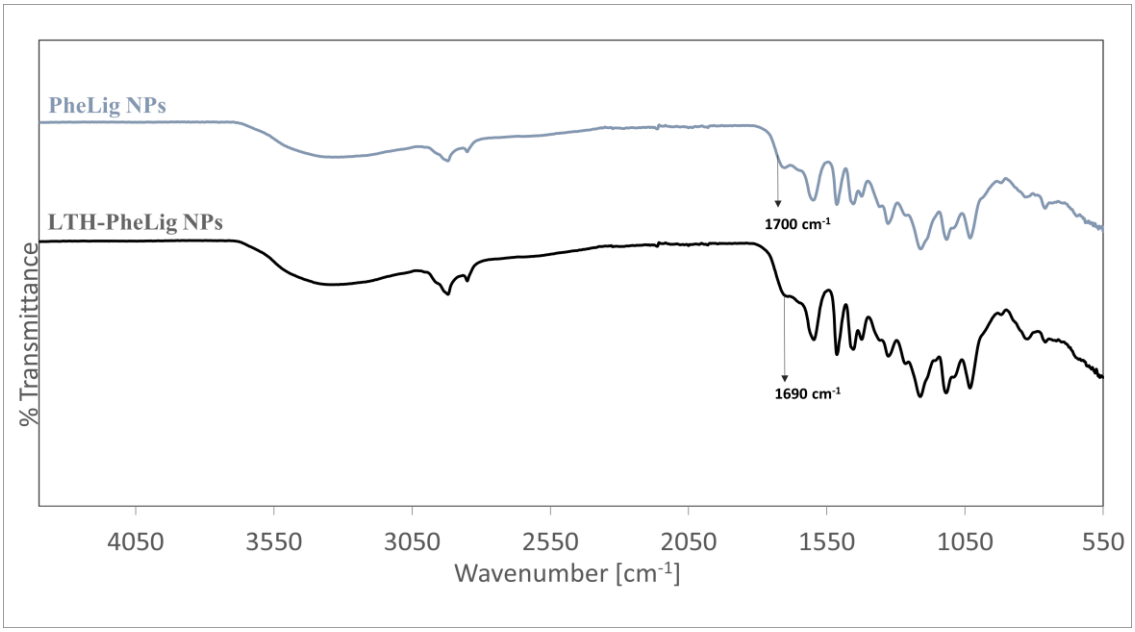


**Figure 28** FT-IR spectra of PheLig NPs and LTH-PheLig NPs: the C=O stretching peak shifted from 1700 $cm^{-1}$ to 1690 $cm^{-1}$, confirming the presence of LTH.

The results of the amino content assay performed on LTH-PheLig NPs were used to evaluate and quantify the presence of LTH in PheLig NPs. The concentration of the amino groups measured was 0.12 ± 0.01 $NH_2$/mg even if the results were considerable untrustworthy since the detected fluorescence of PheLig NPs used as negative control resulted negative. Nevertheless, the outcome can be considerate as a qualitative confirmation of LTH binding.

**Phenolic content**

The phenolic content was measured not only to know the amount of phenolic groups in the synthesized NPs, but also to confirm the results of the amino content assay. Table 4 shows the results: the detected phenolic concentration of LTH-PheLig NPs is slightly smaller than that of PheLig NPs. This reduction is not statistically significant; however, it could be related to the binding of LTH that decreased the number of free phenolic groups of PheLig NPs.

**Table 4** Phenolic content of PheLig NPs and LTH-PheLig NPs.

| Sample | Phenolic content [µmol/ml] |
|---|---|
| **PheLig NPs** | 0.30 ± 0.01 |
| **LTH-PheLig NPs** | 0.28± 0.02 |

## Characterization of Co-LTH-PheLig NPs

**DLS, NTA and SEM analysis**

For obtaining Co-LTH-PheLig NPs, different protocols were tested. The results of this optimization are summarized in Table 5 along with the DLS analysis results. Firstly, the hydrodynamic radius obtained for all conditions tested are minor than that of PheLig NPs and LTH-PheLig NPs, in accordance with the results obtained by *Morena et al.*[26,76] One possible explanation of the dimensional reduction of Co-LTH-PheLig NPs could be connected to the redox reaction used in the synthesis process that allows the formation of more stable interactions between Lig and Co, increasing the compactness of the NPs and reducing their size. Secondly, the size of the NPs synthesized by stirring is slightly higher than the average size of the NPs obtained by sonication. However, the PDI suggests that via stirring it is possible to obtain a better monodispersion. The synthesis via stirring was selected for further optimization since it offered similar size and a better PDI with a preparation requiring a lower intensity energy. By comparing the results deriving from different combinations of LTH-PheLig/$CoNH_3$ used to prepare Co-LTH-PheLig NPs, it is possible to note that a decrease in the concentration and in the volume of Lig solution used corresponds to an increase of ξ-potential from negative to positive values. This could be due to the saturation of the Lig. In this case it could be possible to have residual ionic Co (II) in the solution that could increase the NPs cytotoxicity. Therefore, a negative ξ-potential is preferred.

**Table 5** DLS results for Co-LTH- PheLig NPs obtained using different protocols of synthesis. The best balance between average size, monodispersion and colloidal stability comes from the synthesis obtained starting from a volume ration % of Lig : Co equal to 60 % : 40 %.

| Method | LTH-PheLig [mg/ml) | $Co(NH_3)$ (mg/ml) | Volumes % Lig : Co | Average size (nm) | PDI | ξ-potential (mV) |
|---|---|---|---|---|---|---|
| stirring | 5 | 4 | 50:50 | 146 | 0.299 | - 32.9 |
| stirring | 5 | 4 | 60:40 | 209 | 0.301 | - 22.5 |
| stirring | 5 | 4 | 40:60 | 233 | 0.284 | - 24.0 |
| stirring | 2.5 | 2.5 | 25:75 | 146 | 0.331 | + 22.3 |
| stirring | 2.5 | 4 | 40:60 | 150 | 0.182 | + 18.2 |
| US | 5 | 4 | 60:40 | 138 | 0.370 | -24.9 |

The results were further confirmed by the SEM analysis results shown in Figure 29, even if also in this case the resolution of the resulting images were considered not sufficiently high to obtain significantly quantitative results.

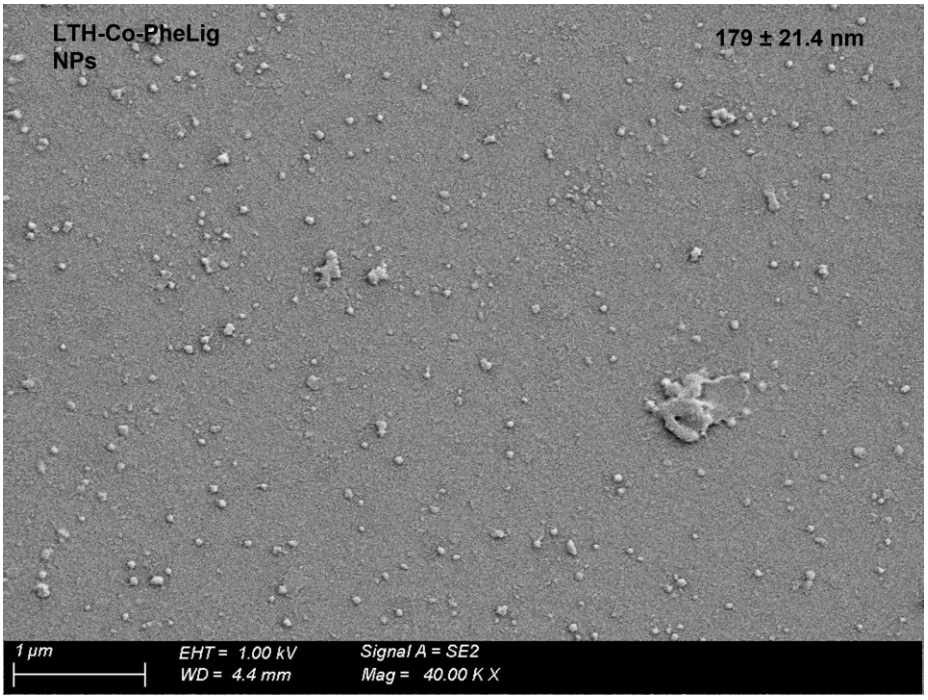


**Figure 29** SEM analysis results of Co-LTH-PheLig NPs. The size of the NPs is reduced by the presence of Co.

The Co-LTH-PheLig NPs with negative ξ-potential were also analysed with the NTA to confirm the results obtained with DLS and measure the particle concentration in the solution. The results are shown in Figure 30 and Table 6.

**Table 6** NTA results: the concentration is compared with that one obtained via freeze-drying (last column).

| **Sample** | **Volume % Lig:$CoNH_3$** | **NPs/ml** | **Mean Size ± Standard error (nm)** | **mg/ml** |
|---|---|---|---|---|
| Co-LTH-PheLig NPs (stirring) | 60:40 | 1,92E+11± 1.44E+10 | 143.9± 1.5 | 3,9 |
| Co-LTH-PheLig NPs (stirring) | 40:60 | 2,10E+11± 8.38E+09 | 96.3 ± 2.1 | 3,7 |
| Co-LTH-PheLig NPs (stirring) | 50:50 | 3,91E+10± 1.20E+10 | 95.8 ± 2.4 | 5,8 |
| Co-LTH-PheLig NPs (US) | 60:40 | 1,78E+11± 1.05 E+11 | 89.9 ± 0.8 | 4,7 |

The size distribution profiles confirmed that the NPS are monodisperse in the case of stirring preparation. Indeed, Co-LTH-PheLig NPs prepared via US shows two different peaks at 60 nm and 95 nm (Figure 30.1), while all the other analysed systems, corresponding to LTH-Co PheLig NPs obtained via stirring, presented a single peak (Figure 30.2-4).
The NPs/ml was similar in every analyzed sample except for Co-LTH-PheLig NPs obtained via stirring starting from a volume ratio of Lig:$CoNH_3$ of 50 % : 50 %.

Giving all these results, the combination LTH-PheLig/Co($NH_3$) 60 % : 40 % with a concentration of 5 mg/ml and 4 mg/ml respectively, was considered the more promising option to obtain a good compromise in terms of size, PDI and ξ-potential. To further confirm this choice, ICP-MS analysis was performed the results of which will be examined in the next paragraph.

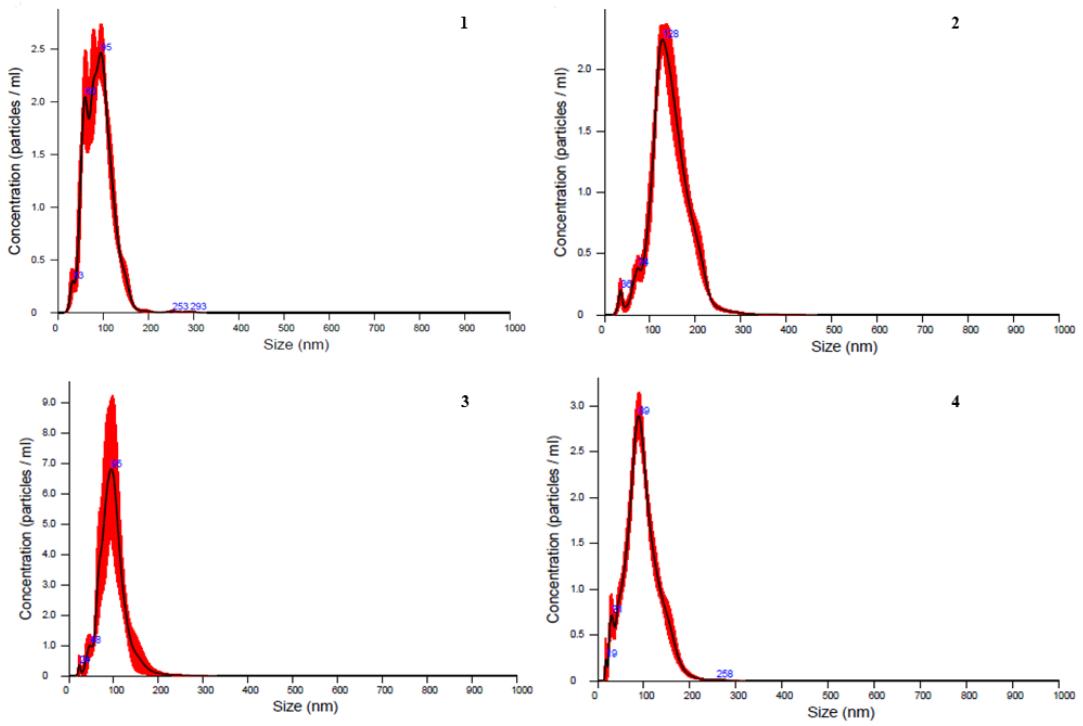


**Figure 30** Size distribution profile of Co-LTH-PheLig NPs: (1) NPs obtained via US; (2) NPs obtained via stirring via a volume ration of 40 % : 60 % of Lig/$CoNH_3$; (3) NPs obtained via stirring via a volume ration of 50 % : 50 % of Lig/$CoNH_3$; (4) NPs obtained via stirring via a volume ration of 60 % : 40 % of Lig/$CoNH_3$; The concentration of Lig and $CoNH_3$ was respectively 5 mg/ml and 4 mg/ml.

**ICP-MS results**

The ICP-MS analysis was used to evaluate the % of Co present in the NPs and the yield of internalization. As shown in Figure 31, the highest concentration of Co was measured in Co-LTH-PheLig NPs obtained via stirring starting from a volume ratio of 60 % : 40 % of Lig/Co $NH_3$. This Co-LTH-PheLig NPs synthesis protocol not only offer the best compromise in terms of size, PDI and colloidal stability, but also improve the % of Co in the NP. In this case, around 34 % of the NP is composed by Co, while the remaining 66 % is composed by LTH-PheLig. In addition, it is noticeable how the % of Co was strongly reduced starting from the same amount of Lig and $CoNH_3$ but using US.

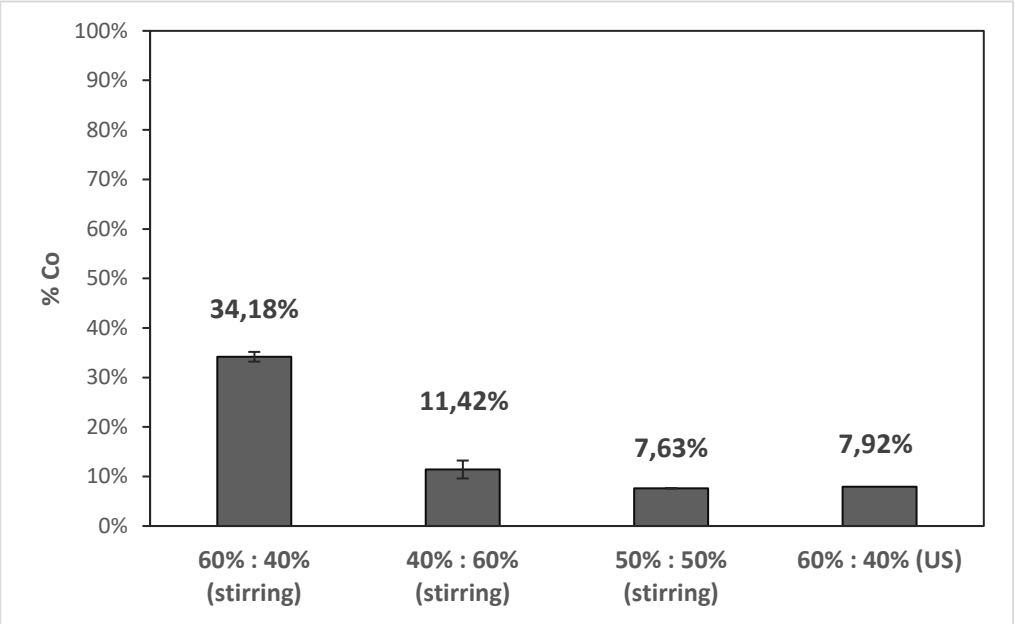


**Figure 31** % of Co in the NPs. The highest concentration was measured in Co-LTH-PheLig NPs prepared via stirring starting from a volume ratio of Lig/$CoNH_3$ of 60 % :40 %.

Furthermore, the ICP-MS analysis was used to evaluate the yield of Co uptake during the synthesis compared to the amount of Co contained in the initial solution of LTH-PheLig (5 mg/ml) and Co nitrate (4 mg/ml), in a volume ratio of 60 % : 40 %. After the first centrifugation (at 6000 rpm) used to eliminate unreacted compounds, 83.62 % of the Co initially used was present in the sample showing that a high amount of Co remained inside the NPs during the first purification step. However, the % of Co decreased to 37.52 % after the second centrifugation step used to eliminate the aggregates and the largest and unreacted compounds. Although the purification process results in a strong reduction of the Co uptake yield, the centrifugation at low intensity was considered fundamental to obtain monodispersed NPs able to guarantee the unique properties NPs can offer only at the nanoscale. Moreover, since metal ions are heavier and precipitate better through centrifugation, the heaviest compound eliminated with the second centrifuge could be Co aggregates, that would have higher toxicity.

**Phenolic content**

The phenolic content assay was used to analyse both the lignin-based material conjugated with TA and LTH (Figure 32) and the NPs obtained from it (Figure 33). The test allowed to verify the conjugation of TA through the increase in phenolic content and also to observe indirectly the phenol consumption due to LTH binding and Co reduction. In Figure 32, the concentration of the phenolic groups is the highest in TA and the lowest in Lig raw materials. This is expected since the number of phenolic groups in TA is significantly higher. Moreover, the phenolation of Lig was confirmed by the increase of the LTH-PheLig phenolic content compared to Lig alone. Figure

32 also shows a comparison between the phenolic content of LTH-PheLig obtained through a single step process (LTH-PheLig$_{SS}$) or through a two-step process (LTH-PheLig$_{DS}$). The phenolic content of LTH-PheLig$_{SS}$ is slightly smaller than the one measured in LTH-PheLig$_{DS}$. Although, the difference is not statistically significant, this reduction could be related to a higher amount of LTH binding in the PheLig that decreases the number of free phenolic groups.

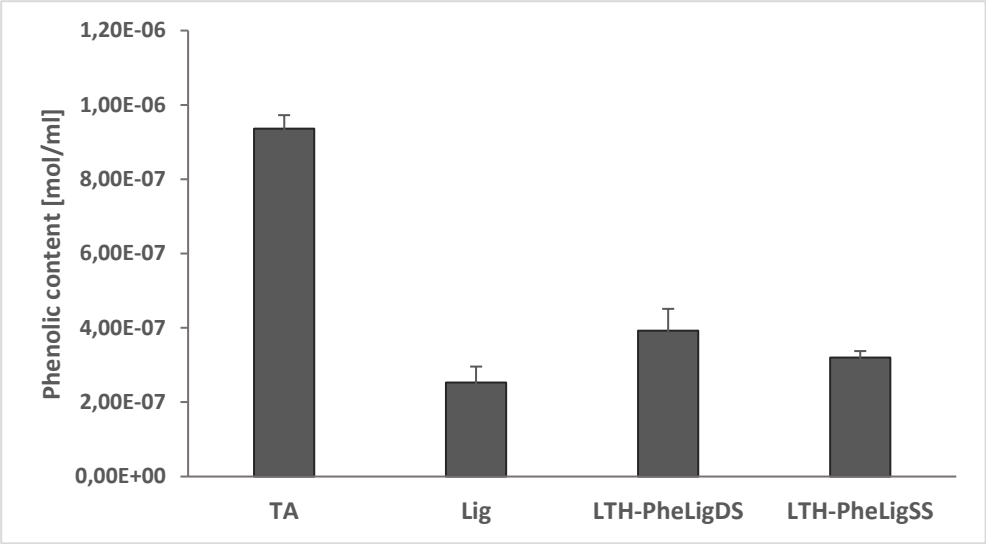


**Figure 32** Phenolic content results: the phenolic content of PheLig is intermediate between the phenolic content of Lig and the phenolic content of TA.

However, this assumption should be verified by evaluating the amino content of the systems. LTH-PheLig$_{SS}$ preparation offered at the same time a comparable phenolic content respect with LTH-PheLig$_{DS}$ with a faster procedure of preparation and may guarantee a better efficacy in the LTH conjugation. Thus, the single step protocol was considered the best option to obtain the LTH-PheLig material to be used for Co-LTH-PheLig NPs synthesis.
The measured phenolic content of Co-LTH-PheLig NPs was 0.12 ± 0.01 μmol/ml.

# Characteristics of PheLig NPs, LTH-PheLig NPs and Co-LTH-PheLig NPs

PheLig NPs and LTH-PheLig NPs has an average size bigger than the Co-LTH-PheLig NPs. This could be the consequence of the different synthesis method: the redox reaction used to reduce Co (II) could create a dependency of the final average dimension to the reducing capacity of LTH-PheLig towards the Co metal ions. In every analysis emerged a decrease in the average size obtained measured via SEM analysis, confirming the hypothesis that the hydrodynamic diameter of the NPs obtained from the DLS is enlarged by the presence of water molecules surrounding the NPs. Comparing the phenolic content of the different NPs it is possible to note that the

phenolic content of Co-LTH-PheLig NPs strongly decrease, testifying a correct reduction of Co (II) after the oxidation of the phenolic groups in LTH-PheLig, as shown in Figure 33.

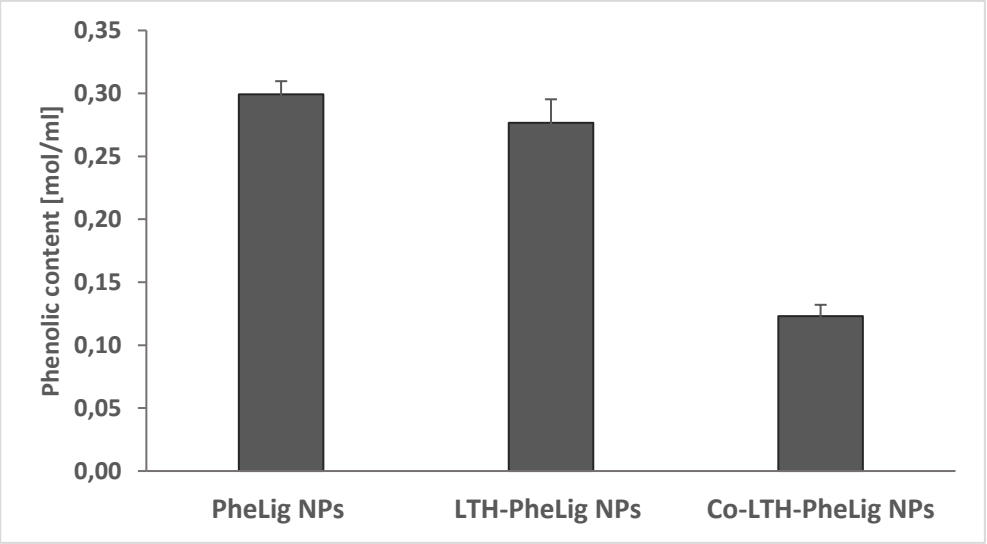


**Figure 33** Phenolic content of PheLig NPs, LTH-PheLig NPs and Co-LTH-PheLig NPs. The strong reduction in the Co-LTH-PheLig NPs phenolic content could be due to Co (II) reduction by the activated phenolic groups of LTH-PheLig.

The actual amino content of NPs remains to be verified, as does a more specific analysis of the morphology of NPs to better understand the molecular arrangement within the different nanosystems.

# Properties of PheLig NPs, LTH-PheLig NPs and Co-LTH-PheLig NPs

## Cytotoxicity

Viability tests were conducted on human fibroblasts (BJ-5tα) and keratinocytes (HaCaT) to assess the cytotoxicity of LTH-PheLig NPs and Co-LTH-PheLig NPs. The results are shown in Figures 34, 35 and 36. As shown in Figure 34, the viability % of fibroblasts in contact with PheLig NPs reached the 100 % at 1.80 mg/ml. Differently, keratinocytes were more sensitive to the NPs presence and showed a lower viability for concentration lower than 1.80 mg/ml (64.37 ± 3.73 %). The unexpected trend of HaCaT cell viability, showing increased cytotoxicity at the lowest NPs concentration, suggests that the test should be repeated to be confirmed. Moreover, the trend diverges from the one obtained for LTH-PheLig NPs (Figure 35). In this case, both BJ-5tα and HaCaT, showed a viability % greater than 80 % at concentrations 1.70 mg/ml and lower, without having increased toxicity at the lowest concentration tested.

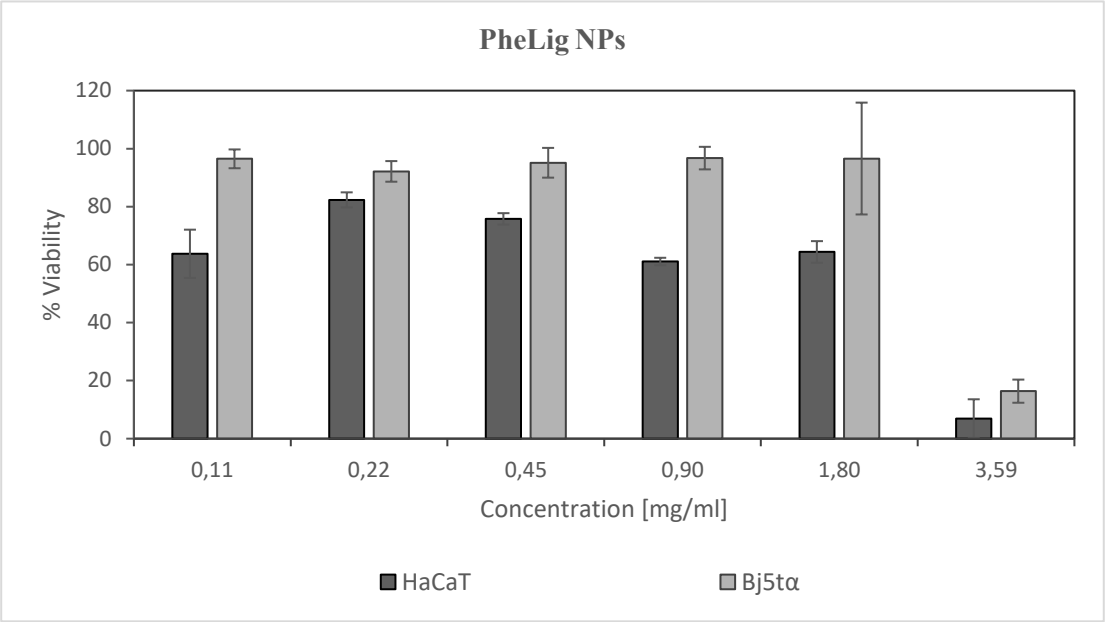


**Figure 34** Cellular viability of keratinocytes and fibroblasts in contact with PheLig NPs. At a concentration of 0,45 mg/ml both BJ-5tα and HaCaT showed a viability % higher than 80 %., The viability of BJ-5tα was around 100 % at a concentration of 1,80 mg/ml.

Co-LTH-PheLig NPs showed a good biocompatibility in contact with BJ-5tα at 1.18 mg/ml at which the viability % measured was around 100 %.

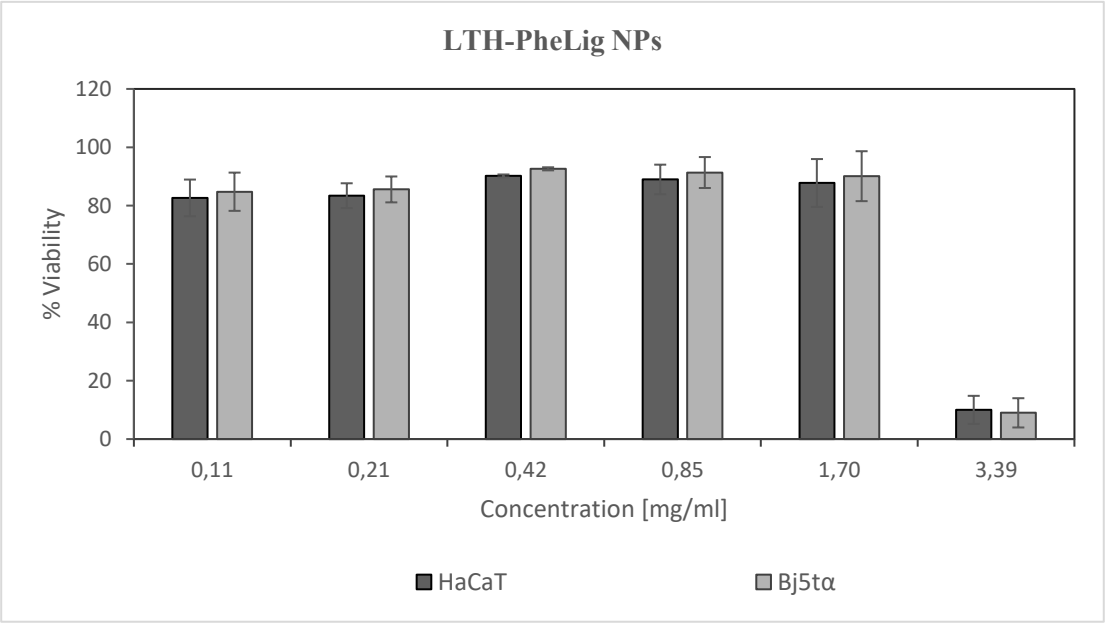


**Figure 35** Cellular viability of keratinocytes and fibroblast in contact with LTH-PheLig NPs .At 1.70 mg/ml the viability % was higher than 80 % for both HaCaT and BJ-5tα.

The biocompatibility was lower in the case of HaCaT cell line: at 1.18 mg/ml the viability % was lower than 40 % (Figure 36) and it was possible to observe biocompatibility only at lower concentration.

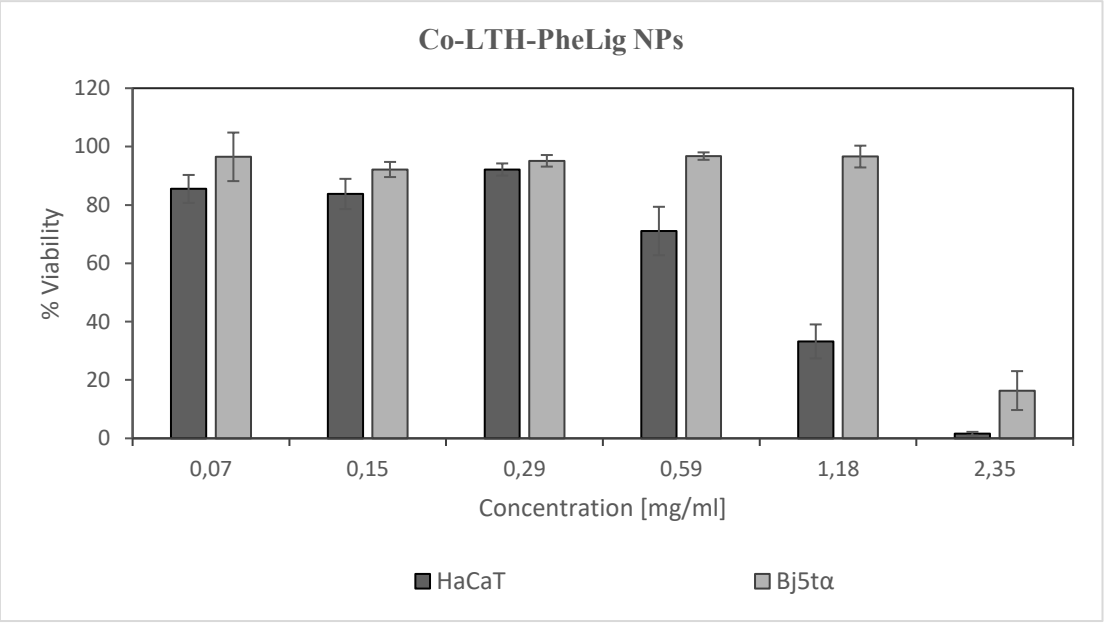


**Figure 36** In presence of Co, the cellular viability of HaCaT was lower. At 0.59 mg/ml around the 71 % of HaCaT was alive.

Overall, the inclusion of a metallic moiety negatively influences the biocompatibility of the NPs, according to predictions. Nevertheless, the results are promising.
In the next section the antibacterial capacity of the NPs is tested to select a concentration showing biocompatibility and that could be used to inhibit bacteria growth.

## Antibacterial Tests: Bacterial Inhibition and Colony Forming Units (CFU)

The antibacterial activity of the different NPs was tested through MIC assay and CFU against two bacterial species common in CWs, *S. aureus* and *P. aeruginosa*. The first test was performed to evaluate the ability of the NPs to prevent bacterial growth. Figures 37 and 38 show the bacterial inhibition % of LTH-PheLig NPs and Co-LTH-PheLig NPsrespectively, indicating the values of

minimum inhibitory concentration (MIC) at which the NPs completely inhibit the bacterial growth.

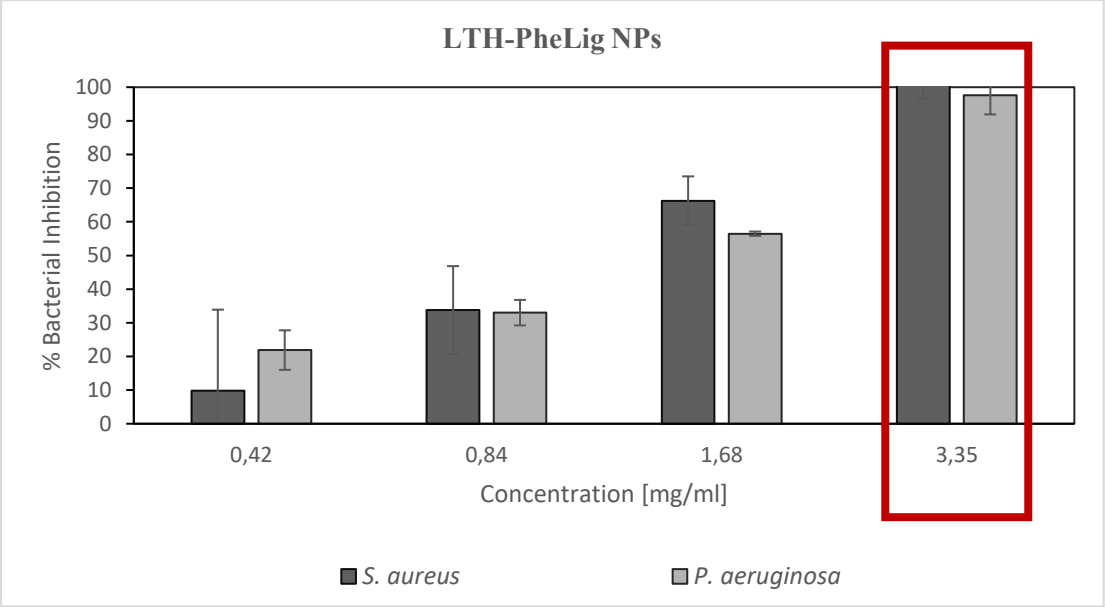


**Figure 37** Bacterial inhibition of *S. aureus* and *P. aeruginosa* against different concentration of LTH-PheLig NPs. The MIC is at a concentration of 3.35 mg/ml.

Both the nanosystems show better inhibitory capacities against Gram-positive *S. aureus*. The inclusion of a metal strongly increases the ability of the NPs to prevent new contaminations. Indeed, the MIC of Co-LTH-PheLig NPs is around 1.18 mg/ml against *S. aureus* and around 2.35 mg/ml for *P. aeruginosa*, while in the case of LTH-PheLig NPs the MIC was around 3.35 mg/ml for both *S. aureus* and *P. aeruginosa.* Results of bacterial inhibition of PheLig NPs remains to be verified.

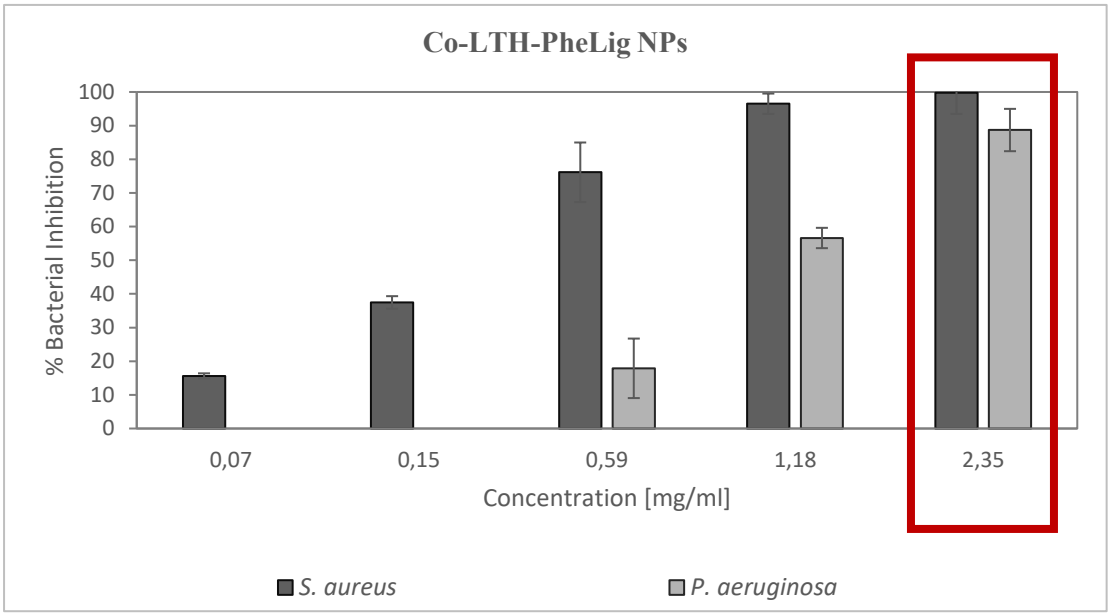


**Figure 38** Bacterial inhibition of *S. aureus* and *P. aeruginosa* against different concentration of Co-LTH-PheLig NPs. The red square indicates the concentration at which the NPs shows the complete inhibition of both *S.aureus* and *P. aeruginosa*. The MIC is at a concentration of 1.18 mg/ml for *S. aureus*, while at the same concentration the inhibition of *P. aeruginosa* reaches almost the 70 %. The MIC for *P. aeruginosa* is at 2.35 mg/ml.

The number of survived bacteria was counted not only to evaluate the bactericidal effects of the NPs, but also to quantify the inhibitory capacities of the synthesized NPs. The initial concentrations of PheLig NPs (1 mg/ml), LTH-PheLig NPs (1 mg/ml) and Co-LTH-PheLig NPs (0.75 mg/ml) were selected starting from the results obtained from the cytotoxicity tests, to ensure a viability greater than 50 %.

Figure 39 reports the qualitative results of CFU test: after 24 h of incubation on the selective agar plate, Co-LTH-PheLig NPs had a full killing effect against *S. aureus* and a strong bactericidal effect against *P. aeruginosa* at concentrations allowing a cellular viability of 100 % for fibroblast and of around 70 % for keratinocytes.

The counting of the bacterial colonies allowed a verification of the bacterial growth inhibition.

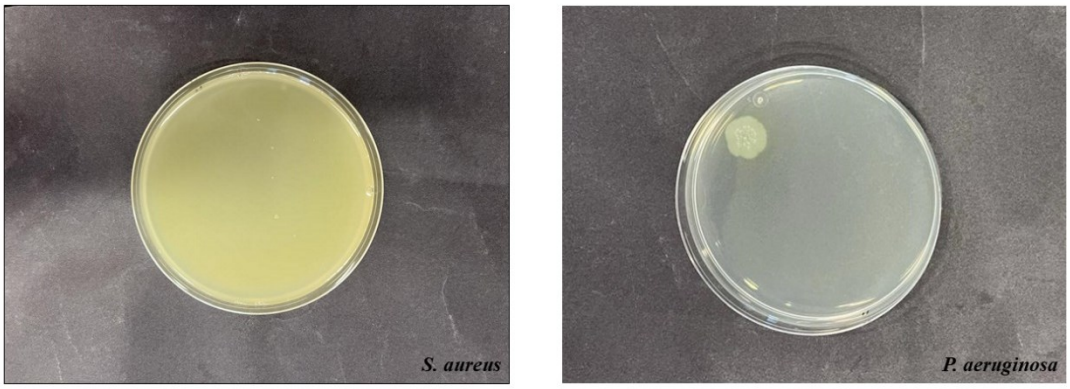


**Figure 39** Qualitative results of the CFU conducted on *S. aureus* and *P. aeruginosa* in contact with multiple dilution of 0.75 mg/ml of Co-LTH-PheLig NPs: the NPs showed a full killing effect against *S.aureus* since no colonies can be seen after 24 h of incubation with NPs.

As shown in Figure 40, the logarithmic reduction of CFU/ ml of bacteria treated with PheLig NPs and LTH-PheLig NPs was lower than 20 % in contact with *S. aureus* and 0 % with *P. aeruginosa,* while in contact with of Co-LTH-PheLig the *S. aureus* colonies were completely eliminated, and the number of *P. aeruginosa* colonies was strongly reduced.

Overall, the results suggest that at biocompatible concentrations, the antimicrobial activities of PheLig NPs and LTH-PheLig NPs are low, especially in presence of *P. aeruginosa*. Thus, this

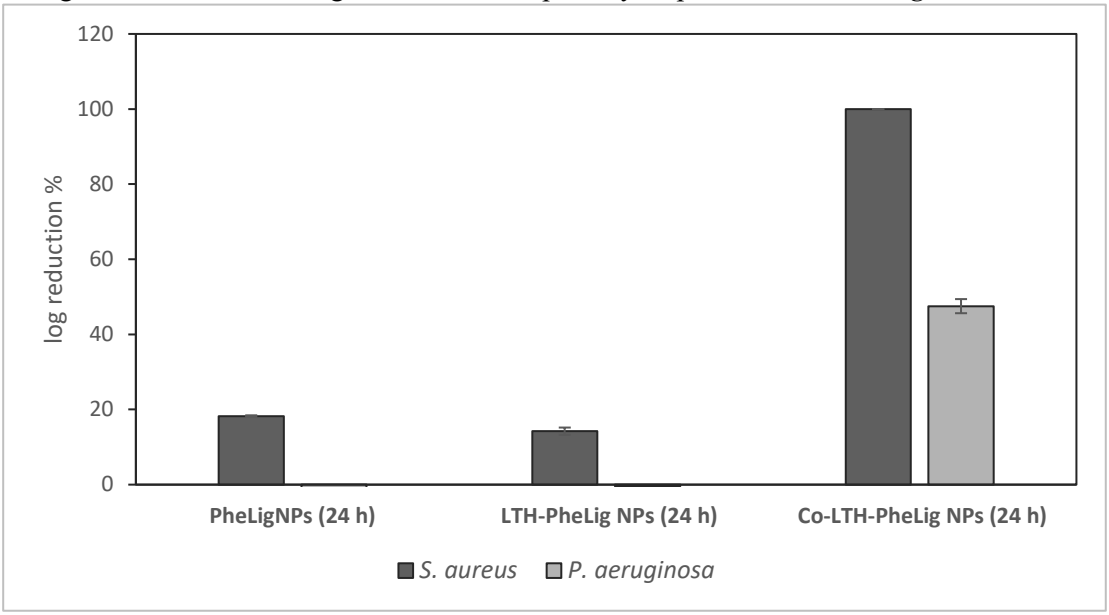


**Figure 40** log reduction % of PheLig NPs, LTH-PheLig NPs and Co-LTH-PheLig NPs against *P. aeruginosa* and *S. aureus*: the presence of Co strongly enhances the bactericidal effects of the NPs.

this type of NPs should be used in contact with not-infected wound, thanks to their lower cytotoxicity. The inclusion of the metal in Co-LTH-PheLig NPs significantly enhances the bactericidal effects of the NPs not only against *S. aureus* but also against *P. aeruginosa* even if slightly reduced the biocompatibility of the system. For this reason, the last system is suitable when the CW is subjected to a bacterial infection that cannot be treated by using PheLig-based nanoparticles alone. However, it remains to optimise the best concentration to not excessively impair cell viability, especially for keratinocytes.

## MPO inhibition assay

The MPO inhibition capacity of the NPs was assessed. The test is based on Guaiacol reaction with $H_2O_2$ mediated by MPO, which results in the comparison of an absorbance peak at 470 nm. The available MPO incubated with the analyzed samples produce a signal that could be compared with the signal deriving from a positive control of MPO in water. The trend of the absorbance over time was analyzed to determine the % of MPO activity of. After 3.5 min the absorbance curves of each analyzed sample had reach a maximum and then start to progressively decrease. Therefore, in this test is advisable to quantify MPO activity by comparing the velocity of the reaction progression by measuring the linear regression of the absorbance curve in the range 0 s – 210 s. This velocity depends on the enzyme activity and could be used as an index of the residual MPO activity in the different conditions. The slope of the regression line was compared with the reaction speed of the positive control (100 % of activity) to measure inhibitory effect of each

sample. Figure 41 shows the results obtained for Lig, TA, LTH and in bulk LTH-PheLig (used then to produce Co-LTH-PheLig NPs).
The lowest inhibitory activity was observed in presence of Lig alone, while TA showed an

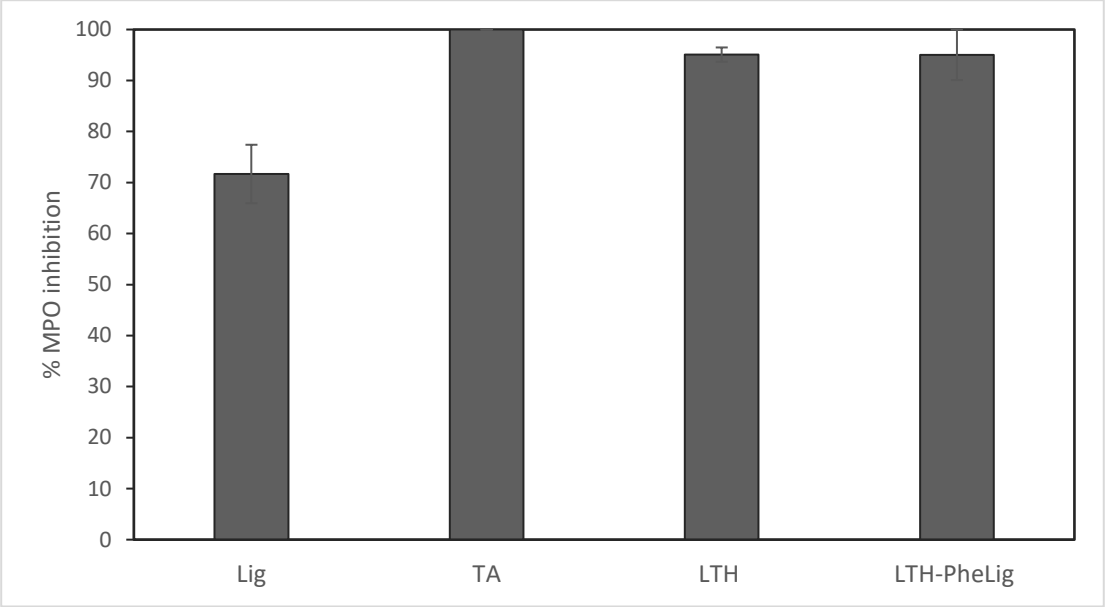


**Figure 41** % MPO Inhibition: the phenolation of Lig and the presence of LTH have a good impact on the ability to inhibit the MPO activity.

inhibition equal to 100 %. For this reason, the phenolation of Lig demonstrated to strongly increase the inhibition effects of Lig over MPO activity. Also, LTH has a good inhibitory capacity against MPO activity: thus, the conjunction of LTH with PheLig should also have a positive effect on the ability of PheLig to reduce MPO activity %.

Finally, the inhibitory effects of PheLig NPs, LTH-PheLig NPs and Co-LTH-PheLig NPs are shown in Figure 42.

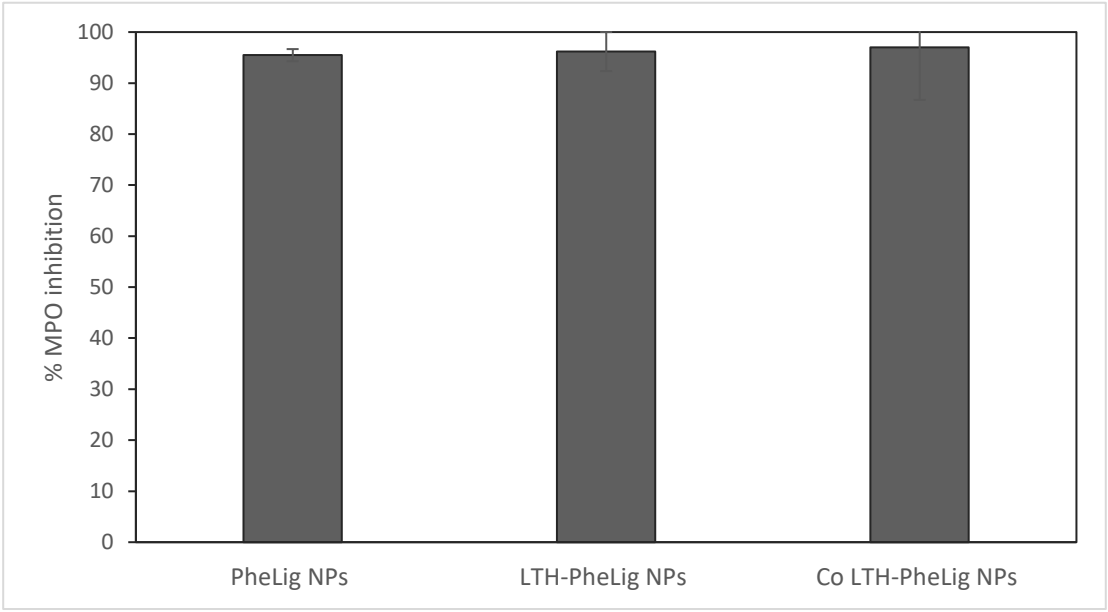


**Figure 42** % MPO inhibition of PheLig NPs, LTH-PheLig NPs and Co-LTH-PheLig NPs: all the NPs totally inhibit the MPO activity.

All the NPs at the concentration of 2 mg/ml have a high inhibitory effect over MPO activity. The nanosize is probably contributing as well in obtaining a higher efficacy compared to the in bulk counterpart LTH-PheLig thanks to the higher surface/volume ratio that can interact with the enzyme. Overall, the synthesized NPs could successfully help to restore MPO levels at physiological concentrations, which could in turn contribute to reduce free radicals, promoting the termination of the inflammation state.

## MMP inhibition assay

Figure 43 reports the results of the MMPs inhibition assay. The residual activity of MMPs contributes to the perpetuation of the inflammatory state. For this reason, the ability of the NPs to control the activity of MMPs was another fundamental factor to be considered. Overall, 2 mg/ml of PheLig NPs and LTH-PheLig NPs demonstrated to have excellent inhibitory effects, while the presence of Co seems to reduce the inhibitory capacity of the nanosystems. This could be due to

further interaction of Co with the MMPs active site that could preserve the catalytic activity of the enzyme[97].

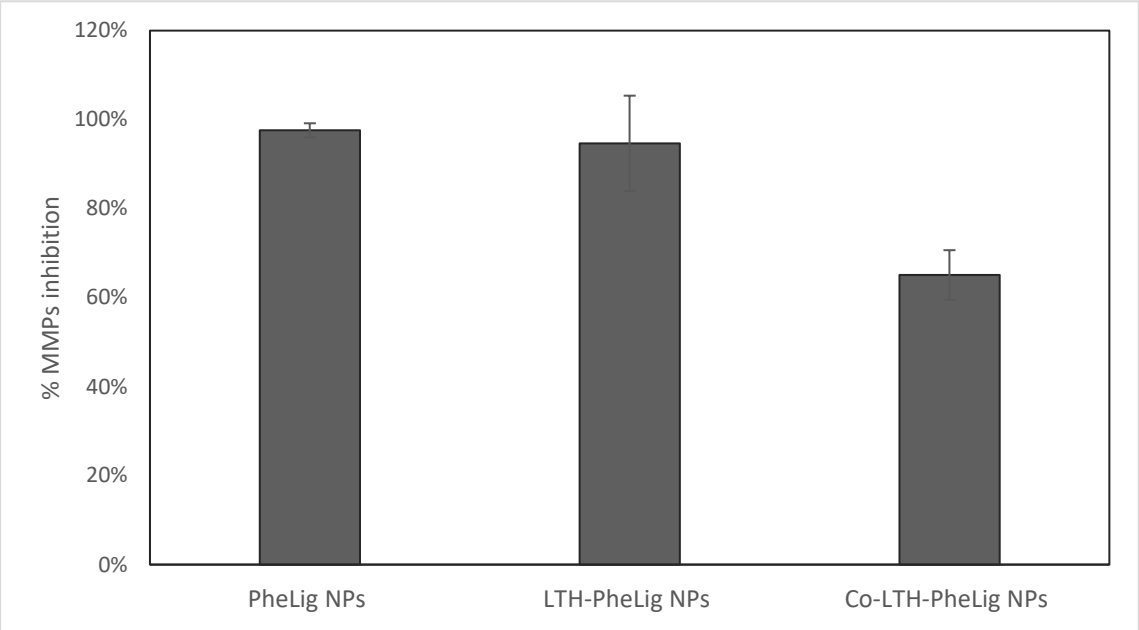


**Figure 43** MMPs inhibition of PheLig NPs , LTH-PheLig NPs and Co-LTH-PheLig NPs. The presence of Co reduced the inhibitory effects of the NPs.

Overall, the assay demonstrated that the presence of PheLig and LTH seems to have a positive impact over the ability of the NPs to inhibit the MMPs, but further investigation should be carried out to better understand the benefits connected with the presence of LTH within the NPs. In fact, if the polyphenols have an unspecific inhibitory effect over MMPs, the LTH should promote a new active targeting that could enhance the efficacy of the treatment. Further investigations should be carried out to find the LTH concentration at which the active targeting is maximally promoted.

# Conclusions

The aim of this section was to develop and characterize new nanosystems, the inclusion of which should offer to the hydrogel inhibitory capacity against MMPs and MPO and antimicrobial properties. PheLig NPs previously synthesized by *Morena et al.*[76] were considered good candidates for the purpose thanks to their antibacterial effects against Gram-positive and Gram-negative bacteria and their low cytotoxicity. PheLig NPs were characterized and consequently modified with an hydroxamic group, LTH, to obtain an active targeting on MMPs, overexpressed during the development of a chronic infections. However, the role of LTH over MMPs inhibition is not yet clear since no differences were found in the inhibitory effects of PheLig NPs and LTH-

PheLig NPs. As future perspective, an alternative strategy to assess their efficacy in the MMPs activity inhibition could be the use of zymography techniques.

The next step consisted in the synthesis of Co-LTH-PheLig NPs using LTH-PheLig as Co (II) reducing agent. The new synthesized NPs demonstrated to have the highest effects over bacterial activities. Moreover, they showed not only higher inhibitory effects against the bacterial growth of *S. aureus* and *P. aeruginosa*, but also a strong bactericidal effect with a bacterial reduction close to 100 % for both S. *aureus* and *P. aeruginosa* at biocompatible concentrations. Other characterization tests should be carried out to complete the study of these NPs. Firstly, EDX spectroscopy could be useful to study the chemical composition of Co-LTH-PheLig NPs, while via XRD it could be possible to evaluate their crystalline structure and the oxidative state of cobalt in order to demonstrate the correct reduction of Co (II) to Co. Finally, TEM analysis could offer high-resolution images of the different synthesized NPs.

To conclude, PheLig NPs, LTH-PheLig NPs and Co-LTH-PheLig NPs can be considered interesting alternatives to treat chronic infections. Moreover, the green synthesis used to obtain PheLig NPs, LTH-PheLig NPs and Co-LTH-PheLig NPs is another fundamental key aspect as it allows the production of systems with low-cost and environmentally friendly methods without the use of chemical additives.

Among all the proposals, Co-LTH-PheLig NPs were considered the most promising nanosystem. The use of Co in the treatment of a CW represents an innovative proposal, still scarcely studied in the state of art Compared to the most common silver or gold NPs, Moreover, the combination of Co and polyphenolic groups should act on multiple and unspecific targets thus avoiding the development of bacteria resistance. In this sense, further investigations on the interactions between the NPs and bacteria surface are required.

.

# Chapter 4

# Poly(ether urethane)-based hydrogel containing PheLigNPs, LTH-PheLig NPs and Co-PheLig NPs

## Introduction

The final part of the project was focused on the incorporation of the PheLig NPs, LTH-PheLig NPs and Co-LTH-PheLig NPs into the poly(ether urethane)-based hydrogel to allow *in situ* release, offering enhanced antimicrobial and antioxidant effects and, at the same time, a stable physical defence against external contaminants maintaining meanwhile a moist environment. In addition, the combination of the *in situ* release promoted by gel and the active targeting of the hydroxamic groups could enhance the efficacy of the treatment.

The preparation of the poly(ether urethane)-based hydrogel containing PheLig NPs, LTH-PheLig NPs and Co-LTH-PheLig NPs was performed by following two alternative protocols to investigate possible interactions between the NPs and CDs that could interfere in the formation of PPRs. Moreover, the phenolic groups present on the NPs could interact with other components of the hydrogel, such as the primary amines exposed by SHF68. To assess the presence of these interactions, the hydrogel was prepared without the addition of α-CDs in order to observe if PheLig NPs alone could promote the transition from sol to gel.

Finally, the hydrogels loaded with NPs were analysed to study their mechanical properties and to quantify the NPs release in order to gain insight on the applicability of the final system in the wound healing field.

## Materials and methods

### Preparation of the PEU-based hydrogels containing PheLig NPs, LTH-PheLig NPs and Co-LTH-PheLig NPs

#### Preparation of CHP407-SHF68 (3 %) and α-CDs (10 %)-based hydrogel containing PheLig NPs, LTH-PheLig NPs or Co-LTH-PheLig NPs

The preparation of poly(ether urethane)-based hydrogels containing PheLig NPs, LTH-PheLig NPs and Co-LTH-PheLig NPs was performed by following several protocols to investigate the presence of potential interactions between the NPs and PEUs and/or NPs and α-CDs.

PEUs CHP407 and SHF68 were solubilized in PBS in the required amount at 4 °C overnight. Then, a solution of CDs (14 % w/v) in PBS was prepared under stirring (500 rpm) at 60 °C.
In the first protocol (referred to as Protocol I) PheLig NPs, LTH-PheLig NPs and Co-LTH-PheLig NPs were collected in the required amount by centrifugation (20000 xg for 20 min), added to the solutions of CDs and sonicated for 1 min at 50 % of amplitude (Sonics and Materials instrument, Ti-horn, 20 kHz and 50 % amplitude) to promote the resuspension of NPs. Then, the solutions of α-CDs and NPs were mixed with the PEUs solutions and vortexed for 1 min, thus obtaining two solutions with a concentration of 3 % w/v of PEUs, 10 % of α-CDs and 2.5 mg/ml of NPs. Finally, the solutions CHP407 /α-CDs/NPs -SHF68/α-CDs/NPs were mixed in a weight ratio of 80 % : 20 %, and the final solution was stored at room temperature to promote the transition from sol to gel. After appropriate studies, this synthesis protocol was selected and used for the subsequent characterisation tests of rheology, stability, release and cytotoxicity.
In the second protocol (referred to as Protocol II), a solution of CDs in PBS was prepared (14 % w/v) under stirring (500 rpm) at 60 °C, added to the PEUs solution and mixed using a vortex for 1 min, thus obtaining 2 solutions with a concentration of 3 % w/v of PEUs and a concentration of 10 % w/v of α-CDs. Then, the solutions CHP407/α-CDs-SHF68/α-CDs were mixed in a weight ratio of 80 % : 20 %, and the final solution was added in the NPs previously collected via centrifugation (20000 xg for 20 min) in order to have a final NP concentration of 2.5 mg/ml. Finally, the solution was sonicated for 1 min at 50 % of amplitude (Sonics and Materials instrument, Ti-horn, 20 kHz and 50 % amplitude) to promote the resuspension of NPs and stored at room temperature to allow gelation.

**Preparation of CHP407-SHF68 (3 %)-based hydrogel containing PheLig NPs, LTH-PheLig NPs or Co-LTH-PheLig NPs without α-CDs**

To understand the role of NPs in the formation of the hydrogel, α-CDs were eliminated from the hydrogel composition to verify if PheLig NPs alone could promote the transition from the sol to the gel phase. In more details, the two PEUs were weighted in the required amount and dissolved in two separate solutions of PBS at 4°C overnight. Then, a solution of PheLig NPs was added and vortexed for 1 min, thus obtaining samples with a concentration of 3% w/v of PEUs (CHP407 SHF68 80%:20%, respectively) and a concentration of 2.5 mg/ml of PheLig NPs.
In a second test, the enzyme laccase (348 U/ml) was added to the final solution to promote the oxidation of the phenolic groups in the NPs promoting a crosslinking reaction between the nucleophile amino groups exposed by SHF68 and the phenoxy radicals on the NPs surface. The solution was maintained under stirring for 2 h at 50 °C to induce the activation of the laccase and then stored at room temperature to promote the gelation.

## Rheology

To study the effects of PheLig NPs, LTH-PheLig NPs and Co-LTH-PheLig NPs on the mechanical properties of the hydrogel, a frequency sweep test and an amplitude sweep test were performed using the rheometer Anton Paar RheoCompass, MCR 302, in accordance with the protocol used by *Torchio et al.*[47] The rheological results of the hydrogels obtained through Protocol I were compared with the results obtained for the corresponding hydrogels prepared with Protocol II. To perform this test, the samples were prepared using the two described protocols and stored in a syringe for 48 h at room temperature; finally, around 0.4 ml of each sample were injected on the plate of the instrument to be analysed. Amplitude sweep test was performed at 37 °C on 25 points using a shear strain % in the range of 0.01 % - 500 % and fixing the angular frequency at 10 rad $s^{-1}$. The frequency sweep test was performed on 16 points at room temperature and at 37 °C using angular frequencies in the range of 0.1 - 100 rad/s and fixing the shear strain at 0.1 %, within the linear viscoelastic range (LVE). The results were compared with the rheology outcomes of a negative control without NPs.

## Stability

The SM hydrogel stability in aqueous media was investigated by monitoring the swelling and dry weight loss over time for SM hydrogels containing PheLig NPs, LTH-PheLig NPs and Co-LTH-PheLig NPs. In the test, 0.5 ml of hydrogel were put in contact with either 500 µl and 100 µl of phosphate buffered saline (PBS, pH 7.4), mimicking two extreme pathological conditions of CW, the case of a wound rich in exudates and the case of a wound poor in liquids. The stability tests were conducted at 37 °C to determine the swelling and the dry weight loss of each hydrogel. For each condition, the time point selected were respectively 6, 24, 48 , 72 and 144 h, and each measurement was performed in triplicate. Initially, the hydrogels were weighted ($w_{wet_0}$). Then, the PBS was added to each sample and the hydrogels were incubated at 37 °C. At each time point, the residual PBS was removed, the SM gels were weighted without PBS ($w_{wet_f}$), while the other samples were completely refreshed with new PBS. Then, the swelling was calculated as follows:

$$Swelling\ \% = \frac{w_{wet_f} - w_{wet_0}}{w_{wet_0}}\ 100$$

The same samples were then freeze dried and weighted again ($w_{dry_f}$) to quantify the percentage of dry weight loss, as follows:

$$Weight\ Loss\ \% = \frac{w_{dry_f} - w_{dry_0}}{w_{dry_0}}\ 100$$

where $w_{dry_0}$ refers to the weight of the hydrogel freeze dried at $t_0$.

The results were compared with the stability outcomes of a negative control (without NPs).

## Release

### Cumulative release

PheLig NPs, LTH-PheLig NPs and Co-LTH-PheLig NPs showed an intrinsic excitation and emission peak at $\lambda_{excitation}$ = 480 nm and $\lambda_{emission}$ = 640 nm respectively. This property was exploited to study the cumulative release of the hydrogels containing PheLig NPs, LTH-PheLig NPs and Co-LTH-PheLig NPs. To study the kinetics release of each type of NP, 500 µl of PBS were added in each sample at time 0h. Then, at 6, 24, 48 and 72 h the supernatant was removed and refreshed with 500 µl of PBS. The volume of the collected PBS was measured and analyzed in fluorescence at $\lambda_{excitation}$ = 480 nm and $\lambda_{emission}$ = 640 nm. A positive control was also prepared by completely dissolving each type of hydrogel in 4 ml of PBS to know the amount of NPs included in the system. A calibration curve was obtained via multiple dilution of each NP in PBS. Using the calibration curve obtained for each type of NP, the concentration of each supernatant was calculated and consequently the total mass of NPs in each analyzed volume was obtained. Then, the cumulative mass and the % of cumulative release were calculated using the following equations:

$$mc_{t_i} = m_{t_i} + m_{t_{i-1}}$$

$$\%\ Cumulative\ release\ = \frac{mc_{t_i}}{m_{100\,\%}} 100$$

Where $m_{t_i}$is the mass calculated at $t_i$, $mc_{t_i}$ is the cumulative mass measured at each analyzed time point and $m_{100\,\%}$ is the total mass measured in the positive control. All the samples were prepared and analyzed in triplicate.

### ICP- MS Analysis

ICP-MS Analysis was used to quantify the amount of Co released by the hydrogel over time. To do this, the supernatants collected at each time point from hydrogels containing Co-LTH-PheLig NPs were analyzed by ICP-MS analysis. Before the analysis, the supernatants were prepared as previously described in Chapter 3.

## Cytotoxicity

The cytotoxicity of the UV-sterilized hydrogel containing PheLig NPs, LTH-PheLig NPs and Co-LTH-PheLig NPs was tested toward human fibroblasts (cell line BJ-5tα) and human keratinocytes (cell line HaCaT) and compared with the results of a control (hydrogel without NPs). Firstly, the hydrogels containing PheLig NPs, LTH-PheLig NPs, Co-LTH-PheLig NPs and the negative control were prepared following the protocol previously described under the hood to ensure the maintenance of sterility. The samples were prepared in a syringe and stored under the hood for

48 h. Fibroblast and keratinocytes were grown in 100 µl of Dulbecco's Modified Eagle's Medium (DMEM, Sigma-Aldrich) in a 96-well plate (60 000 cells per well) in a controlled humidified atmosphere with a $CO_2$ concentration constant at 5 % and a temperature of 37 °C. After 24 h of cell growth, 20 µl of UV-sterilized hydrogels containing 2.5 mg/ml of PheLig NPs, LTH-PheLig NPs and Co-LTH-PheLig NPs were incubated at 37 °C. After 24 h, the wells were washed with PBS twice and the cell viability was assessed using the AlamarBlue assay, evaluating the metabolic activity of cells incubated with hydrogels. To do so, 100 µl of AlamarBlue (10 % v/v) were added and incubated at 37 °C for 3 h. Then, the fluorescence was measured ($\lambda_{excitation}$ = 550 nm, $\lambda_{emission}$ = 590 nm). The maximum percentage of cell viability was calculated using the fluorescence values of a control samples containing cells not incubated with the hydrogels. In addition, wells containing only AlamarBlue reagent were used as the blank group. The percentage of cell viability was calculated as follows:

$$Cell\ viability\ \% = \frac{(Fluorescence_{sample} - Fluorescence_{\ blank})}{(Fluorescence_{control} - Fluorescence_{\ blank})}\ 100$$

The same test was repeated to evaluate the cytotoxicity of the release solution deriving from the hydrogel with Co-LTH-PheLig NPs. More in detail, the hydrogel containing 2.5 mg/ml of Co-LTH-PheLig NPs was prepared following the already described protocol and incubated with 500 µl of culture medium DMEM at 37 °C. After 24 h of incubation, the release solutions were collected and diluted 1:2 in fresh cell medium. Then, 100 µl of the release solution were incubated with fibroblasts and keratinocytes at 37 °C for 24 h. After the incubation, the AlamarBlue assay was performed as previously described.

# Results

### Gelation time of the hydrogels containing PheLig NPs, LTH-PheLig NPs or Co-LTH-PheLig NPs

The gelation time was measured for the different hydrogels loaded with NPs. The preparation protocols of the hydrogels did not influence the hydrogel gelation capacity: the inclusion of PheLig NPs, LTH-PheLig NPs or Co-LTH-PheLig NPs did not hinder the formation of the hydrogel, but it slowed down the sol-to-gel transition from 2 to 4 h either when the NPs were placed in solution with the CDs or when they were added directly into the final solution of PEUs and α-CDs.

**Gelation study of the hydrogel containing NPs without α-CDs**

Solutions of the PUs with the different NPs were prepared and incubated at room temperature to observe the gelation. However, gelation was not observed in the absence of α-CDs, as shown in Figure 44.

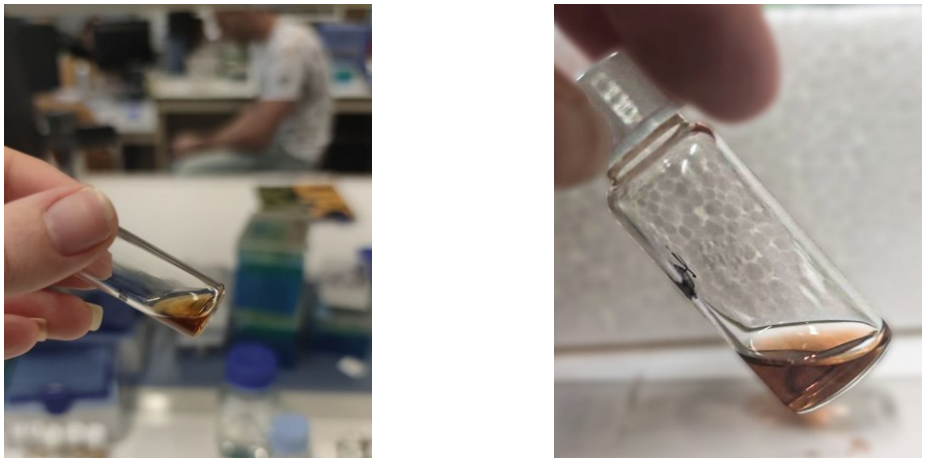

**Figure 44** 3 % CHP407- SHF68 solution containing PheLig NPs at time 0 (left) and after 1 day (right). No gelation was observed even if the turbidity of the solution changed with time.

Nevertheless, an increase of the solution turbidity over time suggested the interaction of the NPs with the PUs and the formation of a hydrogel may be possible by tuning the reciprocal amount of the components. However, increasing the concentrations of PEUs and PheLig NPs could have cytotoxic effects. Moreover, the strength of this PPRs -based hydrogel is the capacity of obtaining stable hydrogels at low concentration of components. The formation of PPRs becomes prevailing over micelle formation only in the presence of a low concentration of PEUs and a high concentration of CDs as previously demonstrated by *Torchio et al*.[47] As a consequence, the deriving SM-hydrogels will release a lower amount of synthetic polymers during their progressive erosion, reducing the overall cytotoxicity of the system. This justified the preservation of the original hydrogel composition for all the subsequent characterizations.

## Rheology

Figures 45 and 46 report the results of the frequency sweep test conducted on the PEU and α-CDs based hydrogels containing PheLig NPs and Co-LTH-PheLig NPs, showing the comparison between the results obtained with the two tested protocols conducted at 25 °C and 37 °C.

Protocol I refers to the hydrogel preparation process in which the NPs were suspended in the 14 % wt/v α-CDs solution before being mixed with PEU solutions. Protocol II refers to the hydrogel

preparation process in which the NPs were directly resuspended in the final solutions of PEU (3% wt/v) and α-CDs (14 % wt/v).

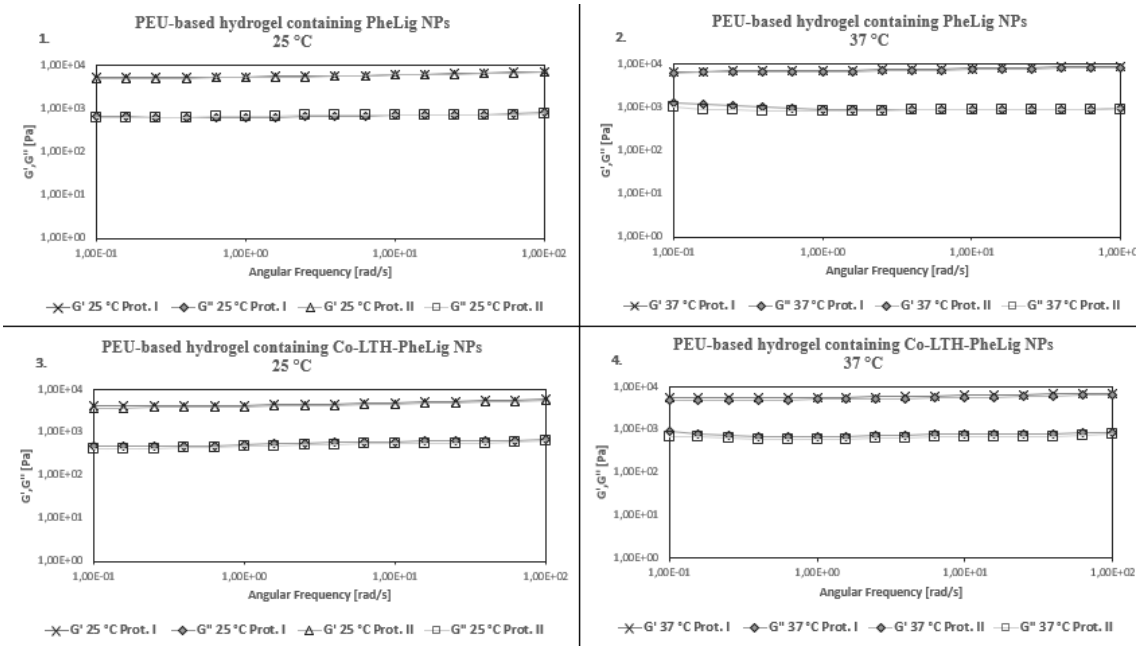


**Figure 45** Frequency sweep test of hydrogel with PheLig NPs prepared using protocol I and II at 25 °C (1) and 37 °C (2). The rheological behaviour of the systems was not influenced by the preparation protocol. Analogue results were obtained for hydrogel with Co-LTH-PheLig NPs.

By the analysis of the results emerged that both at 25 °C and 37 °C the rheological behavior of the hydrogels did not change by varying the preparation protocol, both in presence of PheLig NPs and Co-LTH-PheLig NPs.

In all cases, the hydrogels remained stable in their gel phase as angular frequency varied. The results of the amplitude sweep tests (Figure 46.1, Figure 46.2, Figure 46.3, Figure 46.4) confirmed the similarity in the rheological properties of the hydrogels containing PheLig NPs and Co-LTH-PheLig NPs: the phase transition from gel to sol behavior (due to the complete failure of the gel network induced by the applied deformation) occurred at a shear strain of approximately 0.1 % both at time 0 min, starting from the hydrogel as such, and after 15 min, starting from the hydrogel that had gone previous mechanical failure, demonstrating also a self-healing capacity of the hydrogel. Thus, the first protocol was selected since it was considered the easiest process, and the rheology of each hydrogel was compared with the results obtained on a control sample prepared without the inclusion of NPs.

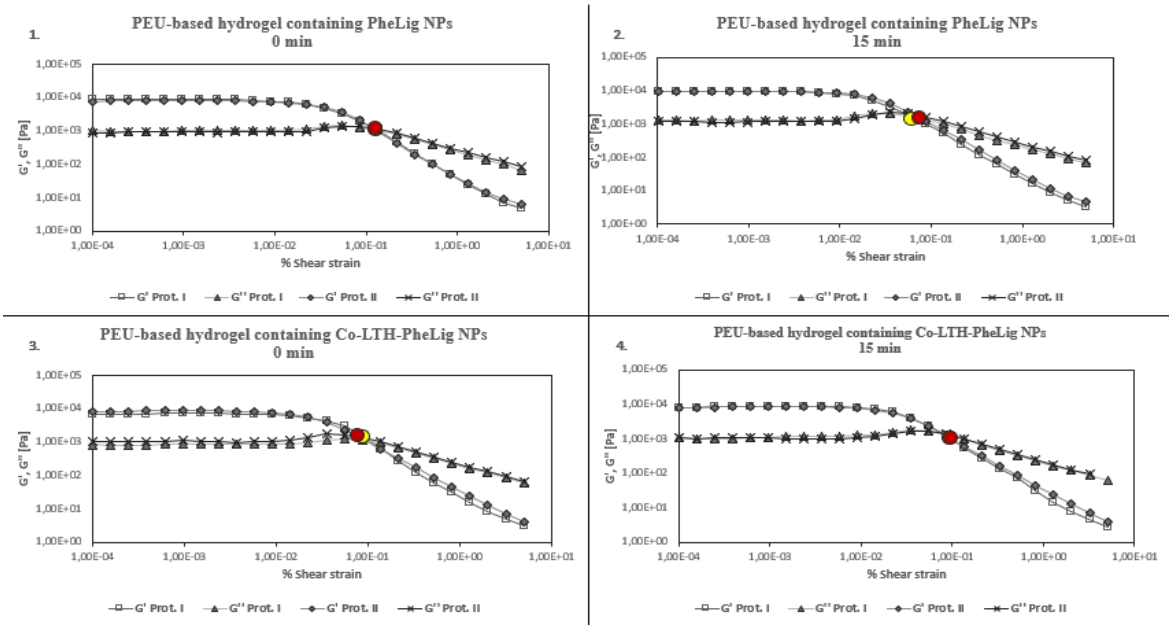


**Figure 46** Amplitude sweep test: comparison between the results obtained for the hydrogels prepared by using protocol I and II. The failure points of Protocol I are indicated with a yellow circle, the failure points of Protocol II are indicated with a red circle. Both in case of the hydrogel with PheLig NPs ((1) and (2)), and in presence of Co-LTH-PheLig NPs ((3) and (4)) the selection of the preparation method did not influence the results.

### Rheology of PEU-based hydrogel containing PheLig NPs

Figures 47 and 48 show the results of the frequency sweep test and the amplitude sweep test conducted on PEU-based hydrogel with PheLig NPs, compared with the results obtained on a control without NPs.

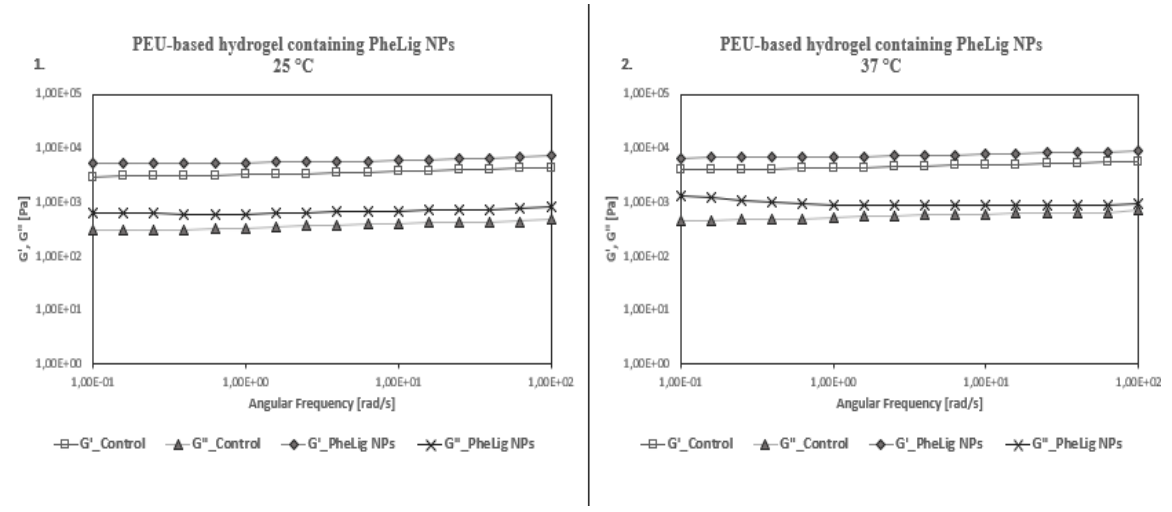


**Figure 47** Frequency sweep test of the hydrogel with PheLig NPs compared to the control. Both at 25 °C (1) and 37 °C (2) the hydrogel with NPs showed higher G' and G'' values.

As shown by the frequency sweep test in Figure 47, the hydrogel remained stable in its gel phase over the range of angular frequency studied.
Moreover, amplitude sweep test in Figure 48 evidenced that the presence of PheLig NPs increased the value of G' and G'' and moved the shear strain % corresponding to the flow point at lower values.

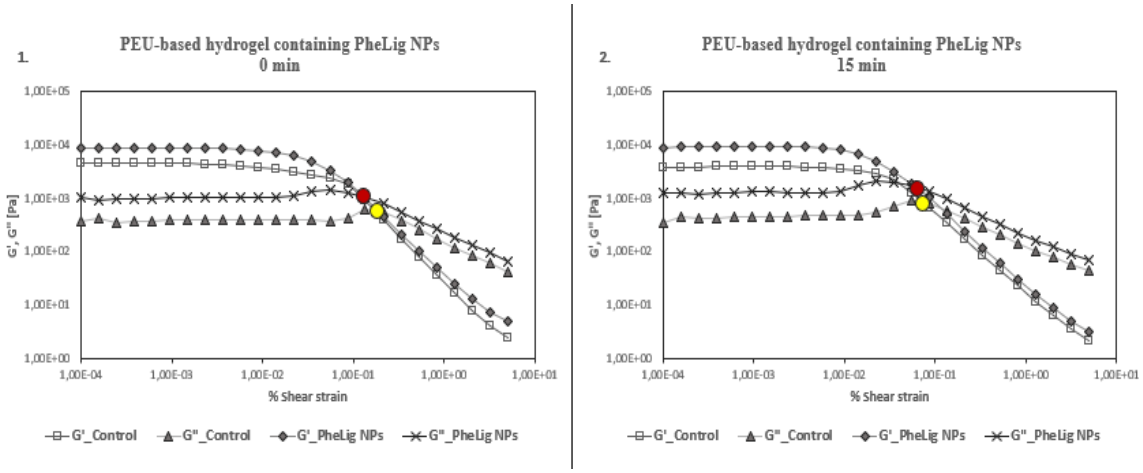


**Figure 48** Amplitude sweep test at time 0 min (1) and 15 min (2) of the hydrogel with PheLig NPs compared to the control. In both cases, the hydrogel with NPs showed higher values of G' and G''. The cross point of G' and G'' of the NP-loaded sample (red circle) was slightly lower compared to the control (yellow circle).

This seems to indicate a higher rigidity of the hydrogel loaded with NPs, which may indicate an interaction between the NPs and the hydrogel. In addition, according to *Boffito et al.*, the differences in the rheological behavior of the hydrogel loaded with NPs compared to the hydrogel without NPs, could be ascribed to the NPs which may act as defects within the hydrogel network.[46] Both the hydrogel containing PheLig NPs and the control without NPs showed a self-healing capacity, as demonstrated by the analysis of the amplitude sweep tests. After 15 min of quiescence at 37 °C, the hydrogel Storage Modulus (G') and Loss Modulus (G'') followed the same trends observed in the amplitude sweep test conducted at time 0 min, *i.e.,* on the as-prepared hydrogel. However, the amplitude sweep test evidenced a slight shift of the phase transition towards lower shear strain %, suggesting hydrogel incapability to recover completely.

**Rheology of PEU-based hydrogel containing LTH-PheLig NPs**

Figures 49 and 50 show the results of the frequency sweep test and the amplitude sweep test conducted on the hydrogel containing LTH-PheLig NPs, compared with the results obtained on a control without NPs.

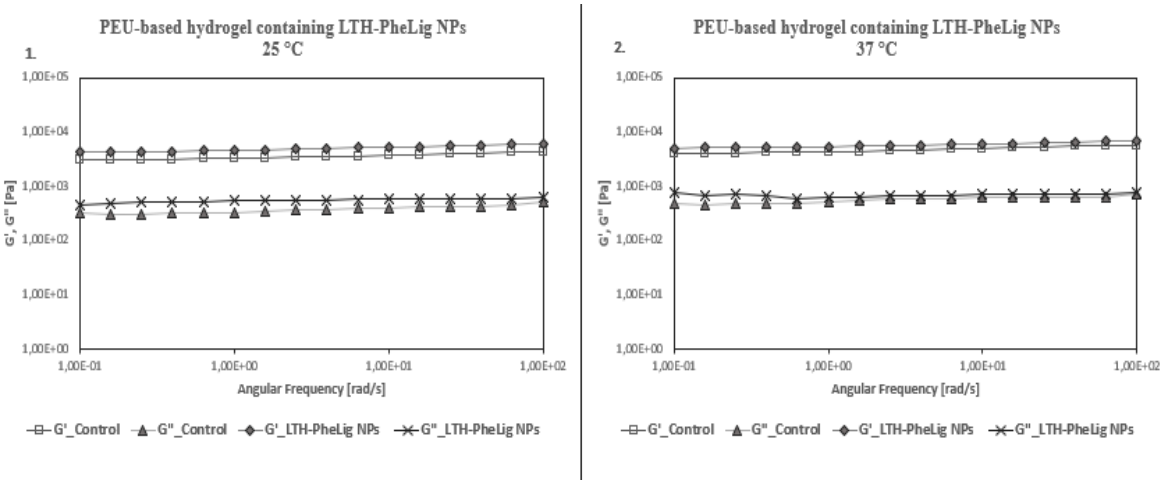


**Figure 49** Frequency sweep test at 25 °C (1) and 37 °C (2) of PEU-based hydrogel with LTH-PheLig NPs compared with the control. The presence of the NPs slightly increases G' and G''.

The rheology of the hydrogel with LTH-PheLig NPs confirmed the previous results obtained for the hydrogel with PheLig NPs: the measured G' and G'' were slightly higher for the hydrogel containing LTH-PheLig NPs. Also in this case, the hydrogel did not fully recover as shown by the reduced shear strain corresponding to the flow point.

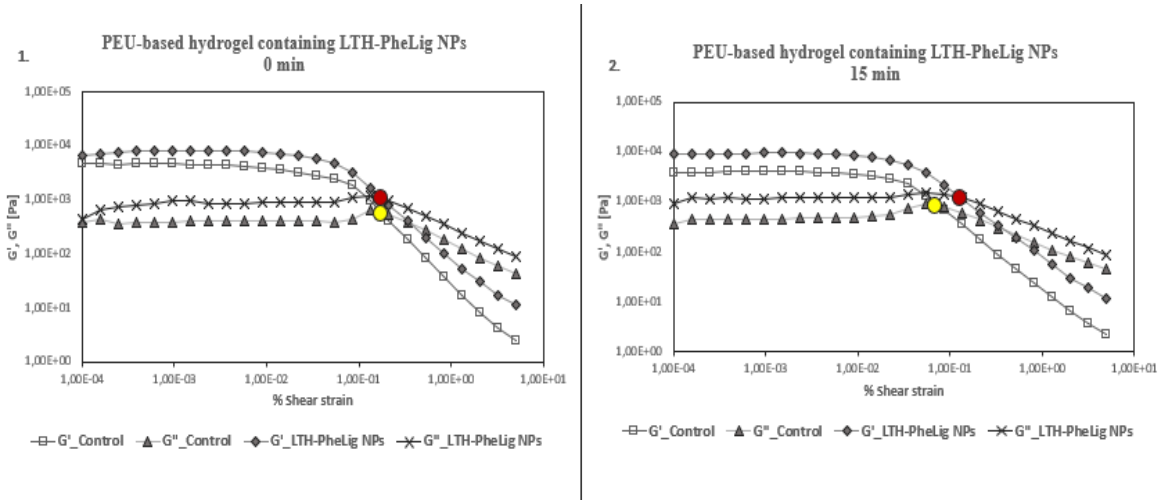


**Figure 50** Amplitude sweep test at time 0 min (1) and 15 min (2) conducted on the PEU-based hydrogel with LTH-PheLig NPs and on the control. The cross point of the sample (red circle) is comparable with the control (yellow circle).

**Rheology of PEU-based hydrogel containing Co-LTH-PheLig NPs**

Finally, Figures 51 and 52 show the results of the rheological tests conducted on the hydrogel containing Co-LTH-PheLig NPs, compared with the results obtained from the analysis of the control: these systems showed the same trend of the hydrogel containing LTH-PheLig NPs with a higher G' and G'' values and a flow point that occurred at lower values of shear strain % compared to the control.

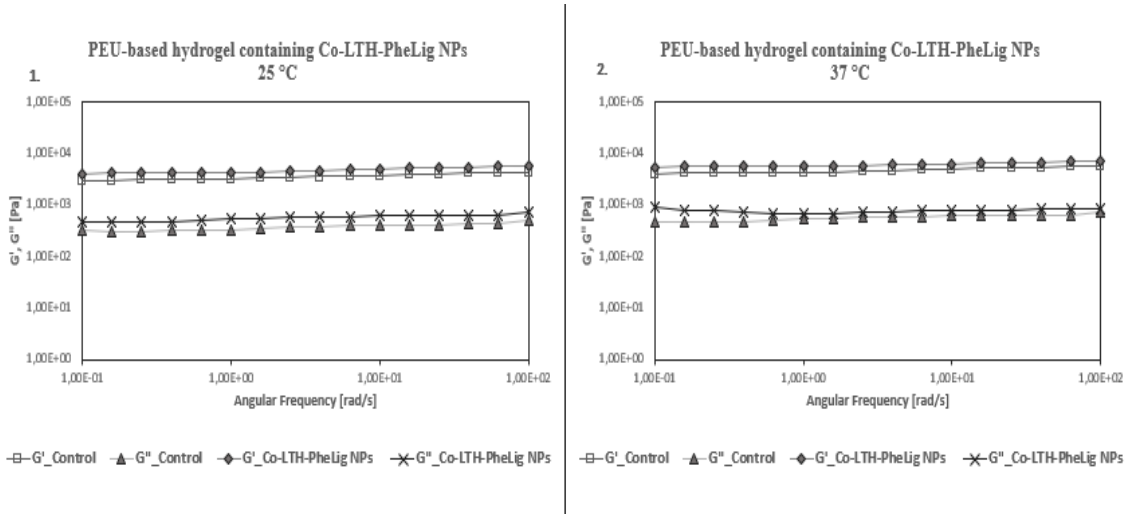


**Figure 51** Frequency sweep test conducted at 25 °C (1) and 37 °C(2) on the PEU-based hydrogel loaded with Co-LTH-PheLig NPs and the control. G' and G'' were slightly higher in presence of the NPs.

Overall, the inclusion of PheLig NPs, LTH-PheLig NPs and Co-LTH-PheLig NPs seemed to slightly increase the toughness of the system, even if the results did not deviate excessively from the control.

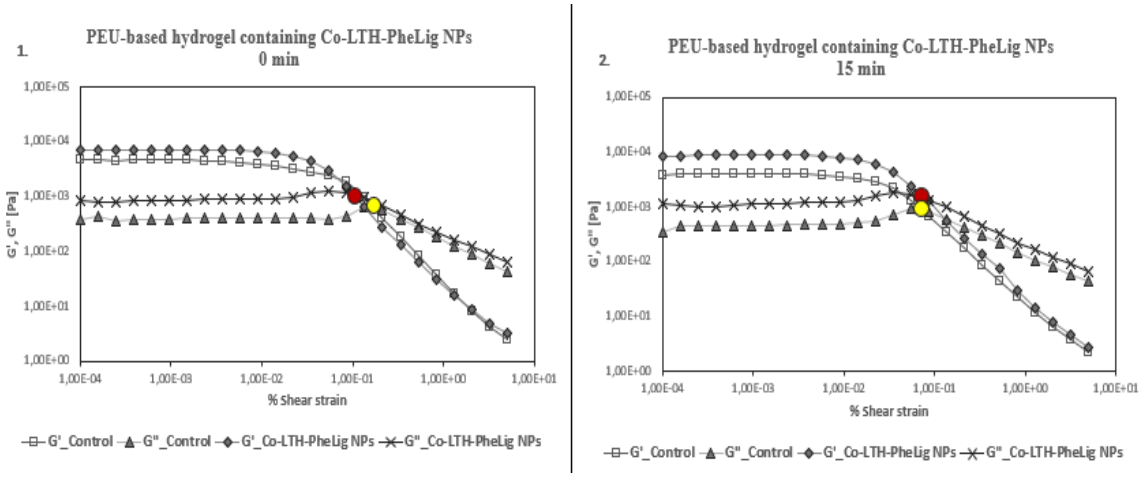


**Figure 52** Amplitude sweep test conducted at time 0 min (1) and after 15 min (2) on the PEU-based hydrogel loaded with Co-LTH-PheLig NPs and the control. The transitional phase of the sample (red circle) at time 0 min is positioned at a lower value of shear strain % but increases after 15 min compared to the control.

It is possible that the inclusion of NPs with phenolic groups allows the interactions with other components of the hydrogel such as the primary amino groups exposed by SHF68, increasing the stiffness of the systems. To confirm these results a stability tests was conducted, as reported in the next paragraph.

## Stability

Figures 53 and 54 report the trends of weight loss % for the hydrogels containing PheLig NPs, LTH-PheLig NPs, Co-LTH-PheLig NPs compared to the control when 500 µl of hydrogel were incubated with 100 µl and 500 µl of PBS at 37 °C. From the stability tests conducted in presence of 100 µl of PBS (Figure 53), within the first 48 h of observation, the measured erosion of the control was around zero, while the hydrogels containing PheLig NPs, LTH-PheLig NPs and Co-LTH-PheLig NPs exhibited a slight loss in dry weight, which remained below 20 % and no significant differences were observed among them.

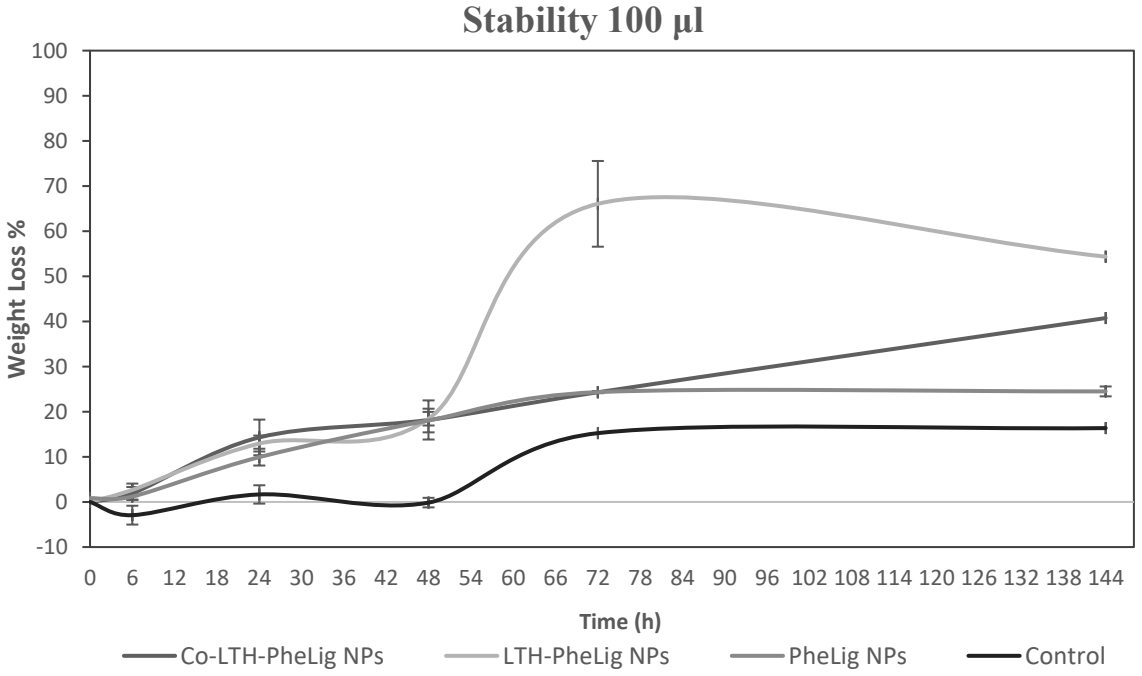


**Figure 53** Dry weight loss % for the hydrogels containing PheLig NPs, LTH-PheLig NPs and Co-LTH-PheLig NPs compared with a control without NPs. The hydrogel containing LTH-PheLig NPs showed the highest dry weight lost after the first 72 h of incubation.

After 72 h of incubation, a differentiation in the erosion process of the different systems was observed with the highest weight loss settled around 54 % measured in the hydrogel containing LTH-PheLig NPs. The highest stability was observed in the control without NPs, with a dry weight loss % that remained lower than 17 % after 6 days. The dry weight loss trend of the hydrogel containing PheLig NPs settled at around 24 % after the first 72 h and remained stable

over time, whereas the system containing Co-LTH-PheLig NPs showed a linearly increasing dry weight loss after the first 72 h that however remained below 50 % after 6 days of incubation.

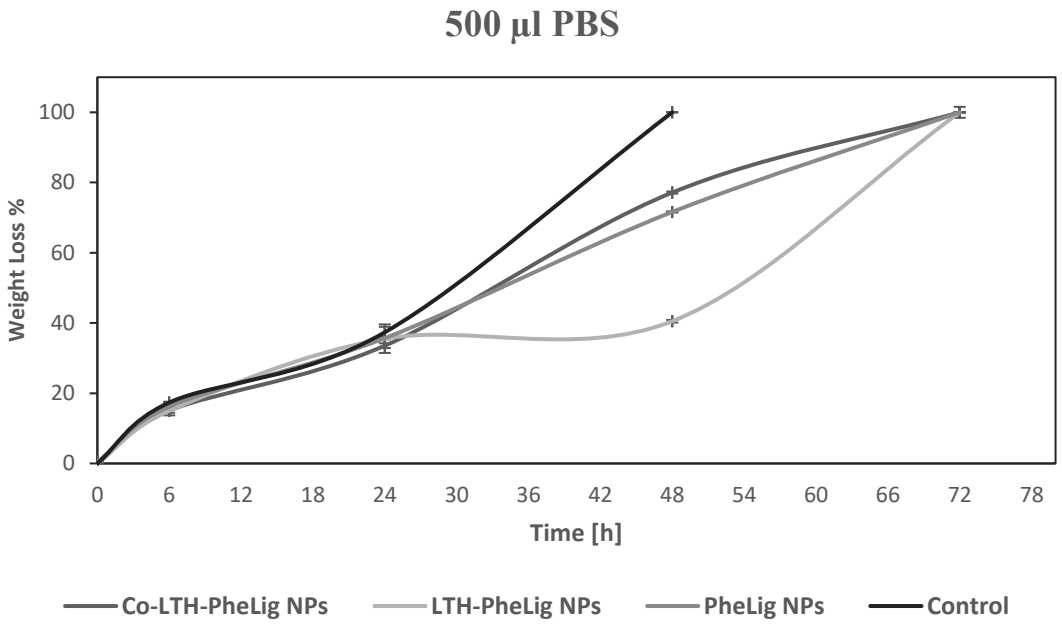


**Figure 54** Dry weight loss (%) for the hydrogels containing PheLig NPs, LTH-PheLig NPs and Co-LTH-PheLig NPs compared with a control without NPs. The control was completely degraded/eroded after 48 h of incubation.

In contrast to the previous results, when the hydrogels were in contact with 500 µl of PBS, the control without NPs showed the lowest stability and, after the first 48 h, the system was completely dissolved. The presence of PheLig NPs, LTH-PheLig NPs or Co-LTH-PheLig NPs increased the stability of the hydrogel which reached a dry weight loss of 100 % after 72 h of incubation. It should be noted that the results obtained were diametrically opposed to those obtained in the previous test:

- during the first 24 h all the systems showed the same trend reaching a dry weight loss of around 36 %
- the hydrogel containing LTH-PheLig NPs showed the lowest dry weight loss after the first 48 with a percentage of up to 40 %.
- the hydrogel containing Co-LTH-PheLig NPs and LTH-PheLig NPs showed a similar trend even if the dry weight loss % of the first system was slightly higher (around 77 %).

Analysing the results concerning the % of swelling of the hydrogels, in contact with both 500 µl and 100 µl, the behaviour of the systems was similar as shown in Figures 55 and 56.

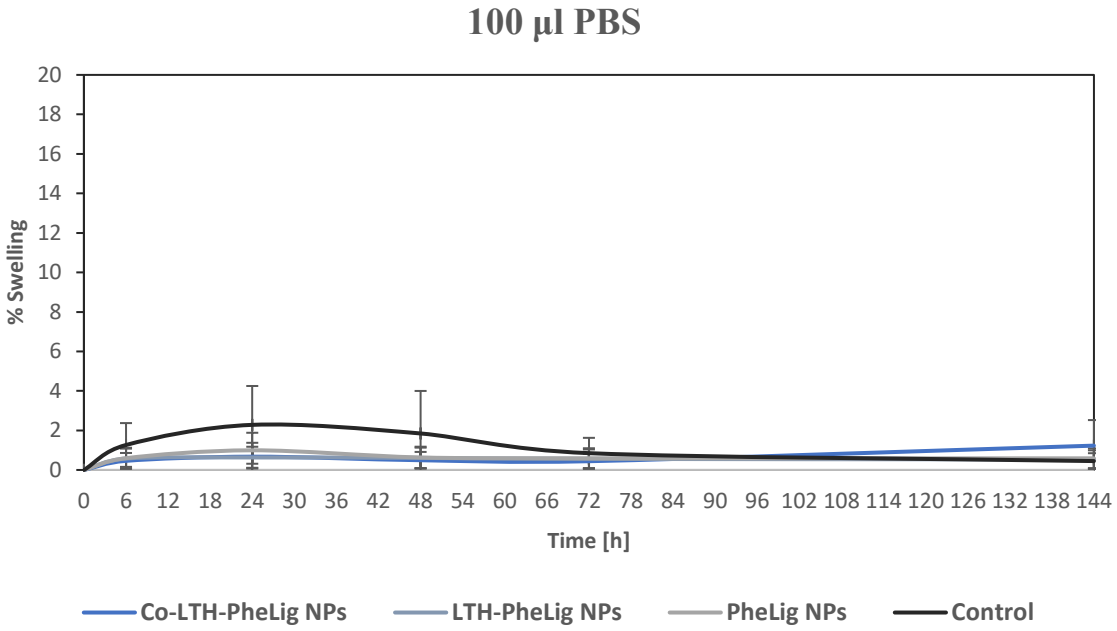


**Figure 55** Swelling (%) of the hydrogels containing PheLig NPs, LTH-PheLig NPs and Co-LTH-PheLig NPs compared with the control. During the samples were in contact with 100 µl of PBS.

The systems containing PheLig NPs, LTH-PheLig NPs, Co-LTH-PheLig NPs and the control maintained their wet weight constant up to 6 days of incubation in contact with 100 µl of PBS and up to 48 h of incubation in contact with 500 µl since the measured swelling % remained stable at zero.

The stability tests confirmed the results obtained by *Torchio et al.*: although the systems maintained constant their wet weight, the increasing of their dry weight loss may be associated with a release of mostly non-crystalline and more unstable components during a concomitant fluid absorption from the external PBS solution.[47] Thus, the stability of the hydrogel depends on its ability to interact with the water environment it is inserted into. A qualitative observation has showed that the inclusion of NPs reduced this capacity. When the control without NPs was put in contact with a higher volume of PBS, its greater retention tendency facilitated the flow of fluids between the internal and external environment, promoting a faster release of the more unstable components by concentration gradient with a faster reduction of its dry weight. On the contrary, the presence of PheLig NPs, LTH-PheLig NPs or Co-LTH-PheLig NPs reduced the hydrogel capacity to exchange fluids and slowed down the release of the components, increasing the stability of the systems.

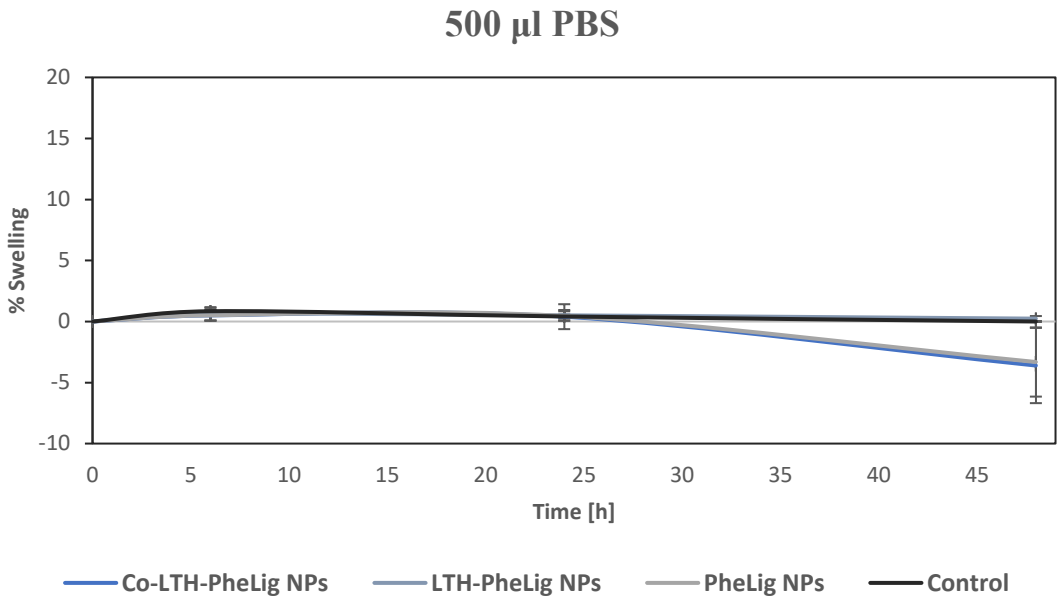


**Figure 56** Swelling of the hydrogels containing PheLig NPs, LTH-PheLig NPs and Co-LTH-PheLig NPs compared with the control in contact. During the test samples were in contact with 500 µl of PBS.

In contact with low volumes of PBS the exchange by concentration gradient was scarcely promoted. In this case the higher crystallinity of the control prevailed over its tendency to exchange fluids with the external solution, resulting in a higher stability compared to the hydrogel containing the NPs which were supposed to be characterized by a higher number of amorphous domains. One influencing factor of the resulting hydrogels stiffness is the average size of the NPs: the larger the NPs dimension, the greater the amorphous phase of the corresponding system should be. At lower volumes of PBS, the degradation/erosion was enhanced due to the lower crystallinity of the system; while at higher volume of PBS the materials exchange was slower and reduced the erosion speed. This could explain the different behaviour observed studying the stability of the hydrogels containing PheLig NPs, LTH-PheLig NPs and Co-LTH-PheLig NPs. However, further investigations should be carried out to confirm these hypotheses and to better understand the molecular structure of the system.

## Release of NPs

**NPs release test obtained through studying lignin fluorescence**

The cumulative release % profiles of NPs from the hydrogels incubated in contact with 500 µl of PBS are shown in Figure 57. The release of PheLig NPs and LTH-PheLig NPs followed the same trend, with a slow linear release during the first 48 h and an increase in the pendency between 48 and 72 h. Co-LTH-PheLig NPs followed a sigmoidal trend. The majority of the release was concentrated between 24 and 48 h. The faster release kinetics of Co-LTH-PheLig NPs may be

associated with their smaller average dimension that promoted diffusion mechanisms. Overall, the cumulative release trend confirmed the stability results obtained by placing the hydrogels in contact with 500 µl. .

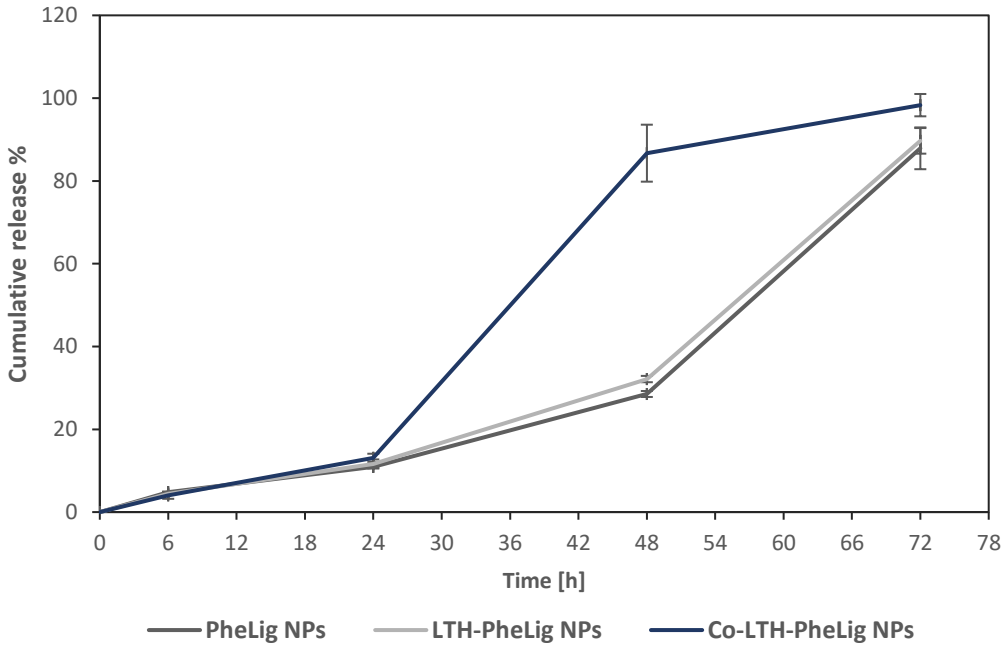


**Figure 57** Cumulative release of NPs from the hydrogels incubated in contact with 500 µl of PBS.

**Co-LTH-PheLig NPs release quantified through ICP-MS Analysis**

ICP-MS analysis was used to quantify the Co released by the hydrogel in order to:

- confirm the results of the release obtained through lignin florescence
- obtain a significant quantitative measurement of the amount of Co-LTH-PheLig NPs released from the hydrogels

Figure 58 reports the cumulative mass of Co released in 72 h by hydrogel in contact with 500 µl of PBS. The results have the same trend of the cumulative release of Co-LTH-PheLig NPs obtained through lignin fluorescence. The cumulative mass of Co released after 72 h was around 0.019 mg.

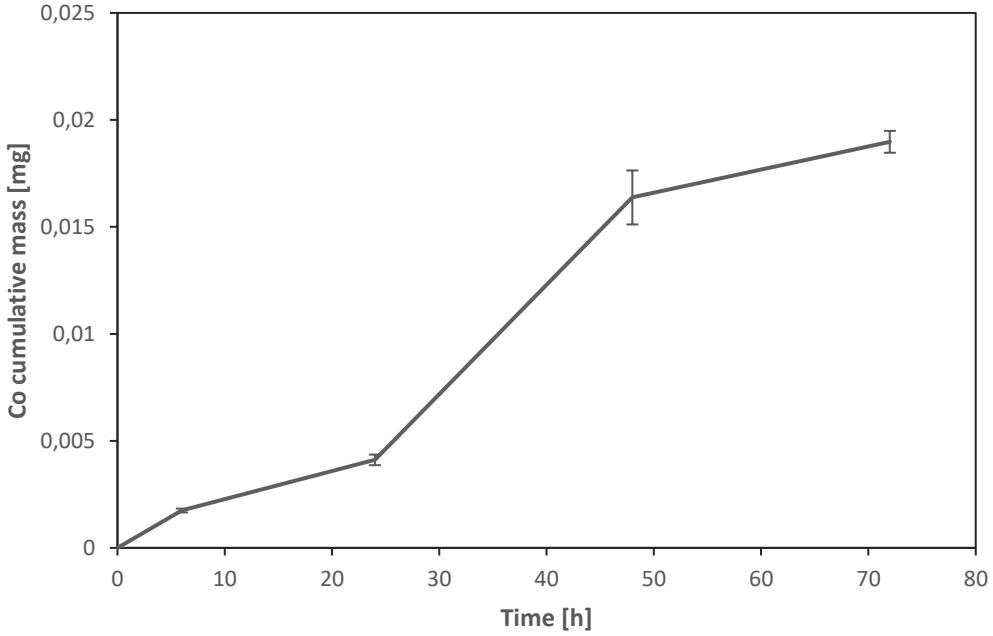


**Figure 58** Cumulative mass of Co released by 500 µl of hydrogel in contact with 500 µl of PBS.

## Cytotoxicity

Figure 59 reports the results of the cytotoxicity test conducted on the hydrogels containing 2.5 mg/ml of Co-LTH-PheLig NPs, LTH-PheLig NPs and PheLig NPs and on a negative control (hydrogel without NPs). In the presence of fibroblasts all the analysed samples, apart from the hydrogel with LTH-PheLig NPs showed a biocompatibility greater than 85 %. The measured fibroblast viability in presence of the hydrogel with LTH-PheLig NPs was lower than 30 % but the associated standard deviation was particularly high. A similar trend was registered in presence of keratinocytes with the highest cytotoxicity observed for the sample with LTH-PheLig NPs. The biocompatibility of the hydrogels was lower in contact with keratinocytes and confirmed previous cytotoxicity results conducted on the Co-LTH-PheLig NPs, LTH-PheLig NPs and PheLig NPs directly in contact with cells. Also in this case, the presence of LTH-PheLig NPs seems to reduce the biocompatibility of the hydrogel even if the corresponding standard deviations was significantly high. Thus, the tests should be repeated to verify the significance of the results. Overall, apart from the sample with LTH-PheLig NPs, the presence of the NPs did not reduce the biocompatibility of the hydrogel.

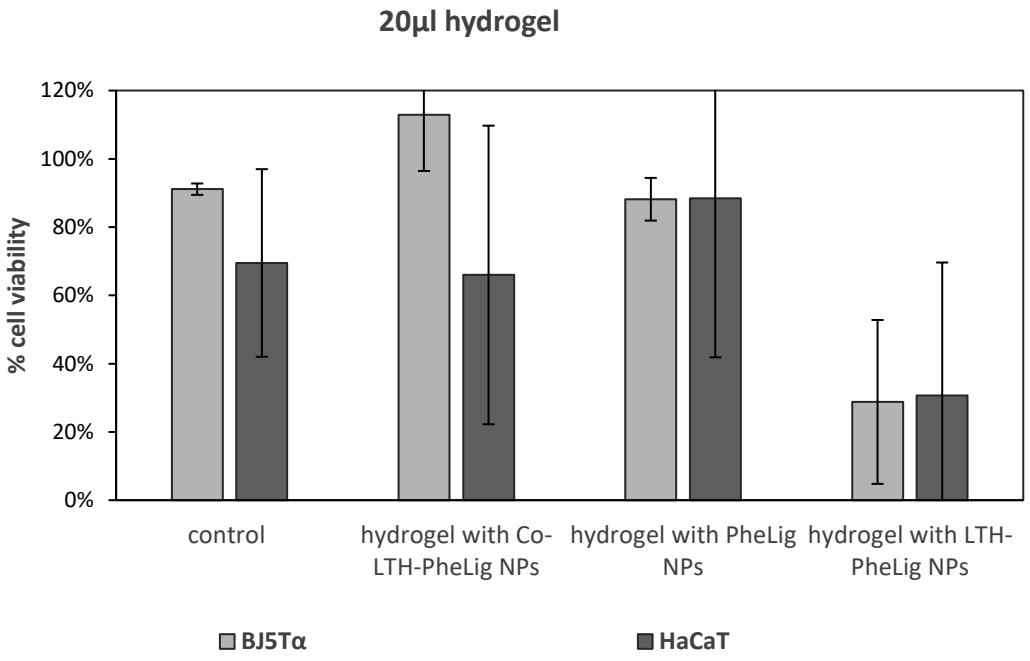


**Figure 59** Cell viability % of fibroblasts and keratinocytes in contact with PEU-based hydrogels containing PheLig NPs, LTH-PheLig NPs and Co-LTH-PheLig NP, and a control. The cytotoxicity of the systems was higher for keratinocytes. The presence of NPs in the hydrogel did not influence the cellular viability.

The biocompatibility test conducted on the release solutions was performed to understand if the release of the hydrogel influences the cellular viability. Figure 60 shows the obtained results: the cellular viability (%) of both fibroblasts and keratinocytes appeared high in the presence of all the types of analysed NPs. The biocompatibility of the solution was lower when the systems were in contact with keratinocytes in comparison with fibroblasts, in accordance with the results already showed. In addition, contrary to the previous outcomes, the presence of PheLig NPs did not change the cellular viability. This supported the hypothesis that the cytotoxicity results of the PheLig NPs previously obtained could be affected by error: one possible cause of the measurement error could be connected to contaminations that could have altered the outcomes.

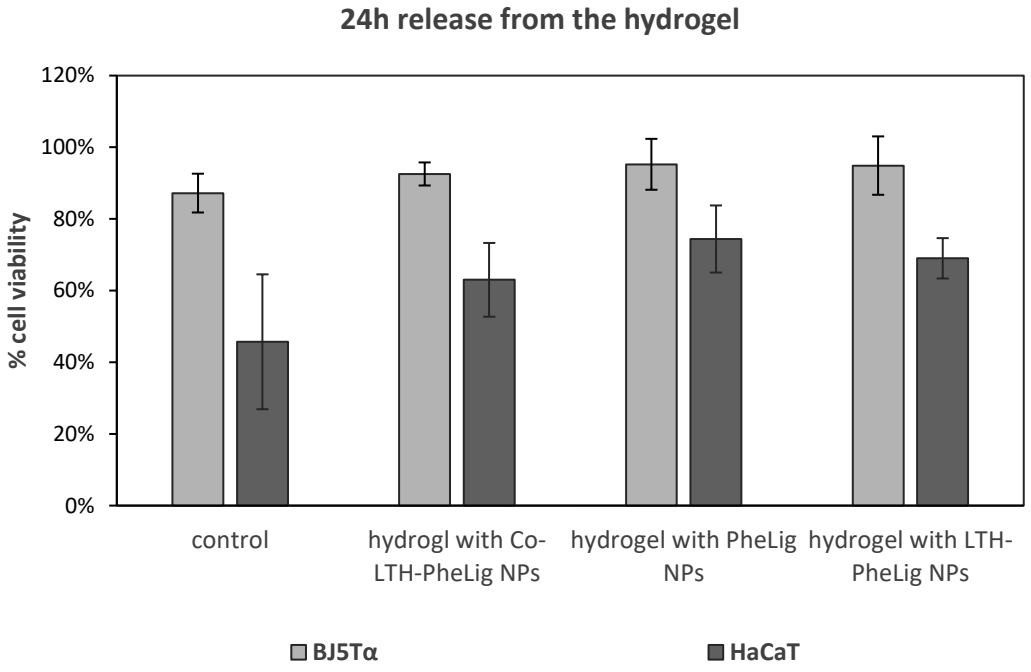


**Figure 60** Cell viability (%) of fibroblasts and keratinocytes in contact with the release solutions of the hydrogel with PheLig NPs, LTH-PheLig NPs and Co-LTH-PheLig NPs.

# Conclusions

The designed PEU-based hydrogels containing PheLig NPs, LTH-PheLig NPs and Co-LTH-PheLig NPs can be considered excellent candidates as treatment systems for CWs. Indeed, the mechanical properties and the biocompatibility of the hydrogels containing PheLig NPs, LTH-PheLig NPs and Co-LTH-PheLig NPs make these systems compatible with the purpose of this thesis project. The hydrogels presented no swelling behaviours but lose their dry weight with time, in accordance with the studies carried out by *Torchio et al*[47]. This means that the degradation mechanism is based on a fluids exchange by concentration gradient between the external aqueous solution and the internal environment. The NPs turned out to be progressively liberated by diffusion with no burst release mechanism during the system erosion and the trend was slowed down by the presence of the NPs in comparison with the control. In addition, the low PEU concentration and the physiological conditions (pH 7.4, 37 °C) at which the hydrogels were prepared and maintained contributed to obtain a highly biocompatible system that did not influence the cellular viability of the area they are in contact with. Moreover, the inclusion of PheLig NPs, LTH-PheLig NPs, Co-LTH-PheLig NPs offers the systems unique MMP and MPO inhibitory properties, making them suitable for reducing the inflammatory state of CWs. In the case of hydrogel containing Co-LTH-PheLig NPs, the release of these NPs not only could prevent the bacterial growth, but it could also fight new microbial infections thanks to the enhanced

bacterial killing effects of the NPs, making this system affordable to be put in contact with infected wound beds.

Further studies should be concentrated on tuning the content of the different components of the system and to measure the precise quantity of NPs released over time. An antibacterial test should be carried out by putting the solutions released over time by the different hydrogels in contact with Gram-positive and Gram-negative bacteria to understand the real antimicrobial power of each type. In addition, a live-and-dead staining could be useful to better understand the cytocompatibility of the hydrogels. Finally, the system should be analyzed through advanced microscopy techniques such as via a Cryo-SEM to observe its structure at the molecular level.

# Chapter 5

# Final remarks

The final aim of this master thesis project was the development of a hydrogel with antimicrobial properties useful in the treatment of CWs. The aim was achieved by the development of a SM-hydrogel including a treatment system that could offer antibacterial properties through unconventional methods that should avoid the development of bacterial resistance.

In this regard, in the framework of this thesis project, a SM hydrogel previously investigated and characterized at the laboratories of the Politecnico di Torino was selected and enriched with antibacterial and antioxidant nanosystems to make it a release system suitable for the final purpose.

The first part of the project was developed in the labs of Politecnico di Torino during the first month of work and involved the synthesis and characterization of the PEUs employed in the hydrogel preparation. After an initial study of the state of art, which however continued for the whole duration of the thesis project, the selected materials were characterized in terms of composition and molecular weight before being used for the hydrogel preparation. The study included the selection of the final composition of the hydrogel starting from previous studies of the mechanical properties of similar systems developed at Politecnico of Turin by the research group of Professor Gianluca Ciardelli, in particular taking into the account the research of *Torchio et al*. and *Boffito et al*.

The rest of the project was carried out in the labs of Universitat Politècnica de Catalunya, in Terrassa (Barcelona) during the successive 6 months, under the supervision of Professor Tzanko Tzanov. The study was focused on the development and characterization of nanosystems to be included into the hydrogel to impart the system unique antioxidant and antibacterial properties.

The first part of the research dealt with the study and modification of PheLig NPs that have been engineered by A. G. Morena. The interest on these nanosystems derived from their strong antioxidant properties, the novel green synthesis method used for their preparation and the unspecific interactions this NPs can form with the bacterial membrane that avoid the development of bacterial resistance. The synthesis of PheLig NPs has required in-depth studies of the chemical and physical properties of natural polyphenolic compounds used as novel medical materials in wound care. The first modification of these NPs with the hydroxamic group LTH, derived from the necessity to include in the NPs a moiety able to offer an active targeting over MMPs, overexpressed during chronic infections. Indeed, the state-of-the-art reported hydroxamic groups as one the most effective compounds used to control the levels of MMPs in several applications. The conjunction of LTH was assessed by the amino content assay and by a slight increase in the average dimension of the NPs. Several studies were conducted to understand the effect on MMPs associated with the conjunction of LTH on PheLig NPs. However, no clear results of the advantages of including LTH were observed. Nevertheless, the inclusion of LTH in PheLig NPs

improved the effect this NPs had on MPO activities and the mechanical stability of the resulting hydrogel. Further investigations are necessary to study the benefits the conjunction of LTH could provide. The NPs demonstrated to have some inhibitory effects against both *S. aureus* and *P. aeruginosa* but no bactericidal effects.

For this reason, the next investigation focused on the inclusion of a metallic compound to enhance the bactericidal properties of the NPs and thus of the resulting hydrogel. Phenolation of Lig was used to prepare in bulk LTH-PheLig: the latter was used as capping agent to reduce cobalt obtaining a new Co-LTH-PheLig NPs. The NPs showed bactericidal effects against both *S. aureus* and *P. aeruginosa*. All the synthesized NPs were also characterized in terms of cytotoxicity, they exhibited good cytocompatibility with both fibroblasts and keratinocytes.

Finally, the last part of the study focused on the inclusion of all the analyzed nanosystems within the hydrogel to understand the effect these NPs have on the mechanical properties and the degradation of the hydrogel as well as to study the release kinetics of NPs from the final systems. The NPs slightly modified the rheological properties of the hydrogels without interfering with the gelation ability of the system. However, some changes at the molecular level were hypothesized due to the possible interactions between NPs and the components of the hydrogel.

The synthesized hydrogels demonstrated to have a stability compatible with the final application they were designed for. In addition, the hydrogel offered a linear cumulative release and a good cytocompatibility in contact with fibroblasts and keratinocytes. Further investigations should be carried out to better understand the ideal concentration of the NPs to obtain the best compromise between antioxidant and antimicrobial effect, and cytocompatibility of the systems.

Finally, the composition of the hydrogels could be arranged to favor further crosslinking reactions between PEUs, CDs and NPs. One possibility could be the increase in the amount of the PEU SHF68 that exposes primary amino groups which could act as nucleophile agent able to interact with the phenolic group exposed by NPs to improve the mechanical properties of the hydrogel.

To conclude, the project offered the opportunity to design a system that could be a viable alternative to treat CWs, offering dual actions against two of the main factors that contribute to develop chronicity, the bacterial contaminations, and the overexpression of MPO and MMPs.

# Bibliography


(1) MacNeil, S. Biomaterials for Tissue Engineering of Skin. *Mater. Today* **2008**, *11* (5), 26–35. https://doi.org/10.1016/S1369-7021(08)70087-7.

(2) Fuchs, E. Scratching the Surface of Skin Development. *Nature* **2007**, *445* (7130), 834–842. https://doi.org/10.1038/nature05659.

(3) Casey, G. Physiology of the Skin. *Contin. Prof. Dev.* 5.

(4) Mackenzie, I. C. Ordered Structure of The Epidermis. *J. Invest. Dermatol.* **1975**, *65* (1), 45–51. https://doi.org/10.1111/1523-1747.ep12598037.

(5) Guillem Rocasalbas Lozano. Development of Multifunctional Biopolymeric Materials for Treatment of Decubitus Ulcers. PHD thesis, Universitàt Politècnica de Catalunya, Barcelona, 2012.

(6) Prost-squarcioni, C.; Fraitag, S.; Heller, M.; Boehm, N. Histologie fonctionnelle du derme. *Ann. Dermatol. Vénéréologie* **2008**, *135* (1), 5–20. https://doi.org/10.1016/S0151-9638(08)70206-0.

(7) Theocharis, A. D.; Skandalis, S. S.; Gialeli, C.; Karamanos, N. K. Extracellular Matrix Structure. *Adv. Drug Deliv. Rev.* **2016**, *97*, 4–27. https://doi.org/10.1016/j.addr.2015.11.001.

(8) Monfort, A.; Soriano-Navarro, M.; García-Verdugo, J. M.; Izeta, A. Production of Human Tissue-Engineered Skin Trilayer on a Plasma-Based Hypodermis: Trilayer Human Skin Equivalent. *J. Tissue Eng. Regen. Med.* **2013**, *7* (6), 479–490. https://doi.org/10.1002/term.548.

(9) Skobe, M.; Detmar, M. Structure, Function, and Molecular Control of the Skin Lymphatic System. *J. Investig. Dermatol. Symp. Proc.* **2000**, *5* (1), 14–19. https://doi.org/10.1046/j.1087-0024.2000.00001.x.

(10) Lindsay B. Baker. Physiology of Sweat Gland Function: The Roles of Sweating and Sweat Composition in Human Health. **2019**. https://doi.org/10.1080/23328940.2019.1632145.

(11) Paus, R.; Cotsarelis, G. The Biology of Hair Follicles. *N. Engl. J. Med.* **1999**, *341* (7), 491–497. https://doi.org/10.1056/NEJM199908123410706.

(12) Fonder, M. A.; Lazarus, G. S.; Cowan, D. A.; Aronson-Cook, B.; Kohli, A. R.; Mamelak, A. J. Treating the Chronic Wound: A Practical Approach to the Care of Nonhealing Wounds and Wound Care Dressings. *J. Am. Acad. Dermatol.* **2008**, *58* (2), 185–206. https://doi.org/10.1016/j.jaad.2007.08.048.

(13) Zhao, R.; Liang, H.; Clarke, E.; Jackson, C.; Xue, M. Inflammation in Chronic Wounds. *Int. J. Mol. Sci.* **2016**, *17* (12), 2085. https://doi.org/10.3390/ijms17122085.

(14) Medzhitov, R. Origin and Physiological Roles of Inflammation. *Nature* **2008**, *454* (7203), 428–435. https://doi.org/10.1038/nature07201.

(15) Nathan, C. Neutrophils and Immunity: Challenges and Opportunities. *Nat. Rev. Immunol.* **2006**, *6* (3), 173–182. https://doi.org/10.1038/nri1785.

(16) Enoch, S.; Leaper, D. J. Basic Science of Wound Healing. **2007**, 7.

(17) Nauta, A.; Gurtner, G.; Longaker, M. Wound Healing and Regenerative Strategies: Wound Healing and Regenerative Strategies. *Oral Dis.* **2011**, *17* (6), 541–549. https://doi.org/10.1111/j.1601-0825.2011.01787.x.

(18) Guo, S.; DiPietro, L. A. Factors Affecting Wound Healing. *J. Dent. Res.* **2010**, *89* (3), 219–229. https://doi.org/10.1177/0022034509359125.

(19) Biggs, A. R. MANAGING WOUND-ASSOCIATED DISEASES BY UNDERSTANDING WOUND HEALING IN THE BARK OF WOODY PLANTS. **1990**, 6.

(20) Frykberg, R. G.; Banks, J. Challenges in the Treatment of Chronic Wounds. *Adv. Wound Care* **2015**, *4* (9), 560–582. https://doi.org/10.1089/wound.2015.0635.

(21) McCarty, S. M.; Percival, S. L. Proteases and Delayed Wound Healing. *Adv. Wound Care* **2013**, *2* (8), 438–447. https://doi.org/10.1089/wound.2012.0370.

(22) Telgenhoff, D.; Shroot, B. Cellular Senescence Mechanisms in Chronic Wound Healing. *Cell Death Differ.* **2005**, *12* (7), 695–698. https://doi.org/10.1038/sj.cdd.4401632.

(23) Cabral-Pacheco, G. A.; Garza-Veloz, I.; Castruita-De la Rosa, C.; Ramirez-Acuña, J. M.; Perez-Romero, B. A.; Guerrero-Rodriguez, J. F.; Martinez-Avila, N.; Martinez-Fierro, M. L. The Roles of Matrix Metalloproteinases and Their Inhibitors in Human Diseases. *Int. J. Mol. Sci.* **2020**, *21* (24), 9739. https://doi.org/10.3390/ijms21249739.

(24) Cui, N.; Hu, M.; Khalil, R. A. Biochemical and Biological Attributes of Matrix Metalloproteinases. In *Progress in Molecular Biology and Translational Science*; Elsevier, 2017; Vol. 147, pp 1–73. https://doi.org/10.1016/bs.pmbts.2017.02.005.

(25) Wang, X.; Khalil, R. A. Matrix Metalloproteinases, Vascular Remodeling, and Vascular Disease. In *Advances in Pharmacology*; Elsevier, 2018; Vol. 81, pp 241–330. https://doi.org/10.1016/bs.apha.2017.08.002.

(26) Morena, A. G.; Stefanov, I.; Ivanova, K.; Pérez-Rafael, S.; Sánchez-Soto, M.; Tzanov, T. Antibacterial Polyurethane Foams with Incorporated Lignin-Capped Silver Nanoparticles for Chronic Wound Treatment. *Ind. Eng. Chem. Res.* **2020**, *59* (10), 4504–4514. https://doi.org/10.1021/acs.iecr.9b06362.

(27) Bessa, L. J.; Fazii, P.; Di Giulio, M.; Cellini, L. Bacterial Isolates from Infected Wounds and Their Antibiotic Susceptibility Pattern: Some Remarks about Wound Infection: Bacterial Isolates from Infected Wounds and Their Antibiotic Susceptibility Pattern. *Int. Wound J.* **2015**, *12* (1), 47–52. https://doi.org/10.1111/iwj.12049.

(28) Munita, J. M.; Arias, C. A. Mechanisms of Antibiotic Resistance. **2017**, 24.

(29) Broughton, G.; Janis, J. E.; Attinger, C. E. A Brief History of Wound Care: *Plast. Reconstr. Surg.* **2006**, *117* (SUPPLEMENT), 6S-11S. https://doi.org/10.1097/01.prs.0000225429.76355.dd.

(30) Schultz, G. S.; Sibbald, R. G.; Falanga, V.; Ayello, E. A.; Dowsett, C.; Harding, K.; Romanelli, M.; Stacey, M. C.; Teot, L.; Vanscheidt, W. Wound Bed Preparation: A Systematic Approach to Wound Management. *Wound Repair Regen.* **2003**, *11* (s1), S1–S28. https://doi.org/10.1046/j.1524-475X.11.s2.1.x.

(31) Liu, K. L.; Zhu, J.; Li, J. Elucidating Rheological Property Enhancements in Supramolecular Hydrogels of Short Poly[(R,S)-3-Hydroxybutyrate]-Based Amphiphilic

Triblock Copolymer and α-Cyclodextrin for Injectable Hydrogel Applications. *Soft Matter* **2010**, *6* (10), 2300. https://doi.org/10.1039/b923472a.

(32) Lee, J. H. Injectable Hydrogels Delivering Therapeutic Agents for Disease Treatment and Tissue Engineering. *Biomater. Res.* **2018**, *22* (1), 27. https://doi.org/10.1186/s40824-018-0138-6.

(33) Li, Z.; Guan, J. Thermosensitive Hydrogels for Drug Delivery. *Expert Opin. Drug Deliv.* **2011**, *8* (8), 991–1007. https://doi.org/10.1517/17425247.2011.581656.

(34) Peppas, N. Hydrogels in Pharmaceutical Formulations. *Eur. J. Pharm. Biopharm.* **2000**, *50* (1), 27–46. https://doi.org/10.1016/S0939-6411(00)00090-4.

(35) Klouda, L.; Mikos, A. G. Thermoresponsive Hydrogels in Biomedical Applications. *Eur. J. Pharm. Biopharm.* **2008**, *68* (1), 34–45. https://doi.org/10.1016/j.ejpb.2007.02.025.

(36) Gil, E.; Hudson, S. Stimuli-Reponsive Polymers and Their Bioconjugates. *Prog. Polym. Sci.* **2004**, *29* (12), 1173–1222. https://doi.org/10.1016/j.progpolymsci.2004.08.003.

(37) Yu, L.; Ding, J. Injectable Hydrogels as Unique Biomedical Materials. **2008**, 9.

(38) Mellati, A.; Akhtari, J. Injectable Hydrogels: A Review of Injectability Mechanisms and Biomedical Applications. *Res. Mol. Med.* **2019**. https://doi.org/10.18502/rmm.v6i4.4799.

(39) Du, X.; Zhou, J.; Xu, B. Supramolecular Hydrogels Made of Basic Biological Building Blocks. *Chem. - Asian J.* **2014**, *9* (6), 1446–1472. https://doi.org/10.1002/asia.201301693.

(40) Akindoyo, J. O.; Beg, M. D. H.; Ghazali, S.; Islam, M. R.; Jeyaratnam, N.; Yuvaraj, A. R. Polyurethane Types, Synthesis and Applications – a Review. *RSC Adv.* **2016**, *6* (115), 114453–114482. https://doi.org/10.1039/C6RA14525F.

(41) Oprea, S.; Timpu, D.; Oprea, V. Design-Properties Relationships of Polyurethanes Elastomers Depending on Different Chain Extenders Structures. *J. Polym. Res.* **2019**, *26* (5), 117. https://doi.org/10.1007/s10965-019-1777-6.

(42) Al Khateb, K.; Ozhmukhametova, E. K.; Mussin, M. N.; Seilkhanov, S. K.; Rakhypbekov, T. K.; Lau, W. M.; Khutoryanskiy, V. V. In Situ Gelling Systems Based on Pluronic F127/Pluronic F68 Formulations for Ocular Drug Delivery. *Int. J. Pharm.* **2016**, *502* (1–2), 70–79. https://doi.org/10.1016/j.ijpharm.2016.02.027.

(43) Barrioni, B. R.; de Carvalho, S. M.; Oréfice, R. L.; de Oliveira, A. A. R.; Pereira, M. de M. Synthesis and Characterization of Biodegradable Polyurethane Films Based on HDI with Hydrolyzable Crosslinked Bonds and a Homogeneous Structure for Biomedical Applications. *Mater. Sci. Eng. C* **2015**, *52*, 22–30. https://doi.org/10.1016/j.msec.2015.03.027.

(44) Sartori, S.; Boffito, M.; Serafini, P.; Caporale, A.; Silvestri, A.; Bernardi, E.; Sassi, M. P.; Boccafoschi, F.; Ciardelli, G. Synthesis and Structure–Property Relationship of Polyester-Urethanes and Their Evaluation for the Regeneration of Contractile Tissues. *React. Funct. Polym.* **2013**, *73* (10), 1366–1376. https://doi.org/10.1016/j.reactfunctpolym.2013.01.006.

(45) Adrian Dominski, Tomasz Konieczny, Piotr Kurcok. A−Cyclodextrin-Based Polypseudorotaxane Hydrogels. **2019**, 28.

(46) Boffito, M.; Torchio, A.; Tonda-Turo, C.; Laurano, R.; Gisbert-Garzarán, M.; Berkmann, J. C.; Cassino, C.; Manzano, M.; Duda, G. N.; Vallet-Regí, M.; Schmidt-Bleek, K.;

Ciardelli, G. Hybrid Injectable Sol-Gel Systems Based on Thermo-Sensitive Polyurethane Hydrogels Carrying PH-Sensitive Mesoporous Silica Nanoparticles for the Controlled and Triggered Release of Therapeutic Agents. *Front. Bioeng. Biotechnol.* **2020**, *8*, 384. https://doi.org/10.3389/fbioe.2020.00384.

(47) Torchio et al. Supramolecular hydrogels based on custom-made poly(ether urethane)s and cyclodextrins as potential drug delivery vehicles: design and characterization *J. Mater. Chem. B*, **2020,** 8, 7696 DOI: 10.1039/d0tb01261k rsc.li/materials-b

(48) Biswas, P.; Wu, C.-Y. Nanoparticles and the Environment. *J. Air Waste Manag. Assoc.* **2005**, *55* (6), 708–746. https://doi.org/10.1080/10473289.2005.10464656.

(49) Yallapu, M. M.; Nagesh, P. K. B.; Jaggi, M.; Chauhan, S. C. Therapeutic Applications of Curcumin Nanoformulations. *AAPS J.* **2015**, *17* (6), 1341–1356. https://doi.org/10.1208/s12248-015-9811-z.

(50) Rajendran, N. K.; Kumar, S. S. D.; Houreld, N. N.; Abrahamse, H. A Review on Nanoparticle Based Treatment for Wound Healing. *J. Drug Deliv. Sci. Technol.* **2018**, *44*, 421–430. https://doi.org/10.1016/j.jddst.2018.01.009.

(51) Chereddy, K. K.; Coco, R.; Memvanga, P. B.; Ucakar, B.; des Rieux, A.; Vandermeulen, G.; Préat, V. Combined Effect of PLGA and Curcumin on Wound Healing Activity. *J. Controlled Release* **2013**, *171* (2), 208–215. https://doi.org/10.1016/j.jconrel.2013.07.015.

(52) Wu, J.; Zheng, Y.; Song, W.; Luan, J.; Wen, X.; Wu, Z.; Chen, X.; Wang, Q.; Guo, S. In Situ Synthesis of Silver-Nanoparticles/Bacterial Cellulose Composites for Slow-Released Antimicrobial Wound Dressing. *Carbohydr. Polym.* **2014**, *102*, 762–771. https://doi.org/10.1016/j.carbpol.2013.10.093.

(53) Im, S. H.; Kim, C. Y.; Jung, Y.; Jang, Y.; Kim, S. H. Biodegradable Vascular Stents with High Tensile and Compressive Strength: A Novel Strategy for Applying Monofilaments via Solid-State Drawing and Shaped-Annealing Processes. *Biomater. Sci.* **2017**, *5* (3), 422–431. https://doi.org/10.1039/C7BM00011A.

(54) Grüngreiff, K.; Gottstein, T.; Reinhold, D. Zinc Deficiency—An Independent Risk Factor in the Pathogenesis of Haemorrhagic Stroke? *Nutrients* **2020**, *12* (11), 3548. https://doi.org/10.3390/nu12113548.

(55) Lin, P.-H.; Sermersheim, M.; Li, H.; Lee, P.; Steinberg, S.; Ma, J. Zinc in Wound Healing Modulation. *Nutrients* **2017**, *10* (1), 16. https://doi.org/10.3390/nu10010016.

(56) Pati, R.; Mehta, R. K.; Mohanty, S.; Padhi, A.; Sengupta, M.; Vaseeharan, B.; Goswami, C.; Sonawane, A. Topical Application of Zinc Oxide Nanoparticles Reduces Bacterial Skin Infection in Mice and Exhibits Antibacterial Activity by Inducing Oxidative Stress Response and Cell Membrane Disintegration in Macrophages. *Nanomedicine Nanotechnol. Biol. Med.* **2014**, *10* (6), 1195–1208. https://doi.org/10.1016/j.nano.2014.02.012.

(57) Koyyati, R.; Kudle, K. R.; Padigya, P. R. M. Evaluation of Antibacterial and Cytotoxic Activity of Green Synthesized Cobalt Nanoparticles Using Raphanus Sativus Var. **2016**, 8.

(58) Díaz-GonzáLez, M.; Rocasalbas, G.; Francesko, A.; Touriño, S.; Torres, J. L.; Tzanov, T. Inhibition of Deleterious Chronic Wound Enzymes with Plant Polyphenols. *Biocatal. Biotransformation* **2012**, *30* (1), 102–110. https://doi.org/10.3109/10242422.2012.646676.

(59) Kobayashi S.; Shoda S.; Uyama H. Enzymatic Oxidation. In *Enzymatic catalysis*; Encyclopedia of Polymer Science and Technology.

(60) Turuvekere Vittala Murthy, N.; Agrahari, V.; Chauhan, H. Polyphenols against Infectious Diseases: Controlled Release Nano-Formulations. *Eur. J. Pharm. Biopharm.* **2021**, *161*, 66–79. https://doi.org/10.1016/j.ejpb.2021.02.003.

(61) Ghuman, S.; Ncube, B.; Finnie, J. F.; McGaw, L. J.; Mfotie Njoya, E.; Coopoosamy, R. M.; Van Staden, J. Antioxidant, Anti-Inflammatory and Wound Healing Properties of Medicinal Plant Extracts Used to Treat Wounds and Dermatological Disorders. *South Afr. J. Bot.* **2019**, *126*, 232–240. https://doi.org/10.1016/j.sajb.2019.07.013.

(62) Mihailovi, M. Lj.; ekovi, ivorad. Oxidation and Reduction of Phenols. In *The Hydroxyl Group (1971)*; Patai, S., Ed.; John Wiley & Sons, Ltd.: Chichester, UK, 1971; pp 505–592. https://doi.org/10.1002/9780470771259.ch10.

(63) Teodor Adrian Enache; Ana Maria Oliveira-Brett. Phenol and Para-Substituted Phenols Electrochemical Oxidation Pathways. *J. Electroanal. Chem.* **2011**. https://doi.org/10.1016/j.jelechem.2011.02.022.

(64) Spiridon, I. Extraction of Lignin and Therapeutic Applications of Lignin-Derived Compounds. A Review. *Environ. Chem. Lett.* 15.

(65) Figueiredo, P. Properties and Chemical Modifications of Lignin: Towards Lignin-Based Nanomaterials for Biomedical Applications. 92.

(66) Spiridon, I. BIOLOGICAL AND PHARMACEUTICAL APPLICATIONS OF LIGNIN AND ITS DERIVATIVES: A MINI-REVIEW. 8.

(67) Cabrera, Y.; Cabrera, A.; Larsen, F. H.; Felby, C. Solid-State 29Si NMR and FTIR Analyses of Lignin-Silica Coprecipitates. *Holzforschung* **2016**, *70* (8), 709–718. https://doi.org/10.1515/hf-2015-0165.

(68) Sahoo, S.; Seydibeyoğlu, M. Ö.; Mohanty, A. K.; Misra, M. Characterization of Industrial Lignins for Their Utilization in Future Value Added Applications. *Biomass Bioenergy* **2011**, *35* (10), 4230–4237. https://doi.org/10.1016/j.biombioe.2011.07.009.

(69) Laurichesse, S.; Avérous, L. Chemical Modification of Lignins: Towards Biobased Polymers. *Prog. Polym. Sci.* **2014**, *39* (7), 1266–1290. https://doi.org/10.1016/j.progpolymsci.2013.11.004.

(70) Domínguez-Robles, J.; Martin, N.; Fong, M.; Stewart, S.; Irwin, N.; Rial-Hermida, M.; Donnelly, R.; Larrañeta, E. Antioxidant PLA Composites Containing Lignin for 3D Printing Applications: A Potential Material for Healthcare Applications. *Pharmaceutics* **2019**, *11* (4), 165. https://doi.org/10.3390/pharmaceutics11040165.

(71) Aracri, E.; Díaz Blanco, C.; Tzanov, T. An Enzymatic Approach to Develop a Lignin-Based Adhesive for Wool Floor Coverings. *Green Chem.* **2014**, *16* (5), 2597. https://doi.org/10.1039/c4gc00063c.

(72) Gülçin, İ.; Huyut, Z.; Elmastaş, M.; Aboul-Enein, H. Y. Radical Scavenging and Antioxidant Activity of Tannic Acid. *Arab. J. Chem.* **2010**, *3* (1), 43–53. https://doi.org/10.1016/j.arabjc.2009.12.008.

(73) Isenburg, J.; Karamchandani, N.; Simionescu, D.; Vyavahare, N. Structural Requirements for Stabilization of Vascular Elastin by Polyphenolic Tannins. *Biomaterials* **2006**, S0142961206001566. https://doi.org/10.1016/j.biomaterials.2006.02.016.

(74) Khan, N. S.; Ahmad, A.; Hadi, S. M. Anti-Oxidant, pro-Oxidant Properties of Tannic Acid and Its Binding to DNA. *Chem. Biol. Interact.* **2000**, *125* (3), 177–189. https://doi.org/10.1016/S0009-2797(00)00143-5.

(75) Strong, P. J.; Claus, H. Laccase: A Review of Its Past and Its Future in Bioremediation. *Crit. Rev. Environ. Sci. Technol.* **2011**, *41* (4), 373–434. https://doi.org/10.1080/10643380902945706.

(76) Morena, A. G.; Bassegoda, A.; Natan, M.; Jacobi, G.; Banin, E.; Tzanov, T. Antibacterial Properties and Mechanisms of Action of Sonoenzymatically Synthesized Lignin-Based Nanoparticles. *ACS Appl. Mater. Interfaces* **2022**, *14* (33), 37270–37279. https://doi.org/10.1021/acsami.2c05443.

(77) Díaz-González, M.; Vidal, T.; Tzanov, T. Phenolic Compounds as Enhancers in Enzymatic and Electrochemical Oxidation of Veratryl Alcohol and Lignins. *Appl. Microbiol. Biotechnol.* **2011**, *89* (6), 1693–1700. https://doi.org/10.1007/s00253-010-3007-3.

(78) Mock, W. L.; Cheng, H. Principles of Hydroxamate Inhibition of Metalloproteases: Carboxypeptidase A. *Biochemistry* **2000**, *39* (45), 13945–13952. https://doi.org/10.1021/bi001497s.

(79) Muri, E.; Nieto, M.; Sindelar, R.; Williamson, J. Hydroxamic Acids as Pharmacological Agents. *Curr. Med. Chem.* **2002**, *9* (17), 1631–1653. https://doi.org/10.2174/0929867023369402.

(80) Cheng, X.-C.; Wang, R.-L.; Dong, Z.-K.; Li, J.; Li, Y.-Y.; Li, R.-R. Design, Synthesis and Evaluation of Novel Metalloproteinase Inhibitors Based on l-Tyrosine Scaffold. *Bioorg. Med. Chem.* **2012**, *20* (19), 5738–5744. https://doi.org/10.1016/j.bmc.2012.08.014.

(81) Liang, H.; Russell, S. J.; Wood, D. J.; Tronci, G. A Hydroxamic Acid–Methacrylated Collagen Conjugate for the Modulation of Inflammation-Related MMP Upregulation. *J. Mater. Chem. B* **2018**, 13.

(82) Giustiniano, M.; Tortorella, P.; Agamennone, M.; Di Pizio, A.; Rossello, A.; Nuti, E.; Gomez-Monterrey, I.; Novellino, E.; Campiglia, P.; Vernieri, E.; Sala, M.; Bertamino, A.; Carotenuto, A. Amino Acid Derivatives as New Zinc Binding Groups for the Design of Selective Matrix Metalloproteinase Inhibitors. *J. Amino Acids* **2013**, *2013*, 1–12. https://doi.org/10.1155/2013/178381.

(83) Lee, G.; Rossi, M. V.; Coichev, N.; Moya, H. D. The Reduction of Cu(II)/Neocuproine Complexes by Some Polyphenols: Total Polyphenols Determination in Wine Samples. *Food Chem.* **2011**, *126* (2), 679–686. https://doi.org/10.1016/j.foodchem.2010.11.020.

(84) W. M. Haynes. *CRC Handbook of Chemistry and Physics*, 97th Edition.; W. M. Haynes, 2016.

(85) Williams, R. J. P. Role of Transition Metal Ions in Biological Processes. *R. Inst. Chem. Rev.* **1968**, *1* (1), 13. https://doi.org/10.1039/rr9680100013.

(86) Siavash Iravani; Rajender S. Varma. Sustainable Synthesis of Cobalt and Cobalt Oxide Nanoparticles and Their Catalytic and Biomedical Applications. *Green Chem.* https://doi.org/10.1039/D0GC00885K.

(87) Khusnuriyalova, A. F.; Caporali, M.; Hey-Hawkins, E.; Sinyashin, O. G.; Yakhvarov, D. G. Preparation of Cobalt Nanoparticles. *Eur. J. Inorg. Chem.* **2021**, *2021* (30), 3023–3047. https://doi.org/10.1002/ejic.202100367.

(88) Chohan, Z. H.; Supuran, C. T.; Scozzafava, A. Metalloantibiotics: Synthesis and Antibacterial Activity of Cobalt(II), Copper(II), Nickel(II) and Zinc(II) Complexes of Kefzol. *J. Enzyme Inhib. Med. Chem.* **2004**, *19* (1), 79–84. https://doi.org/10.1080/14756360310001624939.

(89) Dzidziguri, E. L.; Sidorova, E. N.; Inkar, M.; Yudin, A. G.; Kostitsyna, E. V.; Ozherelkov, D. Y.; Slusarsky, K. V.; Nalivaiko, A. Y.; Gromov, A. A. Cobalt Nanoparticles Synthesis by Cobalt Nitrate Reduction. *Mater. Res. Express* **2019**, *6* (10), 105081. https://doi.org/10.1088/2053-1591/ab3ca8.

(90) Ammar, S.; Fiévet, F. Polyol Synthesis: A Versatile Wet-Chemistry Route for the Design and Production of Functional Inorganic Nanoparticles. *Nanomaterials* **2020**, *10* (6), 1217. https://doi.org/10.3390/nano10061217.

(91) Fiévet, F.; Ammar-Merah, S.; Brayner, R.; Chau, F.; Giraud, M.; Mammeri, F.; Peron, J.; Piquemal, J.-Y.; Sicard, L.; Viau, G. The Polyol Process: A Unique Method for Easy Access to Metal Nanoparticles with Tailored Sizes, Shapes and Compositions. *Chem. Soc. Rev.* **2018**, *47* (14), 5187–5233. https://doi.org/10.1039/C7CS00777A.

(92) Feldmann, C.; Jungk, H.-O. Polyol-Mediated Preparation of Nanoscale Oxide Particles. *Angew. Chem. Int. Ed.* **2001**, *40* (2), 359–362. https://doi.org/10.1002/1521-3773(20010119)40:2<359::AID-ANIE359>3.0.CO;2-B.

(93) Urabe, A. A.; Aziz, W. J. Biosynthesis of Cobalt Oxide (Co3O4) Nanoparticles Using Plant Extract of Camellia Sinensis (L.) Kuntze and Apium Graveolens L. as the Antibacterial Application. **2019**, 9.

(94) Gilca, I. A.; Popa, V. I.; Crestini, C. Obtaining Lignin Nanoparticles by Sonication. *Ultrason. Sonochem.* **2015**, *23*, 369–375. https://doi.org/10.1016/j.ultsonch.2014.08.021.

(95) Chowdhury, P.; Nagesh, P. K. B.; Hatami, E.; Wagh, S.; Dan, N.; Tripathi, M. K.; Khan, S.; Hafeez, B. B.; Meibohm, B.; Chauhan, S. C.; Jaggi, M.; Yallapu, M. M. Tannic Acid-Inspired Paclitaxel Nanoparticles for Enhanced Anticancer Effects in Breast Cancer Cells. *J. Colloid Interface Sci.* **2019**, *535*, 133–148. https://doi.org/10.1016/j.jcis.2018.09.072.

(96) Jian Fui, C.; Xin Ting, T.; Sarjadi, M. S.; Amin, Z.; Sarkar, S. M.; Musta, B.; Rahman, M. Highly Active Cellulose-Supported Poly(Hydroxamic Acid)–Cu(II) Complex for Ullmann Etherification. *ACS Omega* **2021**, *6* (10), 6766–6779. https://doi.org/10.1021/acsomega.0c05840.

(97) Bertini, I.; Fragai, M.; Lee, Y.-M.; Luchinat, C.; Terni, B. Paramagnetic Metal Ions in Ligand Screening: The CoII Matrix Metalloproteinase 12. *Angew. Chem.* **2004**, *116* (17), 2304–2306. https://doi.org/10.1002/ange.200353453.